7-1-2022

Ground Moving Target Detection for Airborne Radar Using Machine Learning Approaches

Rafi Ahmed
Florida International University, rahme007@fiu.edu

FLORIDA INTERNATIONAL UNIVERSITY

Miami, Florida

GROUND MOVING TARGET DETECTION FOR AIRBORNE RADAR USING MACHINE LEARNING APPROACHES

A dissertation submitted in partial fulfillment of

the requirements for the degree of

DOCTOR OF PHILOSOPHY

in

ELECTRICAL AND COMPUTER ENGINEERING

by

Rafi Ahmed

2022

To: Dean John L. Volakis
College of Engineering and Computing

This dissertation, written by Rafi Ahmed, and entitled Ground Moving Target Detection for Airborne Radar Using Machine Learning Approaches, having been approved in respect to style and intellectual content, is referred to you for judgment.

We have read this dissertation and recommend that it be approved.

_____
Ou Bai

_____
Jean H. Andrian

_____
B. M. Golam Kibria

_____
Hai Deng, Major Professor

Date of Defense: July 1,2022

The dissertation of Rafi Ahmed is approved.

_____
Dean John L. Volakis
College of Engineering and Computing

_____
Andrés G. Gil
Vice President for Research and Economic Development
and Dean of the University Graduate School

Florida International University, 2022

DEDICATION

I dedicate this thesis to my parents. Without their patience, understanding, support, and most of all love, the completion of this work would not have been possible.

ACKNOWLEDGMENTS

I would like to acknowledge and give my warmest thanks to my supervisor Dr. Hai Deng, for his insightful advice and proper guidance to complete this dissertation. I would also like to thank my committee members: Dr. Ou Bai, Dr. Jean H. Andrian, Dr. B. M Golam Kibria for their valuable suggestions and comments.

Finally, I would like to acknowledge the financial support provided by the FIU graduate assistantship, and the National Science Foundation under Award AST # 1443909.

ABSTRACT OF THE DISSERTATION

GROUND MOVING TARGET DETECTION FOR AIRBORNE RADAR USING MACHINE LEARNING APPROACHES

by

Rafi Ahmed

Florida International University, 2022

Miami, Florida

Professor Hai Deng, Major Professor

Airborne radar faces many challenges to suppress unknown interferences from ground reflections to detect slow-moving targets. In this dissertation work, a feature-based machine learning approach is proposed to effectively classify target and interference such as ground clutter without actually removing them using traditional methods. Multiple features are considered for developing the target/clutter classification algorithms of airborne radars with digital arrays. The features we use for classification include the clutter proximity measures and target geometric feature.

The proximity feature is extracted to distinguish target, and clutter in location in the Doppler-angle domain for airborne radar. The Euclidean distance between a signal and the locus of the expected clutter ridge is known as clutter proximity feature. The distance feature value is generated for each non-zero signal pixel in the angle-Doppler domain of the radar data. Ground moving target and clutter signals are classified and recognized based on the feature for target detection without removing clutters in traditional filtering methods. The proposed feature method is especially effective for target detection in inhomogeneous clutter environment.

In some radar operational scenarios, a single feature might not be enough, and we further introduce the geometric features as well as proximity feature to the machine-learning target detection method to improve the target detection performance. Several geometric features such as block size, roundness ratio, and bending energy are used to extract the relevant geometric information indicating target and clutter geometric differences. The extracted features are then utilized to classify target and clutters reliably and robustly.

The effectiveness of the proposed feature-based methods is validated by the simulation results based on typical airborne radar systems. This study also demonstrates substantial performance improvement over traditional target detection methods such as space-time adaptive processing (STAP) and Beam-Doppler Image Feature Recognition (BDIFR) methods.

TABLE OF CONTENTS

CHAPTER PAGE

LIST OF TABLES

TABLE PAGE

LIST OF FIGURES

FIGURE PAGE

ABBREVIATIONS AND ACRONYMS

AI	Artificially Intelligent
AMTI	Airborne Moving Target Indication
AMF	Adaptive Match Filter
ANN	Artificial Neural Network
ATR	Automatic Target Recognition
BDIFR	Beam-Doppler Image Feature Recognition
CCM	Clutter Covariance Matrix
CE	Capon Estimator
CNR	Clutter-to-Noise Ratio
CNN	Convolutional Neural Network
CPI	Coherent Processing Interval
CUT	Cell Under Test
CW	Continuous Wave
D3	Direct Data Domain
DBN	Deep Belief Network
DFT	Discrete Fourier Transform
DPCA	Displaced Phase Center Antenna
GMF	Global Matched Filter
GMM	Gaussian Mixture Model
GMTI	Ground Moving Target Indication
HK	Hoshen-Kopelman

ICM	Intrinsic Clutter Motion
IID	Independent and Identically Distributed
kNN	k-Nearest-Neighbor
MaxL	Maximum Likelihood
MDV	Minimum Detectable Velocity
MTI	Moving Target Indication
MV	Minimum Variance
PRF	Pulse Repetition Frequency
PRI	Pulse Repetition Interval
RD	Reduced Dimension
RG	Region Growing
RNN	Recurrent Neural Network
ROC	Receiver Operating Characteristics
RR	Reduced Rank
ST	Space-Time
STAP	Space Time Adaptive Processing
SVM	Support Vector Machine
TACCAR	Time Average Clutter Coherent Airborne Radar

I. INTRODUCTION

Typically, airborne radar systems confront interference and noise to detect small targets with low velocity. The interference can be categorized as ground clutter that is mostly generated from the natural environment of earth's surface. On the other hand, thermal noise is a random and unwanted disturbance that is always present in the radar receiver. However, the most challenging task for a radar is to remove or recognize clutters in an unknown environment. This dissertation mainly focuses on classifying clutter signals non-adaptively to detect the target in the presence of thermal noise.

I.1. General Overview of Airborne Radar

I.1.1. Radar system

In this work, pulsed Doppler (PD) radar is used for ground moving target detection (GMTI). PD radar is suitable for detection and tracking of moving targets with three advantages of digital processing, flexibility and coherence [1]. It has an advantage of better performance than continuous wave (CW) radar in terms of transmitted power and receiver sensitivity as well as reflections of interference [2]. PD radar consists of exciter, transmitter, receiver, array antenna and signal processor. Transmitter contains a microwave power amplifier whereas, receiver comprises in-phase and quadrature detectors. Array antenna consists of several isotropic elements that radiate power to minimize sidelobes [1]. After receiving and digitizing the echo data in the radar system, the further processing could be performed either with conventional or artificially intelligent approach.

I.1.2. Artificially intelligent (AI) and conventional radar

With the technology evolution, radar systems have changed dramatically with the availability of machine learning (ML) approaches. The performance of AI radar improves with the data training. Since the ground clutters are very challenging task to suppress from the radar scene, learning the clutter environment with training data could ensure much more robust and powerful detection than conventional radar. Whereas conventional radars depend greatly on analytical solution and provide unequivocally good performance. However, they have some limitations such as:

- Interference needs to be suppressed or totally eliminated using a filter before the target detection
- To facilitate the filtering process, one needs to estimate the interference such as, clutters in the radar scenario using their statistical information.
- The detection performance is extremely sensitive to the interference estimation accuracy.

Majority of these limitations can be overcome by AI radar classifier. Because-

- Interferences are not actually suppressed rather they are recognized
- AI radar classifies radar data as either interference (H_0) or target along with interference (H_1)

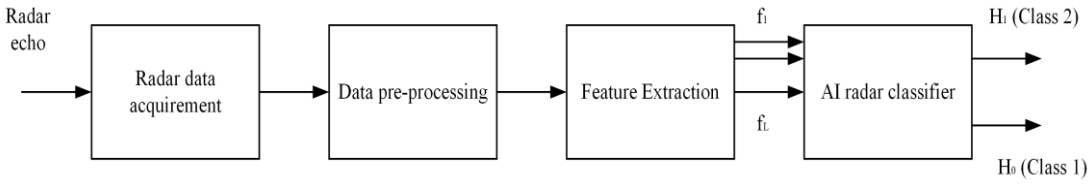

Figure I. 1 AI radar classifier

The steps for AI radar can be visualized with the Fig. I.1. It represents the salient processes to build the AI classifier such as,

- ✓ Preprocessing (Transformation)
- ✓ Feature extraction
- ✓ AI classification

Assume the feature vector extracted from the radar data are: $\mathbf{f} = [f_1, f_2 \ldots f_L]^T$

One way to solve the problem is to find the posterior probabilities (equivalent to a classifier):

$$\begin{aligned} P(H_1|\mathbf{f}) > P(H_0|\mathbf{f}) &\Rightarrow \mathbf{f} \text{ in } \mathrm{H}_1 \text{ subspace} \\ P(H_1|\mathbf{f}) \le P(H_0|\mathbf{f}) &\Rightarrow \mathbf{f} \text{ in } \mathrm{H}_0 \text{ subspace} \end{aligned} \tag{I.1}$$

It is further assumed that the radar feature data components are statistically independent. Likelihood functions for each feature component need to be estimated:

$$p(f_j|H_0),\ p(f_j|H_1),\ j = 1, 2, \ldots L \tag{I.2}$$

To estimate the feature vectors, one can use approximation function utilizing the training data. Alternatively, they can be approximated with histogram functions generated from the training data. However, the training data must be sufficient to cover all possible radar operation scenarios. Simulated radar data are also acceptable for training the AI radar if the mechanism for generating data is clear. AI training data are the labeled datasets

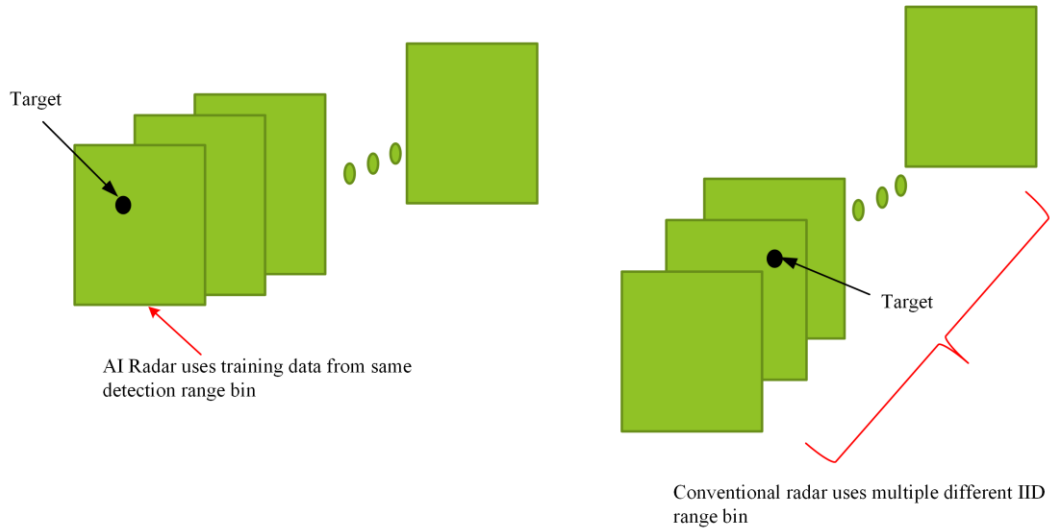

Figure I. 2 AI radar vs. conventional radar

generated by the same or similar radars and simulated under all possible environments and targets.

As for the training data, AI radar does not need to use secondary samples from the adjacent range cells together with cell under test (CUT). In contrast, conventional radar uses multiple different independent and identically distributed (IID) from the adjacent range bins. Fig. I.2 delineates the major difference between them.

The classifier of AI radar could be implemented with perceptron networks (unknown feature distributions) or even deep-learning networks (useful for target recognition). This type of smart radar system is capable of detecting moving targets in heterogenous clutters.

I.1.3. Clutter

Clutter is the most challenging interference encountered by airborne radar. It can be defined as unwanted radar signal echoes that deter the detection of targets. The clutters could be the reflections originated from sea waves, chaff, rain, birds, etc. When clutter echoes come from land or sea, they are categorized as surface clutter. Ground or land

clutter is the most difficult interference in the domain of target detection. The ground terrain's irregularity and dielectric characteristics make it more unpredictable with respect to airborne platform. Clutter environment varies with frequency as well. Usually, rugged surface of hill, vegetation areas have linear relation with frequency [1]. Clutter power is considered to be higher than the receiver noise power. In fact, the clutter power increases with the increase of transmitter power. Besides, clutter distributions vary randomly and make the nature of estimation difficult due to the amplitude variation. There are various types of clutter model used by the radar researchers. Gamma distribution model, K-distributed model and Gaussian distributed model are widely used approaches to simulate clutter spectrum

I.1.4. Thermal noise

Thermal noise is originated from random fluctuation of charge carriers. The noise is also known as white noise which is always present in the radar receiver. Moreover, there are some other noises that have same type probability distribution like thermal noise. They also contribute to generate thermal noise in the radar receiver. In addition, thermal noise greatly depends on the bandwidth of each receiver channel.

I.1.5. Target

Target is the desired signal component of a moving object detected by radar. Usually, the target is described by the azimuth and elevation angles, radar cross section and relative velocity according to the radar platform. Moreover, the target signal shows a point shape feature in the transformed domain with a spread in both angular and Doppler frequency.

I.2. Literature review

I.2.1. Traditional approaches

From the advent of radar technology, various forms of ground clutter suppression technique have been introduced to mitigate the interference. PD radar is the first of kind that can reject clutter in the presence of low-speed targets [2,3]. However, the automatic rejection of interference fails when it confronts the inhomogeneous (the amplitude of clutter patch varies randomly from one range bin to another) clutter [3]. In contrast, moving target indication (MTI) shows better performance than PD radar in the airborne surveillance system. Moreover, MTI Doppler filters can utilize multiple pulse repetition frequencies (PRFs) to reduce the overlapping of target and clutter signal. Some form of MTI uses efficient memory technique to avoid blind velocity phenomenon [2]. Yet, platform motion makes the MTI filtering process difficult to achieve and can cause undesired compensation error on clutter spectrum [4]. Displaced phase center antenna (DPCA) is one of the non-adaptive solutions to the problem of motion compensation. The DPCA also improves the performance when the clutter spectrum width is small. However, the method needs rigorous condition regarding the platform velocity and the pulse interval [5]. Also, non-adaptive DPCA suffers from antenna sensor errors due to phase and amplitude variation [6]. These errors could be resolved by an adaptive MTI system that compensates the differences in phase and amplitude [7]. However, internal clutter motion and non-linear clutter ridge due to the aircraft crab limit the performance of both non-adaptive and adaptive DPCA [6].

Moving platform effects can also be overcome by a compensation technique applied to the Doppler shift in clutter spectrum. Time average clutter coherent airborne

radar (TACCAR) is a well-known method that compensates platform speed by approximating the center Doppler frequency of the clutter [7]. However, TACCAR needs specific order for the range interval and coherent signal generator for the expected compensation [8]. Moreover, clutter coherent method incurs signal to interference plus noise ratio (SINR) loss and may require additional sample data [9]. In contrast, [10] proposed a clutter mitigation technique that uses a matrix that compensates Doppler shift of clutter without using secondary training samples. However, the approach often fails to remove all of the clutter signal and the subspace contains some residues since the compensation operator is not totally perfect.

Space-time adaptive processing (STAP) is a ubiquitous solution to the DPCA and non-adaptive compensation problem that is extensively used to suppress the clutter in phased array radar [5,11–15]. STAP has the ability to detect slow-moving target that are relatively small and suppress inhomogeneous clutter [5]. However, a significant amount of independent and identically distributed (IID) secondary data is required to estimate the clutter covariance matrix (CCM). The RMB rule (coined by Reed, Mallett, and Brennan) suggests that the number of secondary samples must be at least twice the product of antenna element of linear array and number of transmitted pulses in one pulse repetition interval (PRI) to estimate the CCM appropriately [11]. Besides, the STAP has a problem of convergence in CCM estimation and lacks optimum performance for inhomogeneous clutters. These convergence rate can be improved by sample covariance matrix in [12] and asymptotic solution is given in [13] to reduce performance loss. Wu *et al.* proposed an algorithm to get the training data selectively for clutter estimation and thereby reduces secondary sample requirement [14]. Still, the stipulation of [11] makes the

inhomogeneous clutter suppression difficult for operational radars since, the secondary data is hardly available in terms of practical implementation [5,11,15]. Some researchers developed adaptable virtual redundancy sensor elements to estimate the CCM of STAP [16]. Also, subspace method of STAP improves the performance and reduces the number of range bins for inhomogeneous clutter estimation [17].

To reduce the number of secondary training data, reduced dimension (RD) STAP can be adopted to convert it to a partially adapted process [18]. Reduced dimension can be obtained using auxiliary channel method [19], factored technique on space-time data [20] and joint domain algorithm [21]. Nevertheless, implementation of RD techniques becomes difficult due to the lack of sufficient IID secondary data in inhomogeneous clutter environment [22,23]. Whereas sparse recovery (SR) algorithms attain optimum performance with a very few amounts of secondary data samples [24,25]. SR-STAP approach also improves computational complexity of SR dimension problem [26]. However, SR technique show a performance degradation with limited secondary samples of inhomogeneous clutter scenario [27]. Furthermore, clutter inhomogeneity incurs high computational resources to estimate the CCM accurately [18,26,27].

Reduced rank (RR) approach is another solution of adaptive filter processing to achieve dimensionality reduction of STAP. Eigen value analysis is one of the first methods to reduce clutter rank [28]. Cross-spectral metric is also a fine method to the adaptive filter techniques adopted clutter rank reduction [29]. Besides, multistage Wiener filter (MSWF) [30], auxiliary-vector filters (AVF) [31] also provide optimal convergence in achieving reduced-rank adaptive filter. However, these filters are very involved and incur numerical errors in the real-time application [32].

A more viable approach compared to RR technique is the deterministic STAP (also termed as direct data domain or D^3) since it only needs the echo data from the cell under test (CUT). Previously, conjugate gradient approach [33], least squares method [34,35] introduce D^3 concepts to process spatial-temporal snapshot with improved resolution of two-dimensional filter. The purpose of these methods is to eliminate unwanted information in the range gate with the aid of target azimuth and Doppler profile. In fact, some of the developed D^3 methods are suitable for clutter suppression even when the knowledge about the radar operation scenario is not totally accurate [36]. However, the algorithm costs some of the degrees of freedom (DoFs) to suppress the interference effectively [37].

Knowledge-aided (KA) approaches were also popular to address the data required for STAP and DoFs. CCM estimation based on prior information with Kronecker product operation provides significant performance improvement by reducing parameter estimation [38]. Besides, STAP based on Bayesian approach uses prior information about the estimation of covariance matrix. Moreover, terrain data, platform speed, radiation direction of radar sensor array can also be used to detect target-like signals [39]. prior knowledge or information can be achieved via training data or the filter processing [40]. Alternatively, regularized scheme for STAP develops the concept of knowledge aided adaptive matched filter (AMF) ensuring accurate estimate of CCM [41–43]. However, computational burden and large amount of training data are the main obstacles to obtain desirable performance of this method. Thus, [44] introduces a knowledge based parametric approach for matched filter with limited training data. The method has an advantage of having better performance in case of uncertain prior knowledge. On the

contrary, shrinkage model is another KA-STAP technique that reduces the dependency of large training data. Moreover, the model does not need an accurate estimation of CCM [45]. Meanwhile, [46] develops a prior knowledge-based suppression technique to optimize the STAP performance via modification of radar system. However, there are several factors that can adversely affect the KA approaches. Prior knowledge could often contain imprecise information owing to estimation, or obsolete information [46]. Moreover, statistical and structural information about the CCM is quite difficult to obtain for inhomogeneous clutters [48,49].

Compressive sensing (CS) is the process of extracting information from compressed radar data samples without signal reconstruction [50–52,56]. CS technique is very effective in the application of radar target detection. There are various types of CS method used in modern radar systems. Full Nyquist rate-based target detection schemes have been used since the advent of CS application [53,54]. However, these methods do not consider lower the sampling rate under Nyquist rate. Hence, sub-Nyquist sampling system is an alternative approach to detect the Doppler frequency of the target and clutter spectrum [55]. PRF based compression technique is one of them and it can be utilized even when the signal is sampled under Nyquist rate [56]. CS sampling with quadrature has recently gained popularity to reconstruct radar signal in the receiver end. This method is also used to detect the target by using a small amount of training data and thereby improve the detection performance as well as clutter suppression [57,58]. On the contrary, some researchers developed velocity-based clutter suppression approach before applying CS algorithm. With a chosen range corresponding to the clutter velocity, the moving targets can be detected with minimal error [59]. Knowledge aided compressing

sensing is also applied to radar echo as an alternative to STAP. Global matched filter (GMF) with prior information about signal has the capability to detect the target and clutter by one snapshot of spatial-temporal vector [60]. However, CS algorithms have major disadvantages in interference and noise suppression. They often stipulate rigorous condition on radar transmitter that affects the suppression procedure [55, 61,62]. Besides, some approaches lack in detection and elimination performance of real clutter environments [53,63]. Most importantly, CS methods often fails to detect target that are close to the clutter Doppler frequency and might erroneously reject the target signal as a clutter [55,58].

I.2.2. Feature-based approaches

To minimize the requirement of secondary training data with the help of recent machine learning and artificially intelligent (AI) radar technology evolution, GMTI community puts significant effort on the feature-based approaches in the airborne radar signal processing. Depending on different attributes of radar target and interference, researchers have put a lots of successful classification algorithms from late 20^{th} century. In 1982, Doppler frequency features are used to classify radar clutter [64] . Later, parametric statistical classifier demonstrated improved accuracy on target and clutter classification [65]. Afterward, Haykin *et al.* introduced neural network classifier to detect target from different types of clutter. The classifier obtained 89% of accuracy with single snapshot of radar environment. Skewness and kurtosis of magnitude change of samples, relative power and variance of radar signal, signal-to-noise-ratio (SNR) are used as features for the classifier. The features are then fed to a four-layer feed forward network. The classifier also applied back-propagation algorithm to learn the optimal

weights [66]. Another classifier in [67] can identify the clutter amplitude distribution. However, it requires large set of training data to get a proper classification accuracy. Moreover, non-Gaussian distributed clutter classifier were designed in [68] utilizing the shape parameter of the distribution. Alternatively, time-frequency features are also successful in classifying radar clutter [69]. However, clutter features in time-frequency domain are difficult to extract for surveillance radar. Hence, classification method based on statistics such as, Gaussian mixture model (GMM) showed improved target-clutter classification. The algorithm worked with maximum likelihood (MaxL) estimation rule to classify target from real radar data [70]. Recently, artificial neural network (ANN) is used as a radar classifier for target detection in a simulated environment. Polarimetric features generated by the Prony algorithm are then provided to the classifier [71]. Although the method provided good accuracy in simulated data, the classifier often fails to detect target in inhomogeneous clutter environment since the polarimetric features change largely with target Doppler frequency. On the contrary, some researchers consider a large set of simulated training data with different clutter distribution and their statistical features. Subsequently, a neural network with two hidden layers is designed to classify the clutters [72]. Nevertheless, training data about different clutter scenario is expensive and difficult to achieve.

Instance-based learning is also popular in radar community since it does not require any complex network structure and expensive training dataset. [73] proposed support vector machine (SVM) to track the target utilizing the radar cross section, radial velocity and target azimuth or range information. In [74], both SVM and k-Nearest-Neighbor (kNN) machine learning (ML) techniques were presented to detect target in the

midst of sea clutter. Two algorithms were compared and kNN demonstrated lower false alarm rate than the SVM technique. The authors in [74] also suggested that the performance of ML based clutter suppression could be improved with the more training data. Whereas Shui *et al.* explored kNN model to segment ground and sea clutters using phase, amplitude, and Doppler information. The similarity parameter is used to differentiate ground and sea clutter using Doppler frequency range. The approach also showed optimal performance in real data collected by airborne radar [75].

While the NN and instance-based approaches are widely accepted in the detection of ground moving targets, some other feature-based techniques such as linear or polynomial feature space put notable contribution with limited training samples. In [76], linear regression model is applied to find the target Doppler and azimuth information. It implies that, each grid of azimuth-Doppler plane is considered as a separate class. The method worked better than STAP since it can detect target with few numbers of training bins. Although the linear feature model is better than STAP, the performance might degrade due to the variation of SINR. Thus, [77] offered a polynomial classifier that provide more performance and accuracy compared to linear model. To reduce the performance deterioration in the presence of weak target signal, the classifier is arranged with a STAP system in series combination. However, the classification system in [77] brings additional computational resources that makes the system vulnerable for low SINR.

Recent development in deep learning models also shows a way to improved feature based leaning systems in radar target detection. The advancement not only reduces the hard thresholding of hypothesis assessment but also enables the radar to

classify target and interference instead of applying filtering processes to retrieve the target. Recently, deep neural networks have been studied and utilized extensively in various of radar signal processing [78]. Especially, [79] investigated the target detection using recurrent neural network (RNN) to solve signal detection and estimation problem. As for the waveform design, authors in [80] proposed convolutional neural network (CNN) based time-frequency technique that recognized radar waveform and decrease the noise level. For recognition purpose, [81] devised a new Boltzmann machine-based network model to extract different uncorrelated features of radar echo signal. The recognition model works well with low SNR requirement. However, the computational burden of this model is very high without using deep layers inside it. To reduce the complexity of deep learning hardware, some researchers developed methods with reduced arithmetic operations for radar application. There are several algorithms that have made efforts to simplify the backpropagation algorithm of neural networks [82,83]. Using the simplified algorithm of [83], authors in [84] proposed deep belief network (DBN) based radar system that can detect small and slow-moving targets. The DBN used in this system ensured the low complexity by modifying the multiplication operations of the network model. On the other hand, automatic target recognition (ATR) has used alternative DNN model with sparse dictionary learning that is suitable for measured radar data [85].

Since the radar echo data for the target detection of airborne radar in the presence of ground or sea clutter can be transformed into a two-dimensional image (range-angle-Doppler, range-Doppler, angle-Doppler space), CNN has been applied extensively to detect targets regardless of low or high SINR and interference variability. The usage of

CNN is also very successful in detecting radar target under extreme heterogeneous clutter. For example, [86] applied CNN with deep layers to detect moving target in inhomogeneous clutter environment. The proposed approach generated augmented dataset from secondary training data and synthetic moving target to validate the effectiveness. The method was also verified with the radar mountaintop data [87]. On the contrary, authors in [88] employed region-based CNN providing high accuracy for maritime radars to detect point targets. Since radar clutter has the tendency of overlapping with target due to slow moving nature, authors in [89] proposed double channel CNN for the target detection. The model utilized the attributes of both time-frequency and amplitude data form radar echo signal to effectively detect the target. The proposed approach also developed two classifiers to control the false alarm and thereby results in improved detection performance in the real data application. To suppress clutter, another CNN based approach was introduced in [90] comprising a method to detect point target. It also developed an approach to pinpoint the target using convolutional autoencoder. Even though the CNN models are very successful in developing radar systems that can classify and reject clutter successfully, their applications in real time radar signal processing are still impeded with the computational complexity [86,88] and large data requirement [86–90]. In real world scenario, it is quite difficult to achieve such highly efficient computing devices in a limited space of airborne or maritime radar. Moreover, generation of secondary clutter data is very expensive and most of the data are classified in the field of airborne radar systems. Thus, a radar with these high-level requirements is quite impractical in real-time implementation.

To reduce the data requirement and computational burden, some of the radar researchers introduced unsupervised feature-based ML techniques. The feature based unsupervised approach was first proposed by [91] where radar echo data is transformed from the space-time domain to angle-Doppler domain. Subsequently, the transformed data is denoised and region growing algorithm is applied to segment target and interference. Block size is the feature that is used to distinguish between target and interference. Later, [92] extended the work of [91] and coined it as a beam-Doppler image feature recognition (BDIFR). BDIFR method verified the approach in inhomogeneous clutter with intrinsic clutter motion (ICM). The method was also compared to conventional STAP and proved to be effective in providing better performance. The biggest advantage of these algorithms is that they do not require any filtering process and clutter estimation. These algorithms work well even when there is limited training data. In fact, they are applicable with the echo data collected from primary detection range bin. However, algorithms based on these seed based clustering technique could not detect targets overlapped with clutters. Since, the region growing algorithm totally depends on the connected components in an image, target and clutter pixels must have to be disconnected. Otherwise, the target is falsely detected as clutter with the block size. Thus, necessary adjustments in the radar systems must be kept to prevent overlapping scenario in the angle-Doppler radar image.

I.3. Problem Description

Radar target detection with various system approach have been developed in the last few decades. Traditional methods are quite successful since their inception but as technology evolves new robust techniques replace them for the expectation of better

performance. As can be seen from the literature, most of the early methods suffer from accuracy in estimating the inhomogeneous clutter power distribution. In contrast, expected accuracy comes with the expense of large data requirement. Although these methods were proved statistically well enough to filter expected clutter components, artificially intelligent techniques made them obsolete due to their fast decision making and reduction of manual hard thresholding.

The era of machine learning techniques brought significant changes in the radar detection technology. Even before the beginning of this era, few early literature used some of the simple neural network architecture to classify clutter in airborne and maritime settings. Afterward state-of the art ML methods has substituted the adaptive filters and made better automatic radar system. Deep learning models such as, CNN, R-CNN are being effectively utilized to improve the performance of the airborne radar and they greatly reduce the false alarm rate. However, these models require a large set of dataset and powerful computational resources to operate on the real time radar application. These two prerequisites of deep learning methods have prevented lots of potential and effective methods to undergo successful implementation.

In this dissertation, a novel feature-based machine learning techniques are introduced to classify clutter and target from transformed radar echo data. The methods require no clutter estimation and can detect target in inhomogeneous clutters from primary detection bin. Besides, these methods do not use any adaptive filter and secondary training data. An innovative multi-feature based deep learning approach is also proposed to detect target overlapping with inhomogeneous clutter.

I.4. Dissertation Contribution

A new feature-based technique coined as clutter-proximity feature based machine learning approach is proposed to suppress clutters without any filtering process and thereby detect target. The proximity feature extracts the information about the target and clutter signals using Euclidean distance metric with respect to the expected clutter ridge. The technique has also designed a new classifier based on the statistics of training data and determine the detection threshold automatically on test samples. One of the salient features of this method is that it can work well with the few amounts of training data. Then the classifier is designed with the bootstrapped samples of the training data. The performance of this approach is evaluated and compared with conventional STAP method.

Another proximity feature based technique is introduced in this dissertation to suppress non-linear inhomogeneous clutter due to aircraft crab. For this method, proximity distance feature is collected with respect to the major axis of the expected non-linear clutter ridge. The method also has proved to be effective to detect target inside or outside of the clutter boundary.

To detect the target overlapped with inhomogeneous clutters under both Doppler unambiguous and ambiguous case, an effective multi-feature-based target detection technique is developed with the aid of feed forward neural network. The clutter training data is generated using minority sampling technique for the training purpose of the network. The method also automatically detects the boundary of the overlapped target and segments it from the clutter. The performance of this method is verified and

compared with another feature-based technique to detect slow-moving targets in inhomogeneous clutter scenario.

I.5. Dissertation Structure

The organization of the dissertation is as follows:

Chapter II elaborates the overall theoretical radar signal processing aspects of airborne radar. The theory basically comprises of the concepts regarding signal detection and estimation with a detailed statistical derivation and mathematical expression. Null (H_0) and alternate (H_1) hypothesis are defined in the section II.1 to better represent the target absent and target-present scenario, respectively. The airborne radar considers clutter, jammer as the interference, thermal noise as receiver noise and target as the signal of interest. Jammer is not included in this work. The clutter, noise and target model has been developed in the section II.2, II.3, and II.4 to elaborate the context of this dissertation. Lastly, the transformation of the radar echo data is presented in the section II.5 with the estimation criteria known as the minimum variance or Capon estimation operator.

Chapter III delves into the depth of a novel feature-based detection approach termed as clutter-proximity feature. Section III.1 starts with theoretical aspect of proximity feature of clutter ridge. The clutter ridge is defined, and the weights of the expected clutter ridge are mathematically described. The mathematical and theoretical part for clutter ridge is divided into two parts. One is for Doppler unambiguous (DU) case and another one is Doppler ambiguous (DA) case. Section III.2 introduces some terminologies to explain the algorithm properly. Since, the transformed domain is a radar image, some definition and terms related to connected component and image features are

described. Section III.3 discusses the algorithm steps to classify the target and clutter using the denoising threshold and proximity detection threshold. Since the training data is not much available, a statistical approach known as bootstrapping is utilized in this work that has been detailed in the section III.4. In section III.5, a new machine learning classifier is designed to approximate the detection threshold from the statistical parameters of the bootstrapped training data. Confidence interval is needed to be determined to obtain the upper and lower bound of the training data. The procedure is explained in the section III.6. The simulation results is demonstrated in the section III.7. Section III.8 compares the proximity feature based detection with the conventional STAP method. In the end, the summary of chapter III puts some concluding remarks for this chapter.

In chapter IV, ground moving target detection using clutter-proximity feature in the presence of antenna alignment error angle is introduced. Section IV.1 begins with the challenge of non-linear clutter and briefly discusses the signal model corresponding to the theory of direction mismatch. Section IV.2 elaborates the innovative proximity feature for the elliptical clutter. Due to the non-linear relationship between spatial and Doppler frequencies, this section concentrates on the major axis of the clutter and describes about it. Next, simulation results are analyzed and demonstrated for this approach. Section IV.4 puts a summary for this chapter.

Chapter V discusses an innovative multi-feature-based machine learning approach for ground moving target detection. Several features such as, proximity to the clutter ridge, block size, roundness ratio, and bending energy etc. are extracted from the angle-Doppler radar scene and fed to the feed forward neural network. In section V.1, a theory

of the of airborne signal model is again revised for multi feature approach. Section V.2 explores the connected components in the radar image through an algorithm known as Hoshen-Kopelman (HK) algorithm to label the individual connected regions. It also describes the procedure to detect the boundary pixel to process the further target pixel identification. Section V.3 describes different image and geometric features to detect both the non-overlapped and overlapped targets. Geometric features are also mathematically explained in this section. In section V.4, the deep FFNN model is developed to classify the target and clutter. It also discusses the number of layers, regularization parameters, optimizer and losses. In section V.5, generation of synthetic data is described both for target and clutter samples corresponding to each feature. Simulation results for linearly extended clutter ridge is given in the section V.6 for ideal and non-ideal platform velocity. The simulation evaluates the scenario of both overlapping and non-overlapping targets in inhomogeneous clutter environment. Section V.7. demonstrates the simulation results for ground low velocity moving target detection due to velocity misalignment. The method is evaluated when the target overlaps with non-linear clutter ridge segment. In section V.8., The performance of the proposed approach is compared with the previous feature based approach known as beam-Doppler image feature recognition (BDIFR) in Doppler unambiguous scenario. The scenario also considers a target merged with the clutter. Finally, the summary of chapter V is given in the section V.9.

Chapter VI draws some salient points of this research and future work based on this machine learning approach. The chapter also points out some limitation of these proposed methods.

II. AIRBORNE RADAR SIGNAL MODEL

This chapter has been adapted from a previous work by the authors titled “Robust ground moving target detection for airborne radar using a novel feature-based machine learning approach”,©2022 Elsevier. In theoretical perspective, there are four types of signals confronted by airborne radar such as, interference, noise and target. Clutter, and jammer are considered as interference. Whereas thermal or white noise is regarded as a receiver noise. The desired signal or signal of interest is known as target. The objective of an airborne radar is to detect the target from the surrounding noise and interference through the echo data achieved from space-time (ST) domain or a transformed frequency domain from ST domain. Angle-Doppler, range-time or range-angle-Doppler space could be categorized as transformed domain. In this dissertation, radar echo data is transformed from ST domain to angle-Doppler domain. Also, the focus of this dissertation is to detect the target in an environment inflicted with clutter and noise. Hence, jammer is not considered as the one of the models.

This chapter deals with widely used theoretical clutter, noise and target model to obtain the angle-Doppler plane scene. Segment II.1 introduces the radar configuration and hypothesis assumed for the radar signal detection and estimation. Section II.2 elaborates the theoretical model complex clutter model. Section II.3 explains the thermal noise model of target scene. Lastly, target is modeled with a theoretical aspect in section II.4.

II.1 Radar Specifications and Hypothesis

An airborne radar with a linear uniform antenna array of N elements is considered to generate radar echo data in space-time domain for signal processing. The radar’s height

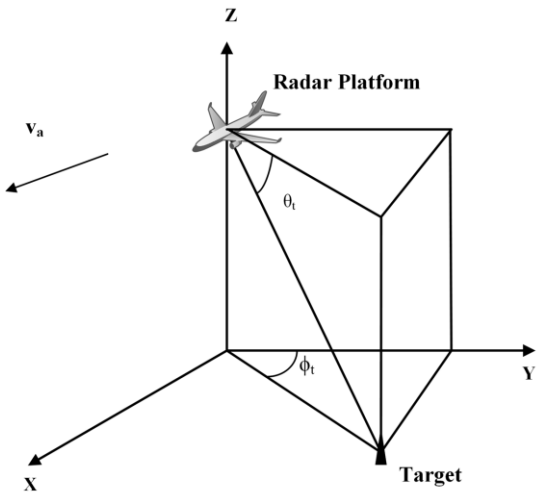

Figure II. 1 The geometry of the airborne radar platform with a ground moving target

to the ground is *h*, and the azimuth and depression angles of the radar's antenna regarding target are ϕ and θ, respectively. The radar operating wavelength is λ. We further assume that the radar platform moves in a direction parallel to the x-axis with a speed of V_x. The antenna element spacing is assumed to be *d*. The radar transmits *M* coherent pulses in one pulse repetition interval (PRI) during each radar beam dwelling. The data are then converted into the angle-Doppler domain using the minimum variance (MV) method [19,92]. shows the geometry of the radar operation.

The space-time samples of the radar data for the target scene can be expressed as,

$$\boldsymbol{S} = [s(0,0), s(1,1), ..., s(N-1, M-1)]^T \quad \text{(II.1)}$$

where $s(i, j)$ is the received echo sample of the *j*-th transmitted pulse at element *i* and each sample contains target, clutters and thermal noise under $\mathbf{H_1}$ hypothesis or clutters and noise only under $\mathbf{H_0}$ hypothesis.

H_0 (null) hypothesis: When the desired signal or signal of interest is not present, then the received echo signal forms null ($\mathbf{H_0}$) hypothesis.

H_1 (alternate) hypothesis: The alternate ($\mathbf{H_1}$) hypothesis is valid if the radar echo signal contains the desired target signal as well as noise and interference.

Thus, the space-time samples can be written as:

$$\begin{cases} \boldsymbol{S} = \boldsymbol{S}_c + \boldsymbol{S}_n \ \textit{under}\ \boldsymbol{H_0}\ \textit{hypothesis} \\ \boldsymbol{S} = \boldsymbol{S}_c + \boldsymbol{S}_n + \boldsymbol{S}_t \ \textit{under}\ \boldsymbol{H_1}\ \textit{hypothesis} \end{cases} \tag{II.2}$$

Where $\boldsymbol{S_n}$, $\boldsymbol{S_c}$, and $\boldsymbol{S_t}$ are the spatial-temporal vectors of the thermal noise, clutter and target, respectively.

The covariance matrix of the radar data can be expressed as,

$$\boldsymbol{R} = E[\boldsymbol{S}\boldsymbol{S}^H] \tag{II.3}$$

with the assumption that target, clutter, and thermal noise are uncorrelated, the covariance matrix in (I.3) can be further represented as the sum of the covariance matrices of $\boldsymbol{S_n}$, $\boldsymbol{S_c}$, and $\boldsymbol{S_t}$ of the thermal noise, clutter, and target, respectively. Hence, the radar data covariance matrix under the $\mathbf{H_1}$ hypothesis is given by,

$$\boldsymbol{R} = \boldsymbol{R}_c + \boldsymbol{R}_n + \boldsymbol{R}_t \tag{II.4}$$

II.2 Radar Clutter

Ground clutter has random amplitude and is dependent on the range. The clutter shape and its orientation significantly depend on the radar platform speed. Whereas range greatly depends on pulse repetition frequency. Thus, radar range has an inherent characteristic of ambiguity. If the two echoes do not have sufficient delay between their round-trip time, the phenomenon could cause range ambiguity. For that, radar must have sufficient wait time to avoid the ambiguous echo. If c is the speed of light and the w is the pulse repetition interval (PRI) then the maximum unambiguous range can be given by:

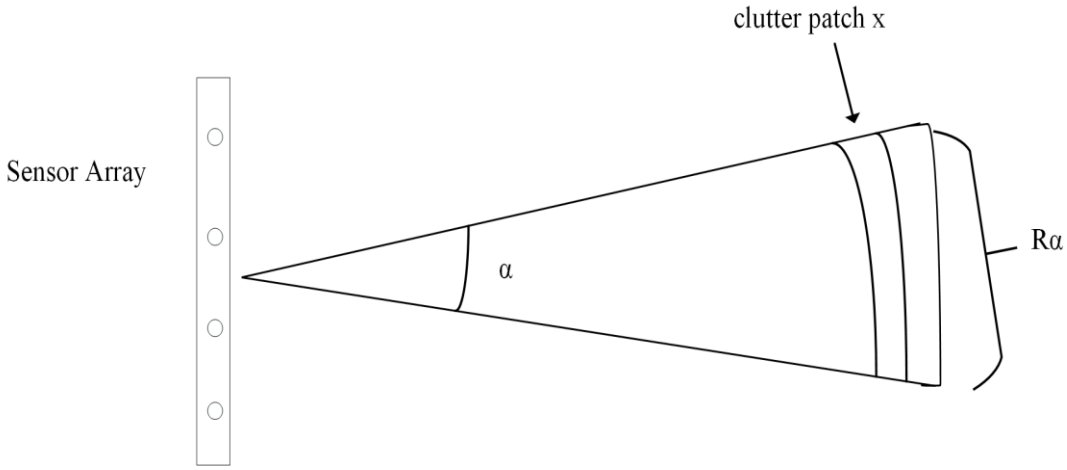

Figure II. 2The clutter patch with respect to the antenna array of airborne radar

$$R_{ua} = \frac{cw}{2} = \frac{c}{2 * PRF} \tag{II.5}$$

Considering the radar ambiguity, the clutter is modeled as individual clutter patches in the azimuth angle location of the radar. This individual clutter patch has an effective area known as clutter patch cross section (ccs). Fig. II.2 Shows the geometric formation of clutter patch from the radar antenna elements. Then the cross section is expressed as:

$$ccs = c_r R\alpha \left(\frac{cw_t}{2} \right) \sec(\varphi_x) \tag{II.6}$$

Where,

c_r = clutter reflectivity coefficient.

A = the angle difference between two consecutive clutter patches;

ϕ_x = the clutter azimuth angle position.

W_t = duration of ON period in one PRI.

Hence, the clutter-to-noise ratio (CNR) for each clutter patch can be expressed as:

$$\frac{C}{N} = \frac{P_{tr} G A_{eff} (ccs)}{(4\pi)^2 R^4 L N_r} \tag{II.7}$$

Where,

P_{tr} = Transmitted power of the antenna array

G = Antenna gain $= \frac{4\pi A_{eff}}{\lambda^2}$

L = Receiver noise figure

N_r = Receiver noise spectral density

The clutter covariance matrix is given by,

$$\boldsymbol{R}_c = \sigma^2 \sum_{x=1}^{N_c} \left(\frac{C}{N} \right)_x [\boldsymbol{b}_c(\varpi_x)\boldsymbol{b}_c^H(\varpi_x)] \otimes [\boldsymbol{a}_c(\vartheta_x)\boldsymbol{a}_c{}^H(\vartheta_x)] \tag{II.8}$$

Where

$\otimes$ denotes the Kronecker product

σ^2 = noise power

N_c =the number of clutter patches

$\boldsymbol{a}_c$ is the spatial steering vector and can be written as:

$$\boldsymbol{a}_c = [\exp(0) \quad \exp(j2\pi\vartheta_x) \ldots \exp(j2\pi N\vartheta_x - j2\pi\vartheta_x)]^T \tag{II.9}$$

with spatial frequency as,

$$\vartheta_x = \frac{d\cos(\theta_c)\sin(\varphi_x)}{\lambda} \tag{II.10}$$

ϑ_x is the spatial frequency, $\boldsymbol{b}_c$ is the temporal steering vector and can be given by

$$\boldsymbol{b}_c = [\exp(0) \quad \exp(j2\pi\varpi_x) \ldots \exp(j2\pi M\varpi_x - j2\pi\varpi_x)]^T \tag{II.11}$$

ϖ_x is the normalized Doppler frequency and defined as:

$$\varpi_x = \frac{f_{dx}}{f_r} \tag{II.12}$$

where f_{dx} is the Doppler frequency at each clutter patch x and f_r is the radar PRF.

The clutter covariance matrix (CCM) can also be expressed in a more simplified manner:

$$\boldsymbol{R}_c = \boldsymbol{\Omega}_c \mathrm{P} \boldsymbol{\Omega}_c^H \tag{II.13}$$

Where

$$\boldsymbol{\Omega}_c = [\boldsymbol{b}_c(\varpi_1) \otimes \boldsymbol{a}_c(\vartheta_1) \quad \ldots \boldsymbol{b}_c(\varpi_x) \otimes \boldsymbol{a}_c(\vartheta_x) \ldots \boldsymbol{b}_c(\varpi_{N_c}) \otimes \boldsymbol{a}_c(\vartheta_{N_c})] \tag{II.14}$$

with $\boldsymbol{b}_c(\varpi_x) \otimes \boldsymbol{a}_c(\vartheta_x)$ has the size of $M \times N$.

And P is diagonal matrix that can given by,

$$\mathrm{P} = \sigma^2 \begin{bmatrix} (C)_1 & 0 & 0 \\ \vdots & \ddots & \vdots \\ 0 & 0 & (C)_{x=N_c} \end{bmatrix} \tag{II.15}$$

Where C is clutter power at each clutter patch x

II.3 Noise Model

The thermal noise is always present in a receiver. Antenna elements in their corresponding receiver inherit this white noise without any correlation to other sensors. The noise could increase from the temperature rise of each element or from the outside environment source that affects the receiver system. The spectral power density of thermal noise is almost uniform in the frequency domain. The noise covariance matrix can be represented as,

$$\boldsymbol{R}_n = E[\boldsymbol{S}_n \boldsymbol{S}_n^H] = \sigma^2 \boldsymbol{I}_M \otimes \boldsymbol{I}_N \tag{II.16}$$

$\boldsymbol{I}_M$ and $\boldsymbol{I}_N$ are identity matrices with dimension $M \times M$ and $N \times N$, respectively.

II.4 Target Signal Model

Target signal is the key point of radar detection approaches. It is the desired signal that can be described by elevation, azimuth angle, Doppler frequency, and cross section area in ST domain [5]. However, in the angle-Doppler domain the target spreads and forms a pointed shape. The target radial velocity and position does not change very much due to the limited data availability and antenna dimension [92].

With the same concept and formula applied on deriving clutter model, the spatial vector for point targets can be obtained as:

$$\boldsymbol{a}_{tg}(\vartheta_{tg}) = [\exp(0) \quad \exp(j2\pi\vartheta_{tg}) \ldots \exp(j2\pi M\vartheta_{tg} - j2\pi\vartheta_{tg})]^T \tag{II.17}$$

Where,

$$\vartheta_{tg} = \frac{d\cos(\theta_{tg})\sin(\varphi_{tg})}{\lambda} \tag{II.18}$$

and the temporal vector is written as:

$$\boldsymbol{b}_{tg}(\varpi_{tg}) = [\exp(0) \quad \exp(j2\pi\varpi_{tg}) \cdots \exp(j2\pi M\varpi_{tg} - j2\pi\varpi_{tg})]^T \tag{II.19}$$

Where normalized Doppler frequency of target is:

$$\varpi_{tg} = \frac{f_{tg_d}}{f_r} \tag{II.20}$$

Here from the target Doppler frequency f_{tg_d}, its radial velocity can be determined as:

$$v_{tg} = 0.5 f_{tg_d} \lambda \tag{II.21}$$

Hence, the covariance matrix for point targets can be obtained as:

$$\boldsymbol{R}_t = \sigma^2 \chi_t [\boldsymbol{v}_t \boldsymbol{v}_t^H] \tag{II.22}$$

where,

$$\boldsymbol{v}_t = \boldsymbol{b}_{tg}(\varpi_{tg}) \otimes \boldsymbol{a}_{tg}(\vartheta_{tg}) \tag{II.23}$$

and χ_t is the SNR.

II.5 Echo Transformation via Minimum Variance Method

The received space-time radar echo data needs to be transformed into angle-Doppler domain for target and clutter recognition using minimum variance (MV) method. For the MV method, the transfer function of the filter at specific spatial and Doppler frequency can be expressed as [92],

$$F(\vartheta, \varpi) = \sum_{p=0}^{M-1} \sum_{q=0}^{N-1} f(p,q) \exp(-j2\pi(p\varpi + q\vartheta)) \tag{II.24}$$

where $f(p,q)$ is the bandpass filter and assume $\boldsymbol{f}$ is the vector of the narrow bandpass filter coefficients in the space and time domain:

$$\boldsymbol{f} = [f(0,0), \ldots f(0,N-1), \ldots f(p,q), \ldots f(M-1,N-1)]^T \tag{II.25}$$

The band-pass filter is optimized with the following constraint:

$$\boldsymbol{f}^H \boldsymbol{v}(\vartheta, \varpi) = \boldsymbol{v}(\vartheta, \varpi) \boldsymbol{f}^H = 1 \tag{II.26}$$

where $\boldsymbol{v}(\vartheta, \varpi) = [1 \ldots \quad \exp(j2\pi[(p-1)\varpi + (q-1)\vartheta]) \ldots \exp(j2\pi[(M-1)\varpi + (N-1)\vartheta])]^T$

Now, the output power can be given by:

$$E\left\{\left|y_{cap}\right|^2\right\} = \boldsymbol{f}^H \boldsymbol{R} \boldsymbol{f} \tag{II.27}$$

Using Lagrange multiplier, the coefficients of the filter $\boldsymbol{f}$ can be obtained. As a result, the solution of the filter under the constraint of (II.26) is given by:

$$\boldsymbol{f} = \frac{\boldsymbol{R}^{-1}\boldsymbol{v}\left(\vartheta,\varpi\right)}{\boldsymbol{v}^{H}\left(\vartheta,\varpi\right)\boldsymbol{R}^{-1}\boldsymbol{v}\left(\vartheta,\varpi\right)} \tag{II.28}$$

Then the minimum variance of the output power y_{cap} is given by [93],[94],

$$\min_{\boldsymbol{f}} E\left\{\left|y_{cap}\right|^{2}\right\} = \frac{1}{\boldsymbol{v}^{H}\left(\vartheta,\varpi\right)\boldsymbol{R}^{-1}\boldsymbol{v}\left(\vartheta,\varpi\right)} \tag{II.29}$$

The Capon estimator in (II.29) yields a radar image of target scene in the angle-Doppler domain with noise, clutter, and possibly targets. Prior to radar target detection, a denoising processing is performed to mitigate the thermal noise from the radar image. The image pixel intensities smaller than a certain denoising threshold are assigned to zeros. The denoising threshold T_N is chosen to be,

$$T_N = \kappa\sigma_w \tag{II.30}$$

where κ is a constant that normally varies between 2 and 3 and σ_w is the standard deviation of the thermal noise after the MV transform [91]. The standard deviation σ_w can be estimated using some radar image pixels with the amplitudes in the bottom 10% of all image pixels that are likely the white noises. After the denoising processing, the radar image contains target and clutter components only.

III. CLUTTER-PROXIMITY FEATURE-BASED GROUND MOVING TARGET DETECTION

This chapter has been adapted from a previous work by the authors titled “Robust ground moving target detection for airborne radar using a novel feature-based machine learning approach”,©2022 Elsevier. Devising new clutter feature is very important in the field of radar target detection. Especially, conventional methods need to apply complex

filtering procedure to estimate the clutter. Since, the clutter is mostly inhomogeneous by nature, adaptive filters could not suppress them efficiently. Moreover, if filters works properly to remove clutters, some of their residues still be present in the target detection system. For these aforementioned disadvantages, an innovative feature is described in this section to detect the clutter and target pixel with respect to the clutter ridge. The attribute is termed as clutter proximity feature.

The first section of this chapter discusses the theory of the proposed proximity feature. The next section defines some terms to elaborate the algorithm. Section III.3 develops the algorithm of the proposed approach. The subsequent section describes statistical method used to obtain the confidence with the training data. III.5 proves the classifier to determine the detection threshold. III.7 and 8 demonstrate the simulation results and performance comparison. The last section summarizes the entire method.

III.1 Theory of Proximity Feature

The new target detection approach is to classify the angle-Doppler space into the target, clutter subspace based on a pixel's proximity to the center of the expected clutter ridges. The clutter proximity of a pixel can be measured by the pixel's distance to the ridge line of clutter mass in the angle-Doppler plane. Without loss of generality, we consider a case of radar moving at a fixed velocity. The clutter ridge is a line segment and can be redefined as,

$$\varpi_x = \frac{f_{dx}}{f_r} = \left(\frac{2v_a}{df_r}\right)\vartheta_x = \beta\vartheta_x \qquad \text{(III.1)}$$

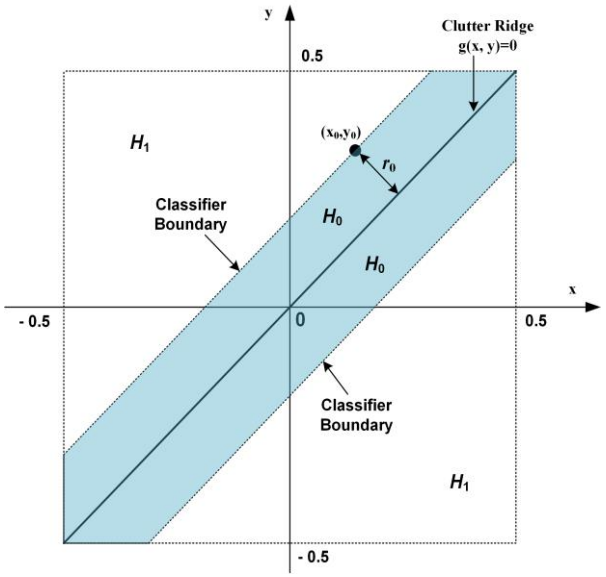

Figure III. 1 Target detection in angle-Doppler domain based on the proximity of a pixel to the clutter ridge center

where v_a is the velocity of the radar platform, f_{dx} is the Doppler frequency at clutter patch x, f_r is the radar pulse repetition frequency (PRF), d is the interelement distance of the antenna array, and β is the clutter ridge slope. Depending on the radar platform's velocity and radar PRF, we will consider the cases of both unambiguous and ambiguous Doppler clutters in formulating the new target detection approach simulations.

Case 1: Let us consider the clutter ridge center equation in the angle-Doppler plane for unambiguous Doppler clutter case. It can be represented as,

$$y - \beta x = 0 \tag{III.2}$$

where, x and y denote the normalized spatial (horizontal coordinate) and Doppler frequencies (vertical coordinate), respectively, as shown in Fig. III.1. The general equation of the central clutter ridge line is given by,

$$g(x, y) = \mathbf{w}^T \mathbf{z} = 0 \tag{III.3}$$

where, $\boldsymbol{w} = [w_2, w_1, w_0]^T$ is the weight vector with the weights corresponding to Doppler, spatial and intercept of clutter ridge respectively and $\boldsymbol{z}$ is the vector containing the normalized Doppler and spatial frequencies of a clutter patch and given by,

$$\boldsymbol{z} = \begin{bmatrix} y & x & 1 \end{bmatrix}^T \tag{III.4}$$

In Fig. III.1, if a pixel appears inside the lightly blue-colored region or located in the central clutter ridge line, i.e., its distance to the clutter ridge is less than the pre-defined detection threshold distance r_0, it is considered to be clutter; otherwise, the pixel is considered to be a target signal. r_0 is decided by the maximum clutter extension for a particular application or estimated from training data. The distance of any pixel (x, y) in Fig. III.1 to the clutter ridge can be calculated from the following equation:

$$r = \frac{g(x, y)}{\|\rho\|} \tag{III.5}$$

where $\|\rho\| = \sqrt{w_1^2 + w_2^2}$

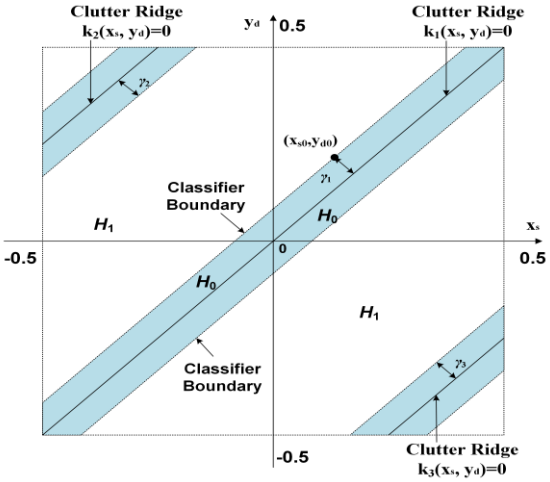

Figure III. 2 Target-clutter scenario in angle-Doppler domain based on the nearest distance of a pixel to any of the clutter ridge center (M = 3)

The *r* from (III.5) for each non-zero pixel is compared with the proximity threshold r_0 to classify target and clutter.

Case 2: This is the scenario of Doppler ambiguous clutter. Usually, clutter spectrum changes or aliases in the normal clutter subspace depending on the platform velocity or pulse repetition frequency. Since the Doppler frequency of clutter depends on the radar pulse repetition interval, interelement spacing, and platform speed, the aliasing often occurs when ϖ_x in (III.1) surpasses certain value. It implies that, if β is greater than 1, then clutter becomes Doppler ambiguous i.e. the clutter Doppler spectrum will alias with the visible Doppler subspace. Hence, the probability of getting same Doppler echo both for clutter and target becomes higher than the previous case. The more the platform speed or the low PRI, the ambiguity becomes higher. Besides, it is also possible for target to be totally overlapped with clutter without even showing a shape change in the clutter subspace. Now, with a high radar platform velocity and/or relatively low radar PRF, assume that the clutter ridge consists of *M* segments in the angle-Doppler plane due to the Doppler ambiguity as shown in Fig. III.2. The multiple clutter ridge equations are rewritten as,

$$\begin{aligned} &g_m(x,y) = w_{m1}x + w_{m2}y + w_{m0} = 0 \\ &m = 1,2,...M \end{aligned} \tag{III.6}$$

where w_{m1}, w_{m2}, and w_{m0} are the ridge equation weights of the *m*-th segment of the clutter.

Consequently, the distances between a pixel at *(x, y)* and the *m*-th clutter ridge segment center is given by:

$$r_m = \frac{g_m(x,y)}{\|\rho_m\|} \qquad m = 1,2,...,M \tag{III.7}$$

where

$$\|\rho_m\| = \sqrt{{w_{m1}}^2 + {w_{m2}}^2}, m = 1,2,...,M \tag{III.8}$$

The minimum distance from a non-zero pixel at *(x, y)* to all possible clutter ridge segments is determined as:

$$r_{\min} = \min(r_1, r_2 ..., r_M) \tag{III.9}$$

To determine if the pixel at *(x, y)* belongs to the clutter or the target space, we simply compare it with predefined threshold r_0 with the following rule:

$$\begin{aligned} r_{\min} \geq r_0 &\Rightarrow H_1\text{: pixel at } (x, y) \text{ as a target} \\ r_{\min} < r_0 &\Rightarrow H_0\text{: pixel at } (x, y) \text{ as clutter} \end{aligned} \tag{III.10}$$

If a pixel appears inside the region satisfying $r_{min} < r_0$, it is considered as a clutter pixel; otherwise, the pixel is considered to be in the target region. Naturally, these target and clutter segments are separated in the Doppler-angle domain due to their different Doppler frequencies. However, low-speed targets could overlap with clutters under some scenarios. But the targets still can be detectable if more than one feature are used for classification or some radar parameters such as radar PRF are slightly adjusted during radar operation.

III.2 Terminologies for the Algorithm

To further describe the procedure of implementing the new target detection method, we need to define the following concepts and terminologies related to the non-zero pixels on the angle-Doppler plane.

Definition 1: The Connected pixels is defined as a set of non-zero pixels in which for any two pixels p and q there exists a minimum distance connected path connecting p and q. A minimum distance connected path is defined as an ordered sequence of non-zero pixels such that the distances of any two adjacent pixels in the sequence are equal to or less than a predefined value C (normally $C \leq 2$).

With Definition 1, we propose the following Lemma for forming a pixel block that is connected.

Lemma 1: If there is a pixel block $\boldsymbol{A}$ consisting of non-zero pixels that are connected based on the minimum distance property with a pixel $q \in \boldsymbol{A}$ and a non-zero pixel $x \notin \boldsymbol{A}$ and their distance satisfying $\|x-q\| \leq C$, then x can be merged into Block $\boldsymbol{A}$ to form a new block $\boldsymbol{A}' = \{\boldsymbol{A} \cup x\}$ that is connected.

Proof: Since $\boldsymbol{A}$ is connected and q is a pixel inside $\boldsymbol{A}$, any other pixel p inside $\boldsymbol{A}$ is connected to q through a minimum distance path $\{p, p_1, p_2, \ldots, q\}$. Because the distance between q and x is less than the minimum distance C, the pixel x is connected to any pixel p in $\boldsymbol{A}$ through the path of $\{p, p_1, p_2, \ldots, q, x\}$. Therefore, x can be merged into $\boldsymbol{A}$ to form a connected block $\boldsymbol{A}'$.

Based on Lemma 1, we can start with a connected block with a single non-zero pixel and expand it by merging it with nearby non-zero pixels until no more nonzero pixels available for merge. Then, another non-zero pixel that does not belong to any connected blocks is selected to form a new connected block until all non-zero pixels belong to a unique connected block. Finally, the denoised radar angle-Doppler image consists of connected blocks only. To further characterize the connected pixel blocks, we introduce the following three definitions.

Definition 2: Clutter Block is a set of non-zero connected pixels that are all classified as clutters.

Definition 3: Target Block is a set of non-zero connected pixels in which at least one of them is classified as target.

Definition 4: Block Size is the maximum distance between any two pixels inside a block.

III.3 Algorithm Steps

With the aforementioned definitions, the step-by-step procedure of target detection using this new approach is listed the steps as follows:

Step 1: Perform radar data transformation from the space-time domain to the angle-Doppler domain using the minimum variance (MV) method. The transformed data is considered as a 2-D image as the pixel indices.

Step 2: Apply a hard threshold to the amplitudes of all the transformed radar image pixels to significantly mitigate thermal noise level. As a result, if any pixel with its amplitude less than the threshold T_N in (II.30) its value is set to be zero; otherwise, the pixel value remains the same.

Step 3: Calculate the distance $r_{m,n}$ from a non-zero pixel (x_m, y_n) with the image indices of m and n to the clutter ridge center or the nearest clutter ridge center if there are multiple clutter ridge segments based on (III.5), or (III.9), respectively. If the distance is less than pre-defined clutter proximity threshold distance r_0, the pixel is classified as a clutter pixel; otherwise, it is considered as a target signal.

Step 4: Repeat Step 3 until all the non-zero pixels in the image are examined and labeled.

Step 5: Declare that a target is detected if there is at least one target pixel. Otherwise, no target is detected.

The critical parameter in the procedure is the clutter proximity distance threshold r_0 used to detect the target pixels. It is directly related to maximum clutter spread across the clutter ridge center and thus it can be determined from the estimation of clutter distribution in the angle-Doppler plane or can be trained based on actual radar data.

Typically, the detection threshold is estimated from the training data, which are normally obtained from the operational radar. However, generating real radar data is very expensive and most of real radar data are classified, and synthesized data (or simulated data) are widely used for verifying the effectiveness of the machine-learning algorithms [95–97]. In this work, we choose the detection threshold based on the typical radar parameters and simulated radar data. However, the new detection approach is applicable for actual radar with real radar data.

III.4 Bootstrapping Procedure

Our goal is to estimate the proximity threshold by approximating the average value of measured distances from clutter ridge using bootstrapping. Bootstrapping is an excellent method to deal with threshold estimation and prediction with small to large samples sizes of data [98−100]. Other method such as, Bayesian technique involves complex manipulation of matrices and incurs expensive computational costs. Whereas bootstrapping considers the estimation with a simple approach that does not require to handle singularity problems [99]. To estimate the clutter proximity distance threshold, we applied bootstrapping on the training data. Assume, each bootstrap sample contains *n* data points that are resampled from the actual training data with replacement. Then the concept of bootstrap can be described as follows:

1. Let $x_1, x_2, \ldots x_n$ be the training data samples from an unknown distribution *F*.

2. $\bar{x}$ is the mean of the training data

3. $x_1^*, x_2^*, \ldots x_n^*$ are the resampled data generated from *F**, where *F** is the empirical distribution function of $x_1, x_2, \ldots x_n$, which gives equal weight to each data point.

4. Compute bootstrap mean using $x_1^*, x_2^*, \ldots x_n^*$

5. Repeat *B* times the step 4 to get $\bar{x}_1^*, \bar{x}_2^*, \ldots \bar{x}_B^*$

Here, we calculated the maximum and minimum distances from any pixel inside the clutter block, and target block to the nearest clutter ridge for the samples. For simplicity, we will consider the approach on the training data of a single block. The training data based on proximity distance can be given by:

$$\boldsymbol{x} = [x_1, x_2, \ldots x_n] \tag{III.11}$$

and $\bar{x} = \frac{1}{n}\sum_{j=1}^{n} x_j$

Now, the generated resampled data can be expressed as,

$$\boldsymbol{x}^* = [x_1^*, x_2^*, \ldots x_n^*] \tag{III.12}$$

Let us assume that there are *B* bootstrapped samples repeatedly computed from this resampled data. The sample vector can then be written as:

$$\bar{\boldsymbol{x}}^* = [\bar{x}_1^*, \bar{x}_2^*, \ldots \bar{x}_B^*] \tag{III.13}$$

Afterwards, the lower and upper bound of the confidence interval (CI) are calculated from the bootstrapped samples.

To find the confidence interval, one has to sort them (sorted in ascending order):

$$\bar{\boldsymbol{x}}^*_{sorted} = sort(\bar{\boldsymbol{x}}^*) \tag{III.14}$$

where $sort(\bullet) = \{t_1 < t_2 < t_3 \ldots < t_B\}$

Following [100], the 95% percentile bootstrap confidence interval (CI) for mean is obtained below:

$$CI = \begin{cases} \bar{x}^*_{sorted}(\lceil 0.025B \rceil): \ Lower\ Bound \\ \bar{x}^*_{sorted}(\lceil 0.975B \rceil): \ Upper\ Bound \end{cases} \tag{III.15}$$

where $\lceil \cdot \rceil$ denotes the ceiling function, $\bar{x}^*_{sorted}(\lceil 0.025B \rceil)$ and $\bar{x}^*_{sorted}(\lceil 0.975B \rceil)$ are the 2.5th and 97.5th percentile points of F^* distribution, respectively.

III.5 Classifier for the Proximity Distance Threshold

The r_0 can be selected based on the upper bound of clutter block CI and lower bound of target block CI. To further describe the procedure, we propose the following Lemma for a unique classifier.

Lemma 2: the optimum predefined threshold distance r_0 in the angle-Doppler domain can be approximated as the value found from *a:b* ratio of the upper bound (UB) and lower bound (LB) CI of clutter block (CB) and target block (TB) data, respectively.

Proof: Since the data for both clutter and target do not overlap, r_0 can be chosen in the range between the UB of clutter block confidence interval (CI_{CB}) and LB of target block confidence interval (CI_{TB}) ($i.e.\ CI_{CB}(UB) < r_0 < CI_{TB}(LB)$), respectively. However, if it is chosen at the edge values of the range, the detection performance might degrade and cause undesired false alarms. Hence, a suitable value needs to be chosen to evade the edge values. Now, based on the mean and standard deviation (σ_{CB}) of the clutter training data, one can choose the value given by:

$$r_0 \approx \frac{bCI_{CB}(UB) + aCI_{TB}(LB)}{a+b} \tag{III.16}$$

where, $a = mean(CB) + 4\sigma_{CB}$, *and* $b = mean(TB)$; here the $4\sigma_{CB}$ is chosen as the guard distance to separate target and clutter pixels robustly.

The guard distance parameter needs to be chosen very carefully. According to the central limit theorem, the large bootstrapping samples for target and clutter block can be approximated by the normal distribution. Thus, about 99.99% of the data will fall within $4\sigma_{CB}$ from clutter block's mean. Since it is highly unlikely to get a clutter block data beyond that value, we chose the guard distance $4\sigma_{CB}$. It should be noted that, a value greater than $4\sigma_{CB}$ tends to misinterpret the target signal as clutter.

Basically, learning of the proximity threshold distance is a machine learning approach i.e., the radar learns the threshold from the upper and lower bound of confidence interval (CI) of bootstrapped sample data in (III.16) with the aid of mean and standard deviation of the training data. The more training data considering different scenarios of ground clutter environment, the r_0 in (III.16) gets more precise to detect the target. As for the training data for estimating feature distribution, the data do not need to be very accurate. In addition, the transfer-learning (the data generated by other radar systems or the same radar at different times or environments) could be utilized to determine r_0 if the sufficient amount of training data is not available.

III.6 Confidence Interval Steps and Complexity of the Algorithm

The procedure to estimate the upper and lower bounds of the confidence interval is as follows:

Step 1: Generate N sets of independent bootstrapping samples with replacement for maximum and minimum distances for any pixel inside each block. The size of each set is

equal to the number of samples collected from the training data. The randomness of replacement in each set is done based on resampling distribution.

Step 2: Determine the mean of each bootstrapping set corresponding to each block.

Step 3: Determine the mean of the aggregated samples from training data of the same block.

Step 4: Perform sort operation for the bootstrapping sample vector for each block and compute the upper and lower bound of the confidence interval.

Since the confidence interval (CI) obtained using the training data provides the information about the maximum clutter spectrum spread with respect to the clutter ridge, the detection threshold r_0 can be generated by means of target and clutter block's average proximity distances and a suitable guard distance parameter ($4\sigma_{CB}$). Once the r_0 is determined using Lemma 2 and training data, the detection method is applicable to the unknown inhomogeneous clutters in which their statistical distributions change from range bins to range bins. It should also be noted that, the simulated data cannot be used to train the classifier/detector to remove the real radar clutter. However, one can fly the radar platform under both $\mathbf{H_1}$ (with moving targets) and $\mathbf{H_0}$ (clutters and noise only) hypotheses to get the detection feature distributions.

The complexity of the algorithm is proportional to the cost of signal domain transformation and distance evaluation for each non-zero pixel in the radar image. Therefore, the time complexity for this detection method is about $O(PQ)$ with $(P \times Q)$ being the radar image size.

III.7 Simulation Results

To validate the proposed target detection method, we applied it to the radar data simulated from a typical airborne radar system. The radar operates at a frequency of 450 MHz with a uniform linear array with 16 half-wavelength placed elements. Each element radiates in isotropic pattern. There are 16 pulses in one coherent processing interval and SNR and CNR are 0, 40 dB, respectively. The pulse repetition frequency (PRF) of the radar waveform is 300 Hz. Slightly different PRF is also applied to find overlapped target with clutter. Other relevant radar parameters for the simulation are listed in Table III.1.

Table III.1. Radar parameters used in the simulation

Radar Parameter	Value
Platform height	9000m
Platform velocity (minimum)	50m/s
Platform Velocity (maximum)	100m/s
Pulse Repetition Frequency (PRF)	300Hz
No. of pulses in CPI	16
No. of clutter patches	360
SNR per pulse	0dB
CNR per pulse	40dB

To simulate the radar data for target detection, we first consider the radar operation scenario where the radar platform velocity is 50 m/s. The moving target is located at 3° in azimuth at a ground range of 10km from the origin. The target Doppler frequency is set to be –32 Hz. We applied the MV method to the space-time data and generated the radar image data in the angle Doppler domain, displayed in Fig. III.3(a). Fig. III.3(b) shows the

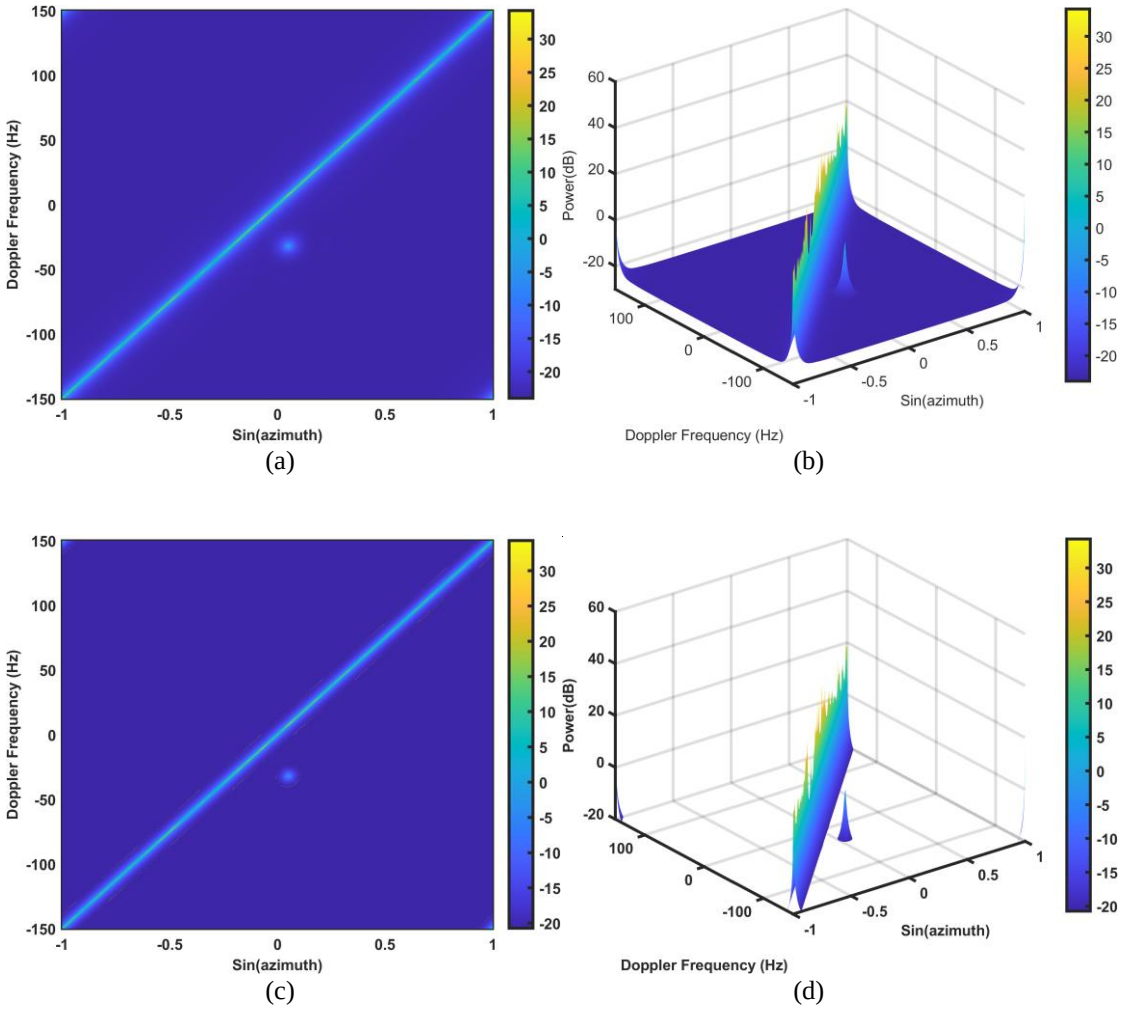

Figure III. 3 Target and clutter detection in angle-Doppler plane with a point target with −32 Hz in Doppler frequency and 3° in azimuth: (a) The transformed 2D-plot; (b) 3D-plot; (c) the denoised 2-D radar image; (d) the denoised 3-D radar image

3-D plot of the radar scene. We further subject it to the denoising processing by applying hard thresholding to all image pixels. Some noise residues could still exist after denoising processing, but they are easily recognizable and would not be considered as targets due to their isolated nature because their block sizes are equal to one. Fig. III.3(c) shows the denoised image after applying thresholding processing to the image in Fig. III.3(a). Fig. III.3(d) shows the denoised 3-D scene of Doppler unambiguous clutter.

The next step in the target detection is to evaluate the distance from all non-zero pixels of the denoised image to the central ridge line. If a pixel's distance to clutter ridge is greater than the pre-defined clutter proximity distance r_0 ,the pixel is considered to be

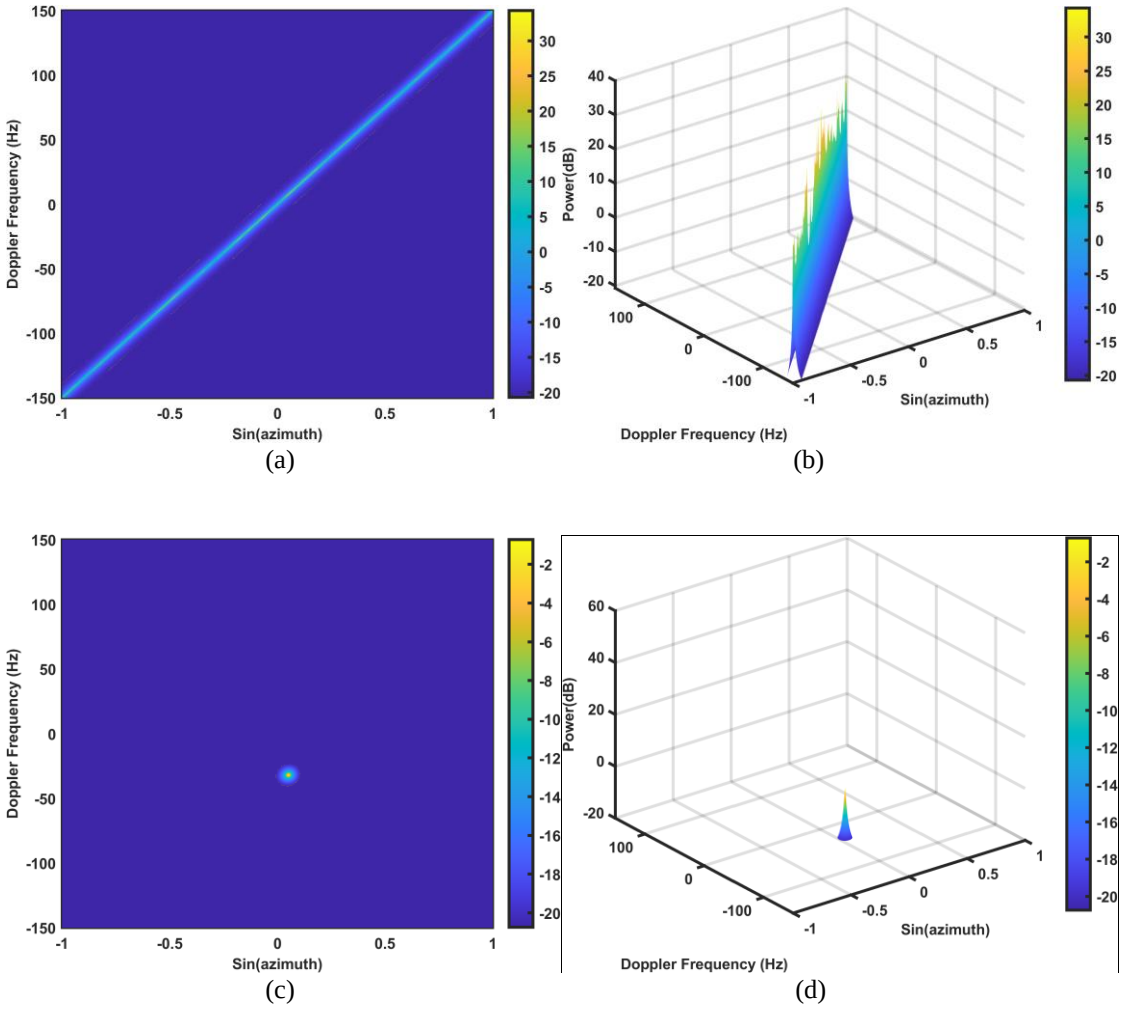

Figure III. 4 Detected target and clutter detection in angle-Doppler plane (a) identified clutter block 2D format; (b) 3D-plot clutter block; (c) detected target block in 2D format; (d) 3-D image of target block

Table III.2 Clutter proximity feature-based target detection results for doppler unambiguous case

	To the clutter ridge			Block Size	Target Detected?
Maximum distance from any pixel in the clutter block	8.35	Clutter Block		507.70	No
Minimum distance from any pixel in the Target Block	24.31	Target Block		17.49	Yes

outside the clutter and thus classified as the target signal; otherwise, the pixel is considered to be in clutter and classified as clutter. From the (III.1), the weights of the linear equation can be found based on a fitting of linear regression technique. Since, the relation of spatial frequency and Doppler is defined in (III.1), the coefficients of this equation can be approximated by either a polynomial fitting algorithm or linear regression. The w_2, w_1, w_0 values for unambiguous case 1 is found to be as 1,1.00 and 0, respectively. As for the detection in this case, the predefined clutter proximity threshold distance r_0 for target pixel classification should be about 16 based on Table III.4 and Lemma 2, which is equivalent to about 8.8 Hz in Doppler frequency or 5.9 m/s in radial speed. Figs. III.4(a) and (c) show the generated clutter, and target from the denoised image in Fig. III.3(c), respectively. Fig. III.3(b) and (d) displayed the 3-D plot of detected clutter and target block, respectively. Table III.2 lists the maximum distance calculated from all clutter pixels to the clutter ridge and the minimum distance from all target pixels to the clutter ridge, which shows reliable detection of slowly moving targets with the new method. The clutter datum in Table III.2 indicates about ±6Hz clutter Doppler extensions due to internal clutter motion (ICM) and limited data length in time domain. However, if the clutters are generated from vegetations as well as terrains, the clutter Doppler spread could be much larger and make the detection of slowly moving target more challenging. We also examined the scenarios where two moving targets exist in the same range bin.

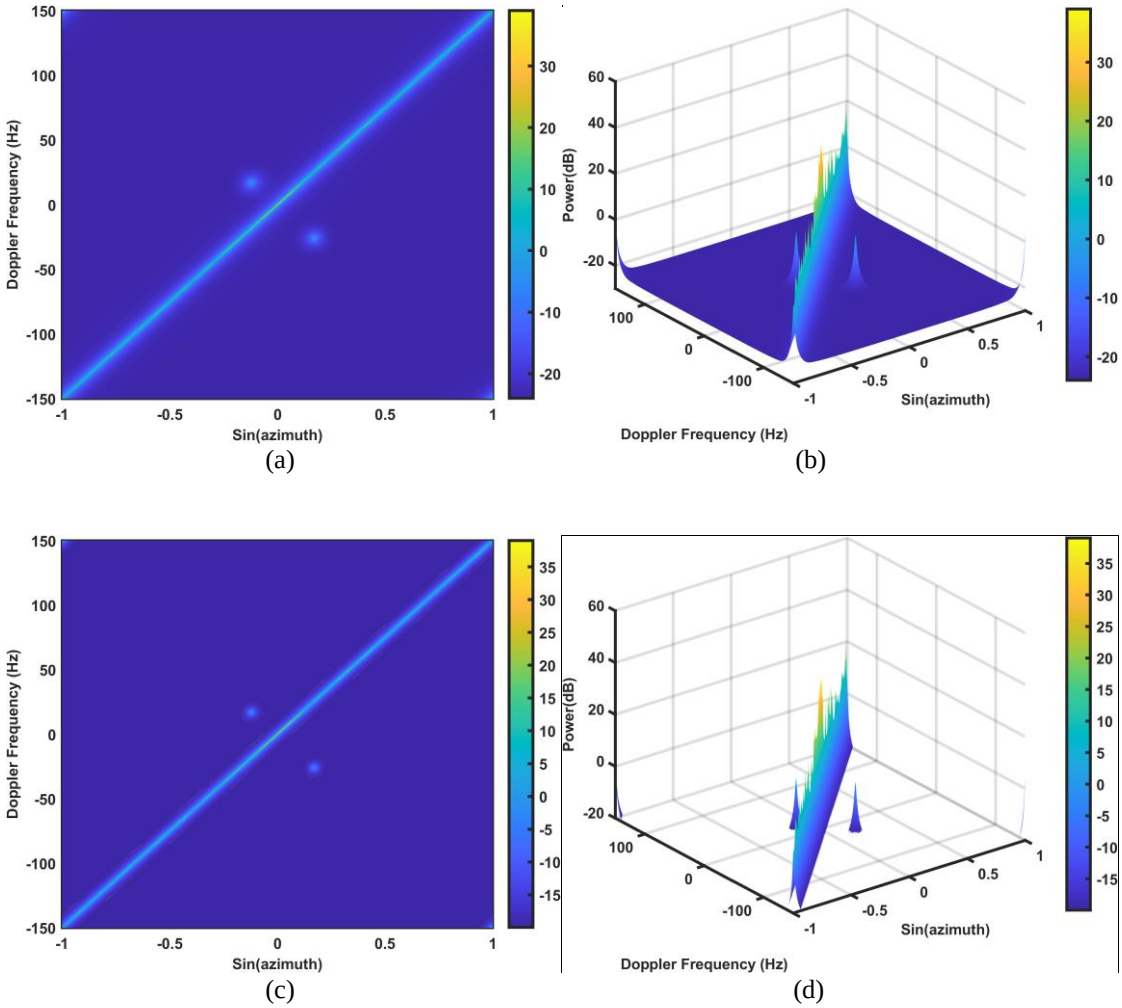

Figure III. 5 Target and clutter scenario in angle-Doppler domain with two moving point targets at 17 Hz in Doppler frequency and –7° in azimuth and –26Hz in 10° in azimuth, respectively: (a) The transformed 2D-plot; (b) transformed 3D-plot; (c) the denoised 2D radar image; (d) the denoised 2D radar image (a) the identified clutter block; (d) the detected target block 1 and (e) the detected target block 2

One target is set at 17 Hz with –7° in azimuth and the other one is at –26 Hz with 10° in azimuth. The same procedure is repeated in the denoised radar image of Fig. III.5(c), and both targets have been extracted using the proximity feature approach. Fig. III.6 show the detected clutter and target blocks in 2D and 3D formats, respectively. The maximum distance from any pixel in the clutter block to the clutter ridge is found to be 9.06. Whereas the minimum distance from any pixel in the target block 1 and target block 2 to

the clutter ridge are 20.21 and 34.94, respectively. Hence, the proposed method performs

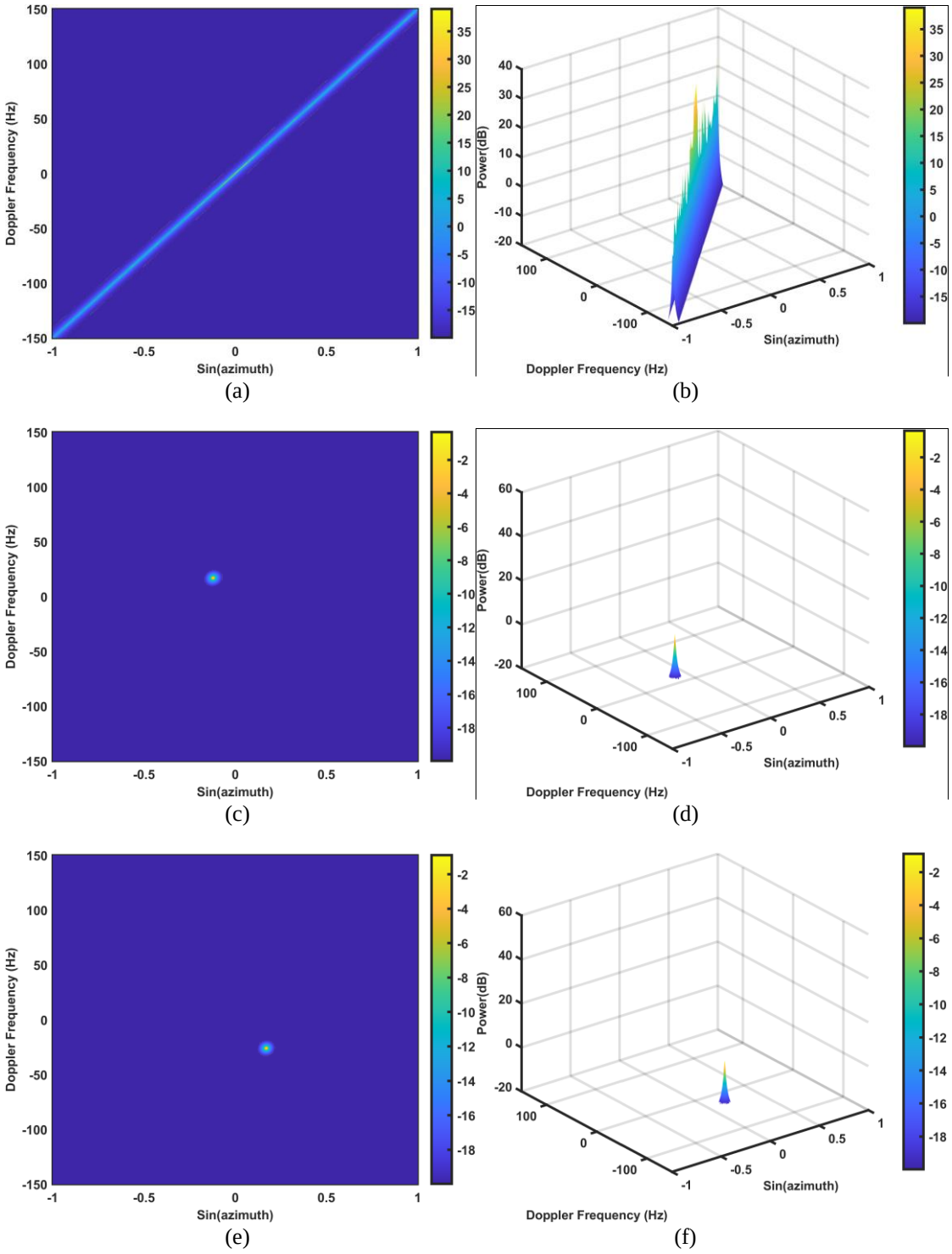

Figure III. 6 Detected target and clutter blocks in angle-Doppler domain with two moving point targets: (a) the identified clutter block (2D) (b) the identified clutter block (3D) (c) the detected target block 1 (2D) (d) the detected target block 1 (3D); (e) the detected target block 2 (2D); and (f) the detected target block 2 (3D)

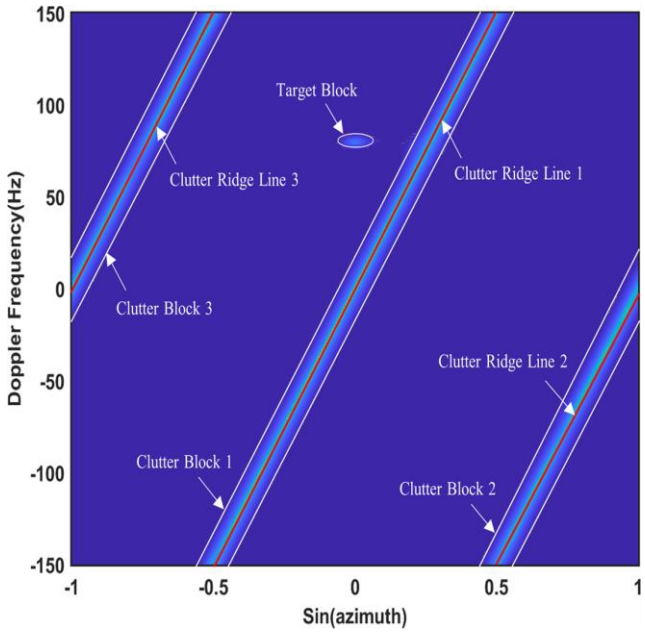

Figure III. 7 Typical multiple clutter ridges for a Doppler ambiguous scenario

well in detecting more than one moving target in the same range bin.

For the Doppler ambiguous case, the platform velocity is increased to 100 m/s. A single target is located at –5° in azimuth and the target Doppler frequency is set at 50 Hz. Fig. III.7 highlights the target and clutter blocks with their corresponding clutter ridges. Fig. III.8(a) and (b) show the MV transformed radar image with a target, clutter (with the slope of the ridge equal to 2), and random white noise. Fig. III.8(c) and (d) show the denoised radar images for 2D and 3D formats, respectively, in the angle-Doppler domain. The same procedure is applied to all non-zero pixels in the image in Fig. III.8 (c) until all pixels are classified. Fig. III.9(a) to (d) show the detected clutter blocks 1 and 2 in 2D and 3D formats, respectively. Fig. III.10 shows the identified clutter block 3 and detected target in 2D and 3D formats. The maximum distances for pixels in a clutter block to the nearest clutter ridge are listed in Table III.3. Since the maximum distance is less than the

threshold distance (which is set to be about 13) for Doppler ambiguous case, the distances of all clutter pixels to the nearest clutter ridge are less than r_0 . Likewise, the distances of all target pixels to the nearest clutter ridge are larger than the threshold distance r_0 .

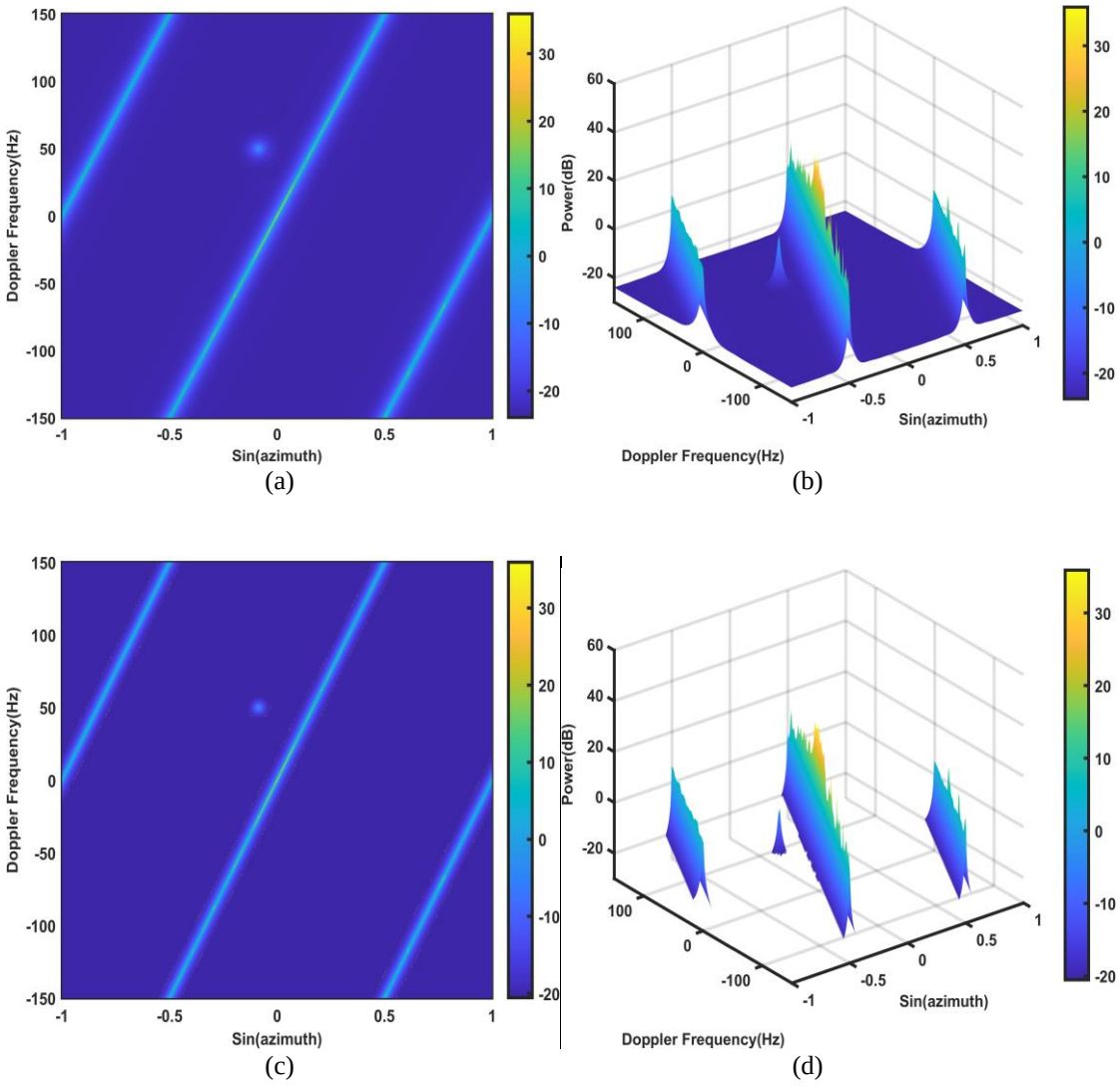

Figure III. 8 The transformed and denoised radar image in angle-Doppler plane with a point target located at 50 Hz in Doppler frequency with -5° in azimuth: (a) The transformed 2D-plot; (b) transformed 3D-plot; (c) the denoised 2D-plot and (d) denoised 3D-plot

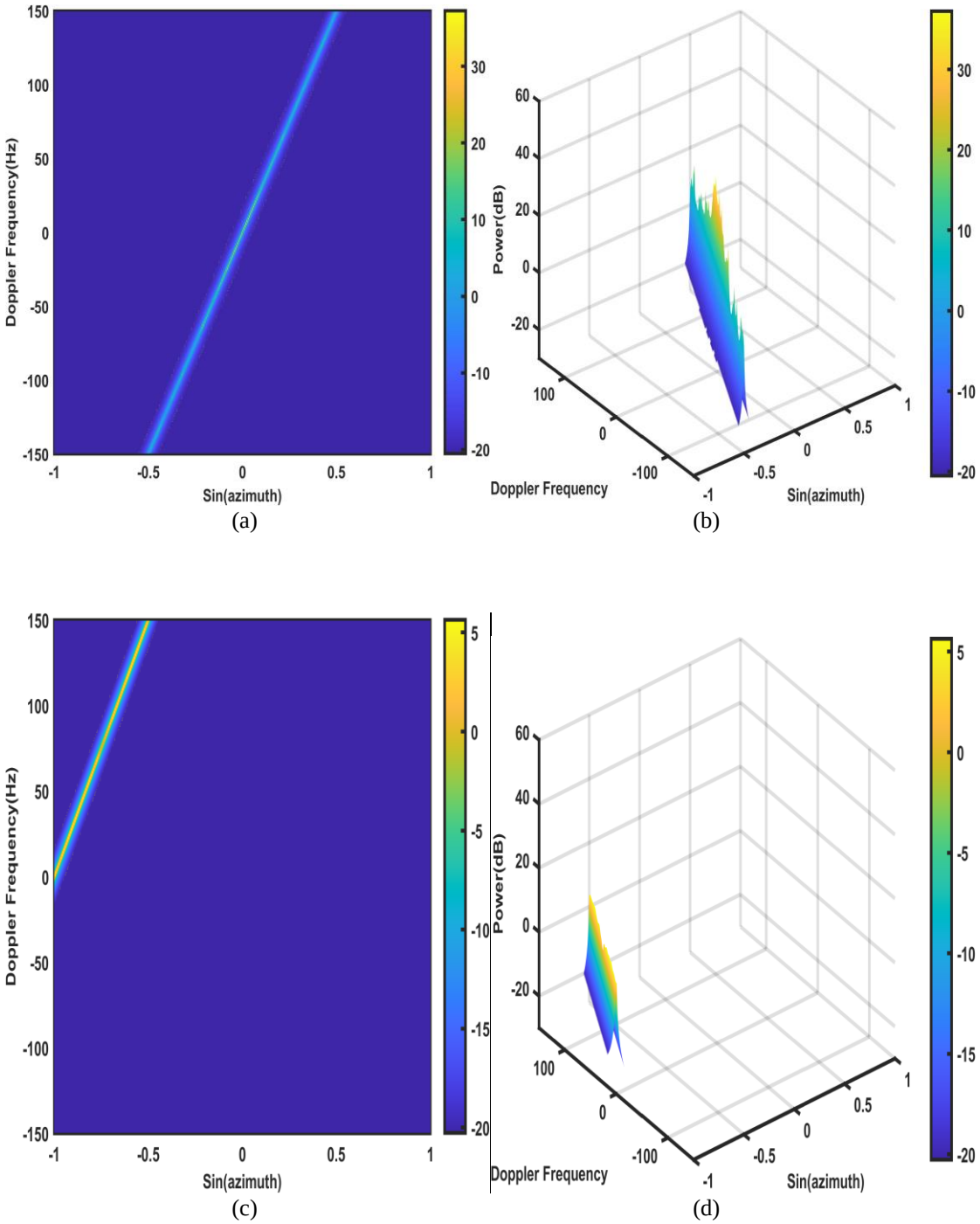

Figure III. 9 The pixels of the image in Fig. III.7 that are classified as clutter block 1 and 2 due to their proximity to clutter ridge: (a) 2D-plots and (b) 3D-plots

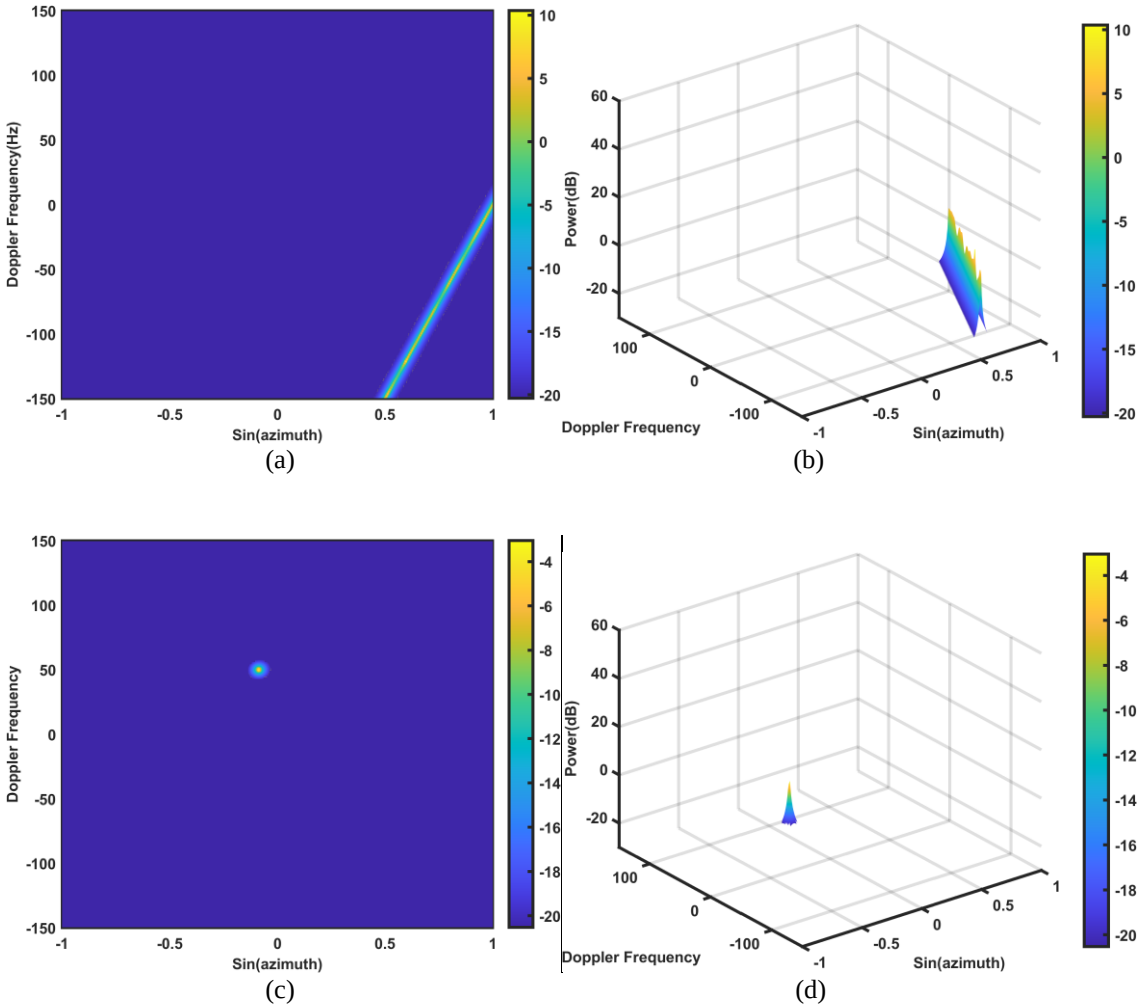

Figure III. 10 The pixels of the image in Fig. III.8 that are classified as clutter block 3 and target due to their proximity to clutter ridge: (a) 2D-plots and (b) 3D-plots

Table III. 3 Clutter proximity feature-based target detection results for doppler ambiguous case

	To the nearest clutter ridge		Block Size	Target Detected?
Maximum distance from any pixel in the Clutter Block 1	6.49	Clutter Block 1	266.18	No
Maximum distance from any pixel in the Clutter Block 2	7.08	Clutter Block 2	138.59	No
Maximum distance from any pixel in the Clutter Block 3	7.24	Clutter Block 3	138.59	No
Minimum distance from any pixel in the Target Block	23.99	Target Block	16.12	Yes

Table III.4 Confidence interval results for threshold estimation

	$\beta = 1$		$\beta = 2$	
	Lower Bound (LB)	Upper Bound (UB)	Lower Bound (LB)	Upper Bound (UB)
Clutter Block (with respect to clutter ridge)	9.43	9.54	7.73	7.78
Target Block (with respect to clutter ridge)	33.87	38.65	23.77	25.66

Table III.5 Confusion matrix chart for clutter/target detection

		Detected Signal	
		Clutter	Target
Actual Signal	Clutter	100%	0%
	Target	0.4%	99.6%

The aforementioned distance thresholds are estimated from the samples of the training dataset of the simulated radar images. The dataset contains samples collected from 2000 simulated radar images, where half of them consist of a target and clutter, and the other half consists of clutter only. It should also be noted that the dataset sample size should be large enough to cover all possible target and clutter parameter variations in estimating detection feature distribution. Since we currently use only one feature for target detection, a sample size of 2000 is a reasonable choice in estimating the feature distribution. These images are generated from the data obtained in the same detection range bin unlike the traditional adaptive methods such as STAP in which a large number of the secondary clutter data are needed for clutter estimation. Subsequently, the dataset is sampled with replacement, and the confidence interval (CI) is achieved via bootstrapping. The distance threshold r_0 is then determined based on the upper and lower bound of 95% confidence interval (CI) of the bootstrapped samples and Lemma 2. In this work, the data in Table III.4 of CI are utilized to set the proximity threshold for separating the clutter and target block. Finally, Table III.5 shows the confusion matrix for

the target and clutter block detection. The number of test samples is 500 for the results shown in Table III.5. Because the detection method is based on radar signal Doppler frequencies and angles, its performance is not affected by the clutter and target variations in amplitude. Furthermore, the detection results presented in Table III.5 are merely the outcomes of simulated test data and not the actual false alarm rate or detection probability. The proposed approach also checks the block size shown in Tables III.2 and III.3 to increase the robustness. Depending on trading off between detection probability and false alarm rate, it is possible that the detection could fail if r_0 is selected too large or too small. However, the proposed method would provide much more robust detection results by utilizing more features such as, block size that can distinguish target and clutters based on the shape feature. Therefore, the target and clutter pixels are classified correctly.

Calculation of distance threshold for DU case (β=1): From Table III.4 and (III.16), we can calculate the approximate threshold r_0 which is given by,

$$\begin{aligned} a &= mean(CB) + 4\sigma_{CB} \\ &= 9.48 + (4 \times 0.9556) = 13.3024 \end{aligned} \tag{III.17}$$

$$\begin{aligned} b &= mean(TB) \\ &= 36.0046 \end{aligned} \tag{III.18}$$

$$\begin{aligned} r_0 &\approx \frac{bCI_{CB}(UB) + aCI_{TB}(LB)}{a+b} \\ &= \frac{(36.0046 \times 9.54) + (13.3024 \times 33.87)}{36.0046 + 13.3024} \\ &= 16.10 \end{aligned} \tag{III.19}$$

Calculation of distance threshold for DA case (β=2):

From Table III.4 and (III.16), we can find the approximate threshold r_0 when platform velocity is increased to 100 m/s. The equations are as follows:

$$\begin{aligned} a &= mean(CB) + 4\sigma_{CB} \\ &= 7.7619 + (4 \times 0.7755) = 10.8639 \end{aligned} \tag{III.20}$$

$$\begin{aligned} b &= mean(TB) \\ &= 24.54 \end{aligned} \tag{III.21}$$

$$\begin{aligned} r_0 &\approx \frac{bCI_{CB}(UB) + aCI_{TB}(LB)}{a+b} \\ &= \frac{(24.54 \times 7.78) + (10.8639 \times 23.77)}{24.54 + 10.8639} \\ &= 12.6866 \end{aligned} \tag{III.22}$$

Results for other platform velocities:

The results are also checked for different platform velocity for Doppler ambiguous case. Since, the clutter ridge changes with the change of the platform velocity, the orientation of clutter is also changed. The analysis is given below:

a) Platform speed is at 150 m/s:

Since the platform velocity is increased, the clutter subspace in Fig. III.11 looks more occupied than the previous β=2. The target Doppler frequency is set at −55 Hz with -5° in azimuth. Fig. III.12(a) and (b) show the 2D and 3D plot of the denoised radar scene of the Fig. III.11(a). As can be seen from the figure, the mainlobe of the clutter is located to the 0° azimuth angle. Moreover, the clutter width and Doppler extension are increased for the increased platform velocity. The proximity detection threshold is also set at 13. Fig. III.13 provides the detected blocks of the clutter and target signals.

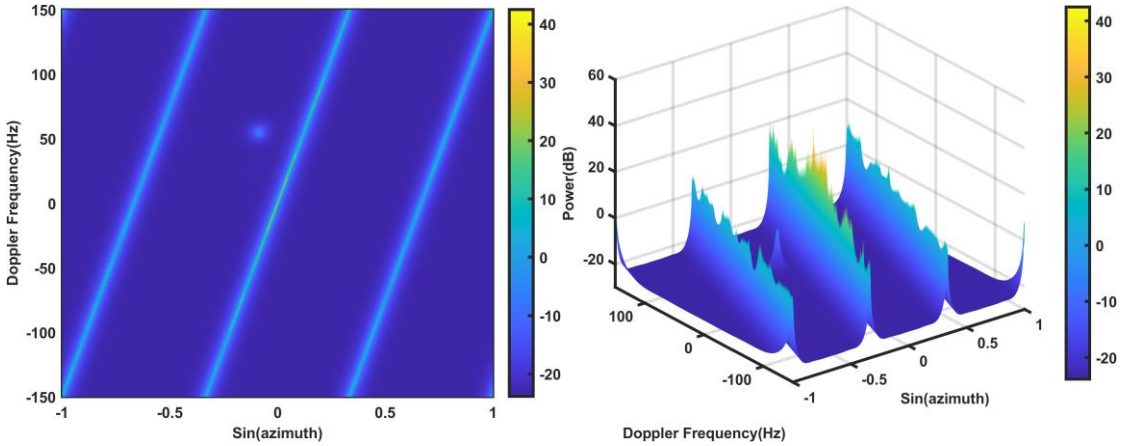

(a) (b)

Figure III. 11 The clutter scenario when the platform velocity is 150 m/s. (a) 2D-plot; (b) 3D-plot

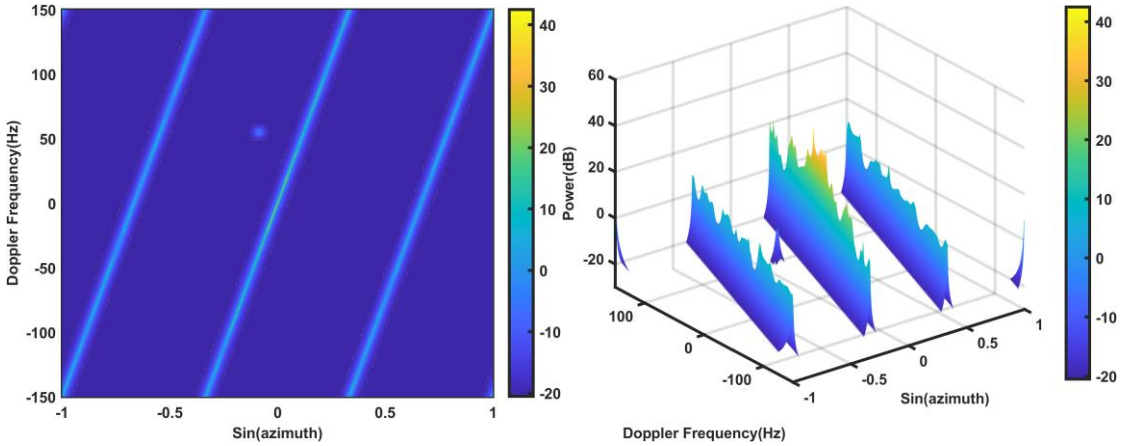

(a) (b)

Figure III. 12 The reduced thermal noise after denoising when the platform velocity is at 150 m/s. (a) 2D-plot; (b) 3D-plot

- The maximum distance from any pixel in the Clutter Block 1 to the nearest clutter ridge is 7.86
- The maximum distance from any pixel in the Clutter Block 2 to the nearest clutter ridge is 7.64
- The maximum distance from any pixel in the Clutter Block 2 to the nearest clutter ridge is 7.73

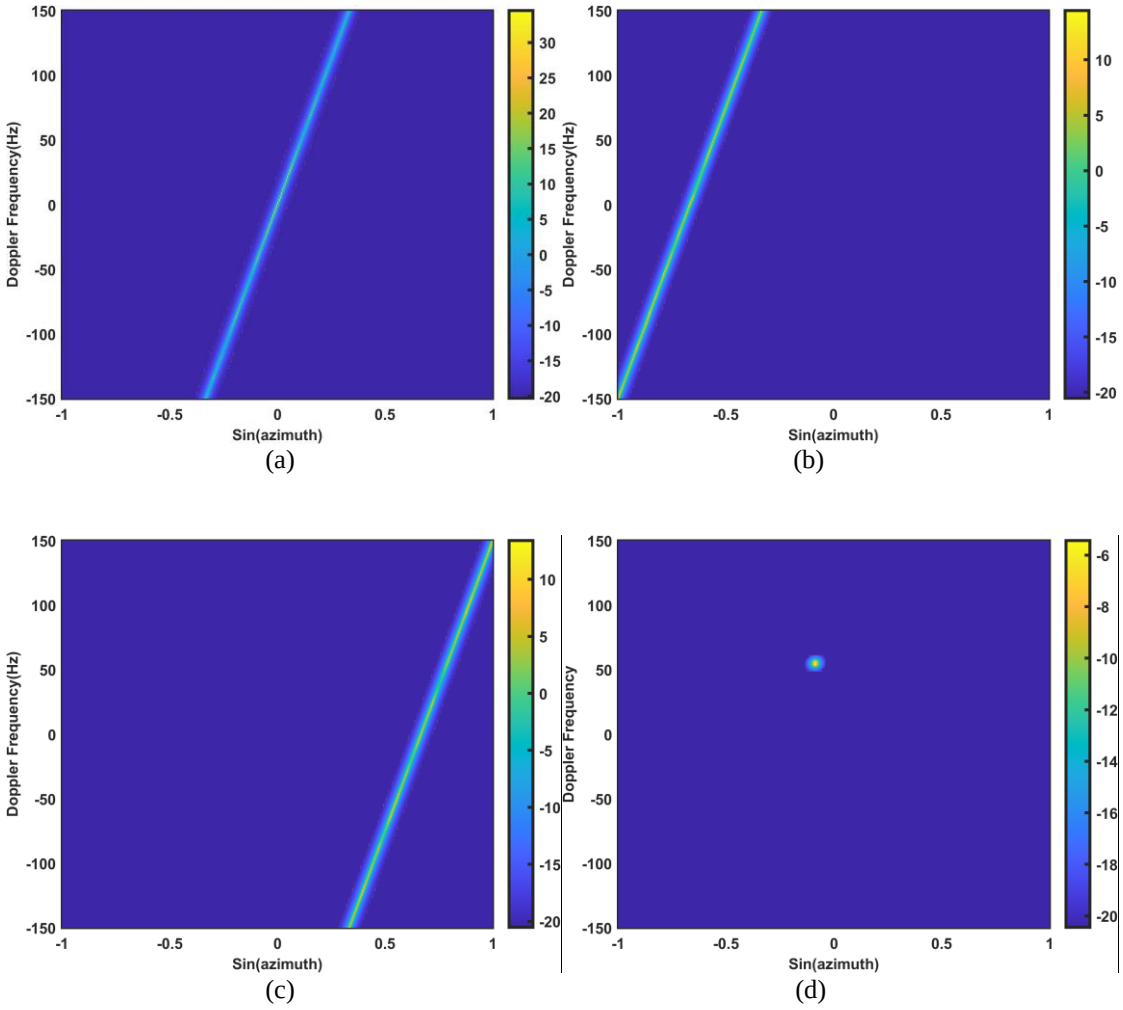

Figure III. 13 The detected clutter blocks and target using proximity feature when the platform velocity is 150 m/s

- Minimum distance from any pixel in the Target Block to the nearest clutter ridge is 23.42.

Since the target is closer to the clutter block 1, the minimum distance is found from the clutter ridge of that particular block. The other clutter ridge distances to the target block is as follows:

- The distance from any pixel in the Target Block to the clutter ridge of the clutter block 3 is 47.07.

- The distance from any pixel in the Target Block to the clutter ridge of the clutter block 2 is 123.

Besides the block size is another useful feature to recognize the target. Typically, the block size of the target is smaller than the clutter block size. The results are as follows:

- The block size of the clutter block 1 is 267.66.
- The block size of the clutter block 2 is 224.86.
- The block size of the clutter block 3 is 224.86.
- The block size of the target block is 18.25.

The detected clutter blocks and the target are shown in Fig. III.13.

Minimum detectable velocity (MDV): The MDV is an important parameter to detect slow moving target. It is defined as the minimum velocity at which the target is recognizable without going completely overlapped with clutter. The MDV in this case is found as 5 m/s due to the decreased width of the spectrum. The velocity less than MDV will overlap with clutter since SINR loss is high.

b) *Platform speed is at 200 m/s:* When platform speed is at 200 m/s, the Doppler spectrum significantly aliases in the visible subspace of angle-Doppler domain. The extended clutters will occupy the target subspace and the probability of false alarm will be much higher than the previous Doppler ambiguity. Thus as platform speed increases, the low radar PRF will cause this kind of clutter ambiguity that are very difficult to remove. However, with the knowledge of the locus of the clutter ridges, it is possible to classify the clutters as well as the target. The target Doppler frequency

is set at 80 Hz. Fig. III.14 shows the 2D and 3D plots of the radar scenario in the angle-Doppler domain. Since, the subspace comprises thermal noise, denoising processing is applied again to greatly reduce it. Fig. III.15 shows the denoised radar image for the platform speed at 200 m/s. As can be seen from the figure the denoised image contain the clutters and target component in the angle-Doppler domain. The proximity distance threshold is set at 12.24. The distance specifications are given as follows:

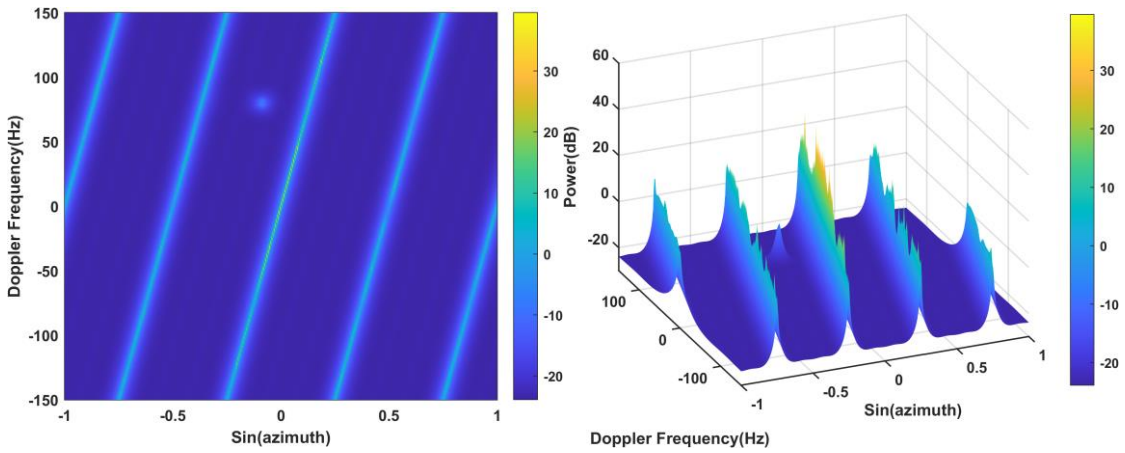

(a) (b)

Figure III. 14 The clutter subspace increased when the platform speed is 200 m/s. (a) 2D-plot; (b) 3D-plot

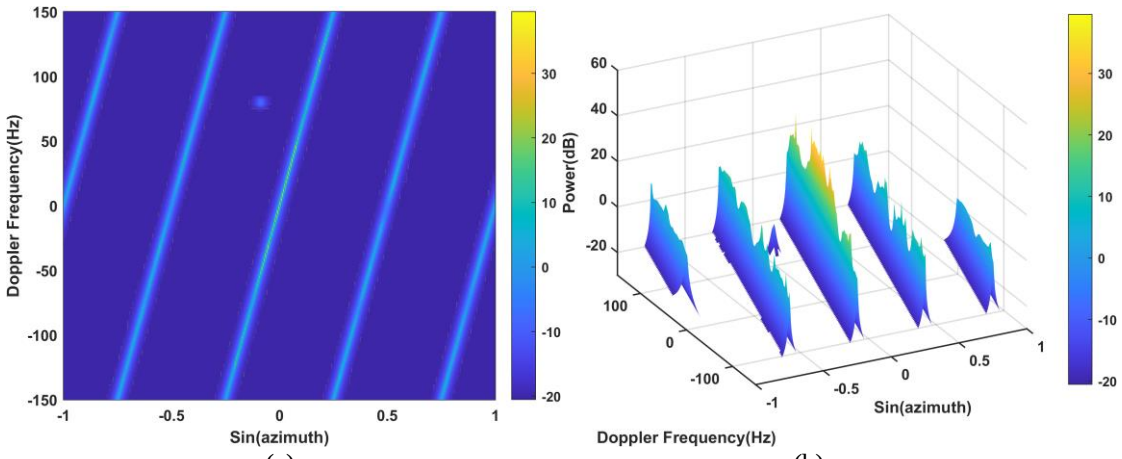

(a) (b)

Figure III. 15 The denoised target and clutter at platform speed 200 m/s. (a) 2D-plot; (b) 3D-plot

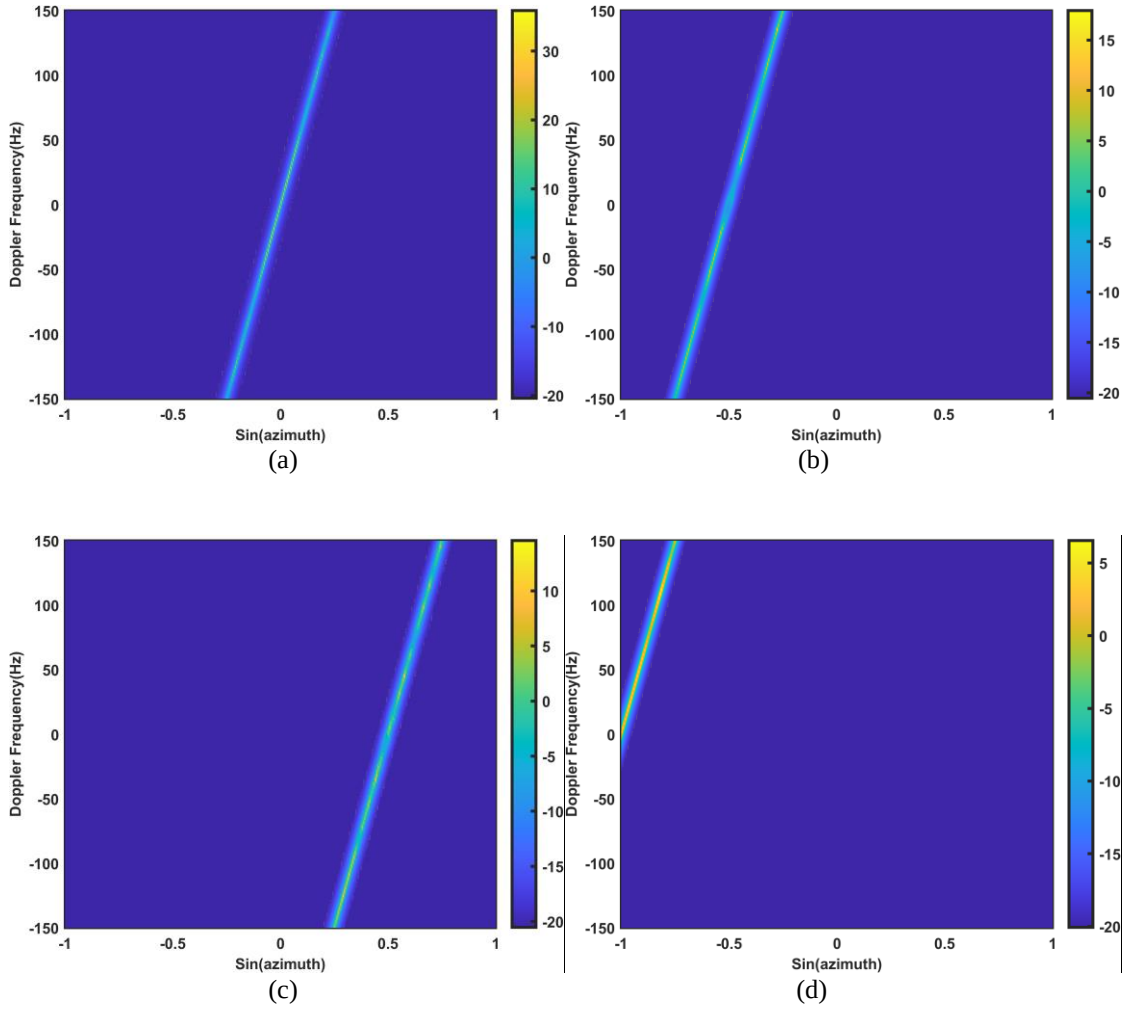

Figure III. 16 The detected four clutter blocks using proximity feature when the platform velocity is 200 m/s

- The maximum distance from any pixel in the Clutter Block 1 to the nearest clutter ridge is 6.74
- The maximum distance from any pixel in the Clutter Block 2 to the nearest clutter ridge is 6.09.
- The maximum distance from any pixel in the Clutter Block 3 to the nearest clutter ridge is 6.42.
- The maximum distance from any pixel in the Clutter Block 4 to the nearest clutter ridge is 6.09

- The maximum distance from any pixel in the Clutter Block 5 to the nearest clutter ridge is 7.02.
- Minimum distance from any pixel in the Target Block to the nearest clutter ridge is 20.22.

Since the target is again closer to the clutter block 1, the minimum distance is found from the clutter ridge of that particular block. The other clutter ridge distances to the target block is as follows:

- The distance from any pixel in the Target Block to the clutter ridge of the clutter block 2 is 25.37 .
- The distance from any pixel in the Target Block to the clutter ridge of the clutter block 3 is 87.88.
- The distance from any pixel in the Target Block to the clutter ridge of the clutter block 4 is 52.25.
- The distance from any pixel in the Target Block to the clutter ridge of the clutter block 5 is 148.81.

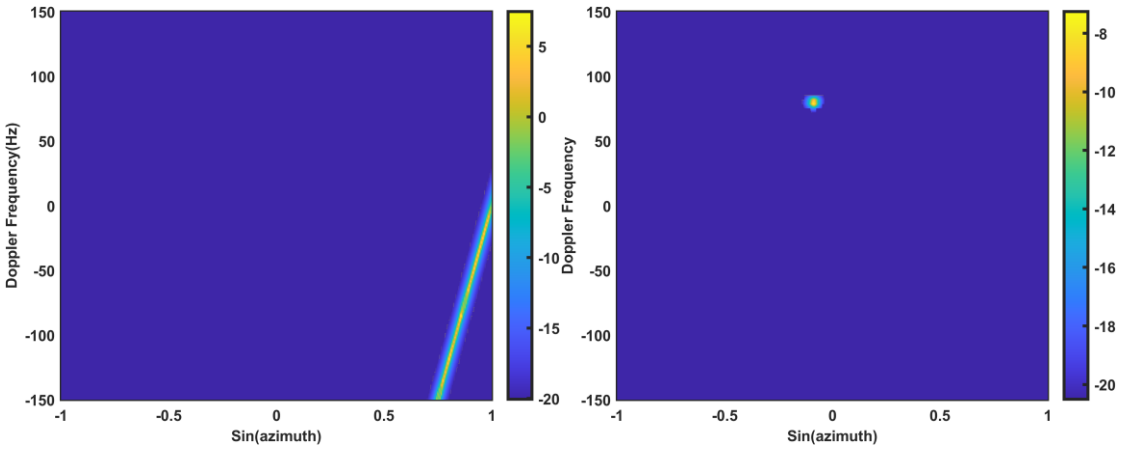

(a) (b)

Figure III. 17 The denoised fifth clutter block and the target at platform speed 200 m/s

Fig. III.16 shows the first four clutter blocks of the denoised image shown in Fig. III.15. Fig. III.17 shows the remaining clutter block and detected target block for this specific platform motion.

Whereas block size for the same radar setting can be found as:

- The block size of the clutter block 1 is 143.53.
- The block size of the clutter block 2 is 142.76.
- The block size of the clutter block 3 is 143.53.
- The block size of the clutter block 4 is 77.78.
- The block size of the clutter block 5 is 77.78.
- The block size of the target block is 19.03

III.8 Performance Comparison

The conventional adaptive method such as, STAP is usually applied to this type of radar system for many years. However, this method does not work well in inhomogeneous clutters. When clutter distribution changes from one range bin to another, adaptive filtering algorithms often fail to remove clutter signals totally. In contrast, the introduced feature-based approach is not affected by such inhomogeneity. Although it is not fair to compare such method with a conventional adaptive algorithm, we simulated same radar data both for the proximity feature method and STAP. The accuracy of target detection using this proximity feature method depends on correct removal of white noise and perfect classification of target and clutter signals in the angle-Doppler domain. Theoretical derivation of the detection probability based on the false alarm rate appears to

be mathematically difficult. However, we can consider a simplified case in which clutter and target are well separated in the angle-Doppler domain by limiting minimum target speed; hence the target and clutter classification using the clutter proximity feature is perfect. The detection probability can be estimated based on the data transform and denoising processing. Given the false alarm rate P_{fa}, the detection threshold for identifying the target from the white noise is obtained as follows,

$$T_t = \sqrt{\sigma_w^2} Q^{-1}(P_{fa}) \tag{III.23}$$

where σ_w^2 is the variance of the white noise after the MV transform and, Q^{-1} is the inverse Q function [101].

With the detection threshold in (III.23), we can estimate the probability of detection using the new method as,

$$P_d = Q\left(Q^{-1}(P_{fa}) - \sqrt{\frac{A_s^2}{\sigma_w^2}} \right) \tag{III.24}$$

where A_s is the average target signal amplitude in the angle-Doppler domain.

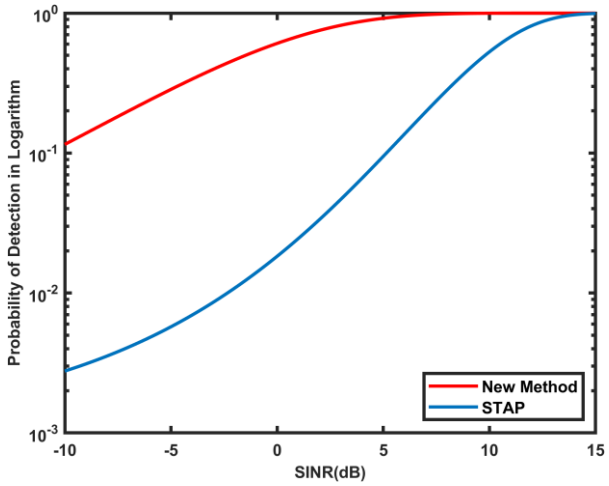

Figure III. 18 Detection performance comparison between the new method and STAP ($P_{fa} = 10^{-3}$)

The detection performance of the new method with $P_{fa} = 10^{-3}$ is shown in Fig. III.18. For comparison, the performance of STAP is also plotted in the same figure (in blue line). In this figure, 3NM secondary clutter data from zero-mean Gaussian variables are generated with their variances randomly changing from $0.5\sigma^2$ to $3\sigma^2$, where σ^2 is the variance of the clutter in the detection unit. If we set the false alarm rate P_{fa} at 10^{-3}, the targets in both cases are undetectable with the STAP approach. We simulated the STAP approach's performance in the inhomogeneous clutters. Similarly, the new method's clutter data is modeled to be independent identical complex Gaussian distributed where the amplitude of each clutter patch has randomly changed with the same range of amplitude variance. Since, the proposed method does not require clutter estimation, the comparison simply indicates that the feature-based detection performance is not affected by inhomogeneous clutters.

III.9 Summary of chapter III

An innovative clutter-proximity feature-based approach was proposed to effectively detect ground moving targets from clutter by recognizing target and clutter features rather than canceling clutter directly through signal filtering [11–15]. The traditional methods [11–49] rely on the adaptive signal processing that proves to be ineffective in the presence of complex and inhomogeneous clutter environment. The new approach can perform more robustly for ground target detection in the unknown clutter environment. The simulation results validated that the new approach can effectively classify target and clutter for ground moving target detection in inhomogeneous clutter. Furthermore, this proposed method is basically a form of the machine learning approach since the radar learns the distributions of the data features under both hypotheses from

either real radar data or synthesized data for target and clutter classification. Other possible interferences such as jammers were not considered in this work, but the new method is equally applicable for identifying jammers as well as target and clutter by including more than one feature in classification. Compared with other feature-based target detection methods, such as those based on the shapes and sizes of target and clutter blocks[91], [92], the clutter-proximity feature is more robust and effective in detecting and identifying slowly moving targets. In fact, this new proximity feature-based approach provided a clear roadmap for future artificially intelligent (AI) radar detection research.

IV. GROUND MOVING TARGET DETECTION USING PROXIMITY FEATURE IN THE PRESENCE OF NON-LINEAR CLUTTER

This chapter has been adapted from a previous work by the authors titled "Proximity Feature Based Target Detection for Airborne Radar with Misaligned Antenna Array", ©2021,IEEE. Aircraft crab is very common problem encountered by airborne radar. It occurs when antenna array elements introduce a phase shift. As a result, the clutter distribution no longer follows linear locus in its extended shape that is observed in the angle-Doppler domain. For this non-linear shape, it is very difficult to remove such clutter with traditional adaptive filtering algorithm and may require additional signal processing. The phenomenon is also known as velocity misalignment [5]. Since proximity feature technique is a non-adaptive approach and does not require secondary data, it can be applied to the non-linear expected clutter ridge such as, elliptical, or circular shape.

The first section of this chapter provides the theoretical aspect of non-linear clutters due to the aircraft crab. The second section elaborates the proposed method in depth. The third section demonstrates the simulation results for elliptical shaped clutters. The fourth section draws some salient remarks of this chapter.

IV.1 Concept of misaligned antenna array

Typically, aircraft moving velocity is assumed to be completely aligned with the spatial axis of sensor array elements. In a forward-looking antenna setting, the aircraft's the sensor array is possibly at the right angle to the platform velocity direction. However, the scenario might not be always true for the side-looking sensors. Array elements axis on this setting might be oblique to the direction of velocity and results a phase distortion. This phase error is always evident to the radar that uses revolving antenna. Consequently, mainlobe and backlobe of the array antenna do not blend together and establish a non-linear shaped clutter. This velocity misalignment causes an angle mismatch known as misalignment angle [5].

To represent the signal model of the airborne radar, a uniform linear antenna array with N elements is considered with M pulses in one coherent processing interval. It is further assumed that the radar antenna array is misaligned with respect to the direction of platform speed. The radar spatial-temporal samples for target, clutter and white noise are expressed as $\mathbf{F_t}$, $\mathbf{F_c}$ and $\mathbf{F_n}$ respectively. The covariance matrices of these vectors can be represented as $\mathbf{G_t}$, $\mathbf{G_c}$ and $\mathbf{G_n}$, respectively under $\boldsymbol{H_1}$ hypothesis. The $\boldsymbol{H_0}$ hypothesis consists of clutter and noise components only. The echo data is then transformed into angle-Doppler domain using minimum variance (MV) method[92]. The domain data

yields a clutter scenario with a possible target in it. Subsequently, the denoising step is performed to obtain the non-zero pixels of clutter and possible target.

IV.2 Proximity feature based nonlinear clutter detection

The denoised image is further processed with the proximity feature of clutter ridge. To extract the necessary feature of the clutter caused by aircraft crab, one needs to examine the normalized Doppler frequency of the ground clutter and that can be given by,

$$\omega_{gc} = \frac{f_{gc}}{f_p} = \left(\frac{2v_r}{f_p \lambda} \right) \cos(\phi) \sin(\psi + \psi_m) \tag{IV.1}$$

Where,

f_{gc} = clutter Doppler frequency

f_p = the radar pulse repetition frequency (PRF)

λ = the radar operating wavelength

v_r = the radar platform velocity

ϕ = depression angle

ψ = azimuth angle

ψ_m = alignment error angle

Now, assume

β = clutter ridge slope;

d = the interelement distance of the antenna array

then (IV.1) can be rewritten as,

$$\omega_{gc} = \beta s_c \cos(\psi_m) + \beta \rho \cos(\psi) \sin(\psi_m) \tag{IV.2}$$

where,

$$\rho = \frac{d\cos(\phi)}{\lambda} \tag{IV.3}$$

and

$$\beta = \frac{2v_r}{df_p} \tag{IV.4}$$

Also, spatial frequency

$$s_c = \rho\sin(\psi) \tag{IV.5}$$

As the normalized spatial and Doppler frequency are having non-linear relationship, (IV.2) can be represented as,

$$g(s_c, \omega_{gc}) = w_3 s_c^2 + w_2 \omega_{gc}^2 + w_1 s_c \omega_{gc} + w_0 = 0 \tag{IV.6}$$

where w_3, w_2, w_1, w_0 are the weights for the normalized spatial-Doppler equation.

(IV.6) represents a rotated ellipse with angle θ for the s_c and ω_{gc}. The angle θ is given by:

$$\theta = \frac{1}{2}\tan^{-1}\left(\frac{w_1}{w_3 - w_2}\right) \tag{IV.7}$$

The problem of (IV.7) can be solved by a couple of standard equations:

$$s_c = s_c^{'}\cos\theta - \omega_{gc}^{'}\sin\theta \tag{IV.8}$$

$$\omega_{gc} = s_c^{'}\sin\theta + \omega_{gc}^{'}\cos\theta \tag{IV.9}$$

(IV.8) and (IV.9) yields the standard form of the rotated ellipse ridge.

Therefore, the equation of the ellipse shaped clutter ridge with respect to the rotated axes can be written as:

$$g^{'}(s_c^{'}, \omega_{gc}^{'}) = w_2^{'} s_c^{'2} + w_1^{'} \omega_{gc}^{'2} + w_0^{'} = 0 \tag{IV.10}$$

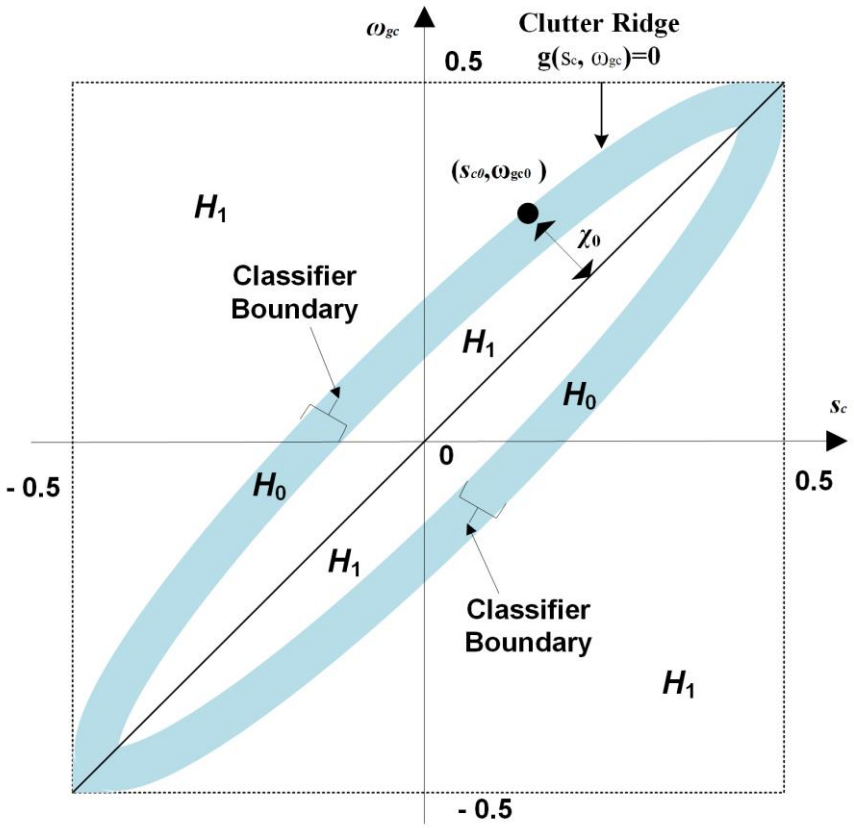

Figure IV. 1 The elliptical clutter ridge and its classifier boundary due to misaligned antenna array axis with velocity vector

where, $w_2^{'}, w_1^{'}, w_0^{'}$ are the new weights for the equation according to the rotated axes.

Since the equation forms a elliptical pattern of the clutter, the locus of the clutter i.e. clutter ridge cannot simplified as the linear relation given in chapter II and III. Hence, the parameters of an elliptical shape such as, major or minor axis, aspect ratio, area etc. could be used as different feature. However, for the proximity feature, major axis of this elliptical shape is a smart choice since it resembles with the clutter ridge segment in a linear setting. Likewise, minor axis can also be used to detect target and clutters. In this chapter, major axis is used for the rotated ellipse to detect the clutter and targe pixels.

If β=1, then the major axis can be found by using vertices of the ellipse:

$$m'(s_c', \omega_{gc}') = s_c' - \omega_{gc}' = 0 \tag{IV.11}$$

$$m'(s_c', \omega_{gc}') = k_2' s_c' + k_1' \omega_{gc}' + k_0 = 0 \tag{IV.12}$$

where k_2', k_1', k_0' are the weights for major axis. In this work, we will consider Doppler unambiguous case only. Hence, the distance formula from a pixel to the major axis can be given by:

$$\eta_{major} = \frac{\left| m'(s_c', \omega_{gc}') \right|}{\sqrt{k_2'^2 + k_1'^2}} \tag{IV.13}$$

Note that, if $g'(s_c', \omega_{gc}') = 0$, then the pixel will be classified as clutter. Now, the target could be outside the clutter or inside of it. Depending on the target location, the recognition can be further divided into two states:

a) *Outside* $(g'(s_c', \omega_{gc}') > 0)$

If a pixel's evaluated distance is greater than the predefined proximity threshold η_0 $(\eta_{major} > \eta_0)$ and satisfies the condition

$$g'(s_c', \omega_{gc}') > 0 \tag{IV.14}$$

then a target pixel will be detected; otherwise, it is a clutter signal.

b) *Inside* $(g'(s_c', \omega_{gc}') < 0)$

In this case, distances are calculated based on a new proximity threshold η_1. Furthermore, each non-zero pixel is examined if it is at the corner side of the clutter ridge. If $\eta_{major} < \eta_1$ and the pixel is not in the corner side, then it will be a target signal; otherwise, it is a clutter pixel.

IV.3 Simulation results

To simulate the proposed detection method, an airborne radar system is considered with operating frequency of 450MHz. There are 18 isotropic antenna elements and their interelement spacing is λ/2. The radar transmits 18 pulses in one coherent processing interval and the pulse repetition frequency is 300 Hz. The signal-to-noise ratio and clutter-to-noise ratio of this radar are considered as 0 and 45 dB, respectively.

For Doppler unambiguous case, the airborne platform is moving at 50 m/s. The antenna alignment error angle (ψ_m) is 10°. The target is located at the Doppler frequency of –51 Hz. Then the space-time echo data is transformed to angle-Doppler image via MV method. Fig. (IV.2) and IV.3 show the 2D and 3D version of possible target and ellipse shaped clutter due to antenna misalignment in the angle-Doppler domain. The echo data

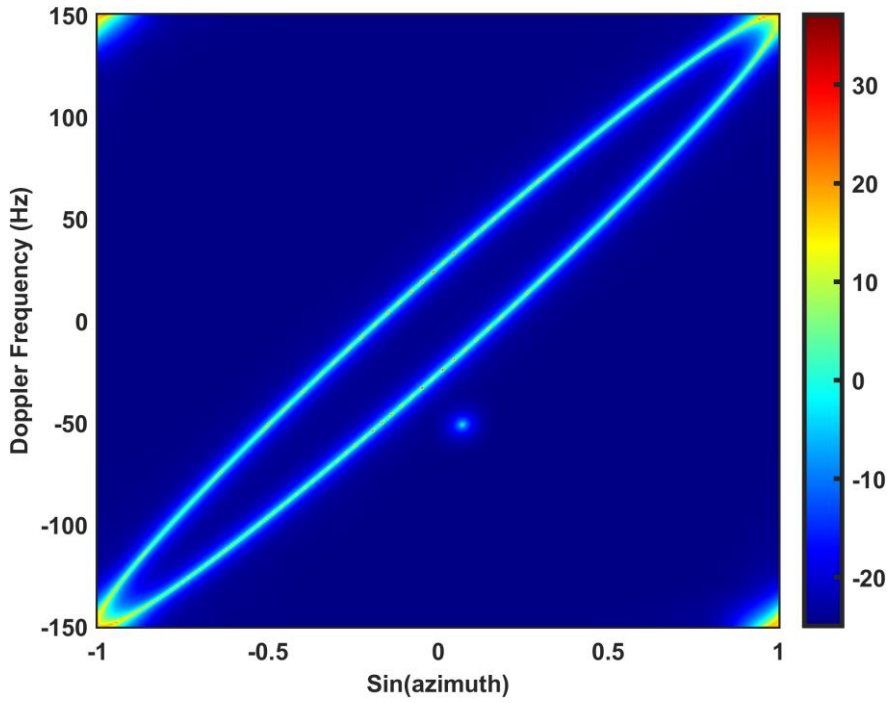

Figure IV. 2 The 10° misaligned elliptical clutter ridge and its classifier boundary due to misaligned antenna array axis with velocity vector

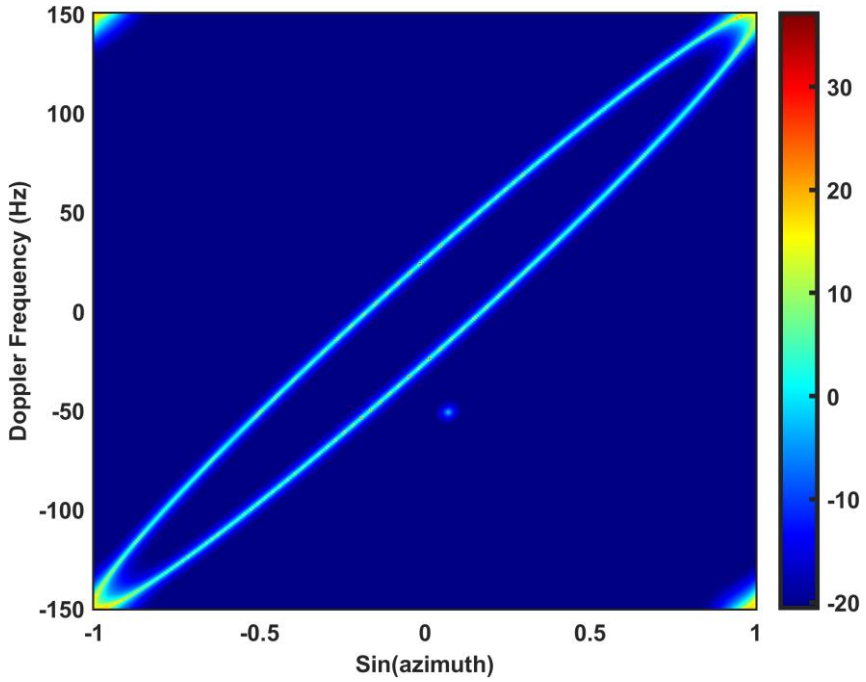

Figure IV. 3 The denoised radar image with non-linear clutter in elliptical form obtained after curtailing bottom 10% of the non-zero pixels

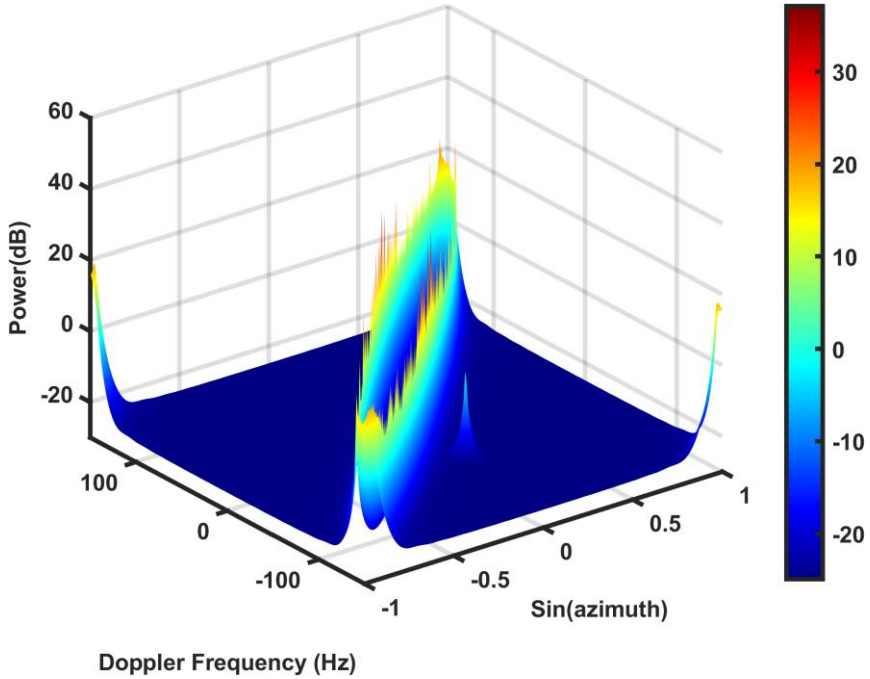

Figure IV. 4 The target located outside the elliptical clutter ridge affected with white noise

has been transformed to angle-Doppler plane through the process of minimum variance

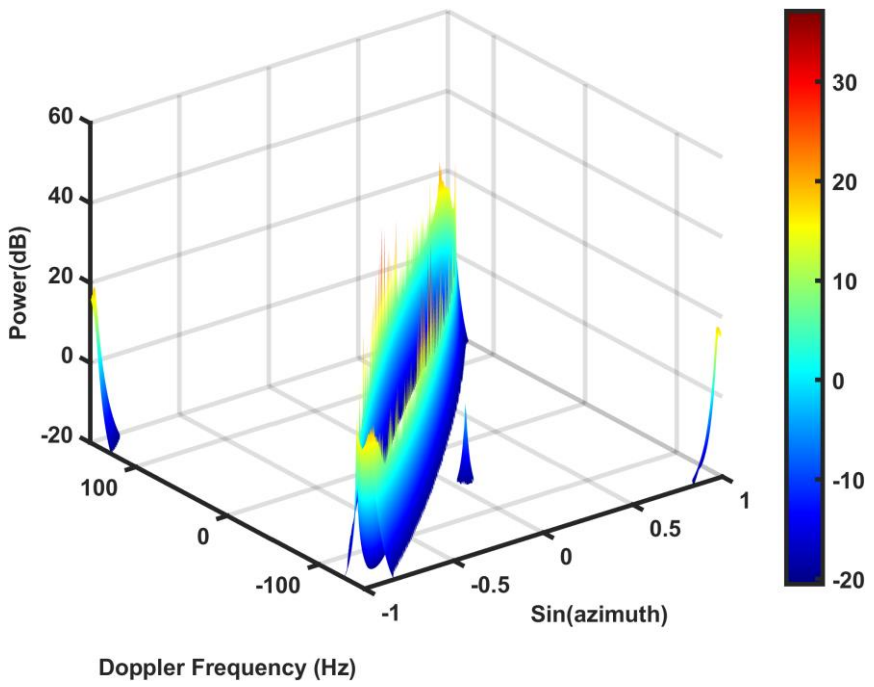

Figure IV. 5 The 3D plot of denoised radar image where target is well separated from the randomly changed elliptical clutter

or Capon estimator operation. Subsequently, a denoising process is applied to reduce the white noise. The white noise can be determined from the standard deviation of that noise. It can be determined from the lowest 10% pixel of the radar image. The mean of that lowest values is found as 0.0040. Next, the threshold is determined by multiplying the mean with a suitable value ranging from 2 to 3. Fig. IV.3 and IV.4 show the 2D and 3D plots of denoised images of elliptical clutter.

Now the next step is performed based on the proposed method. Each non-zero pixel of the denoised image is examined whether it is inside or outside of the clutter. Then, the distances are calculated using (IV.12) and compared with η_0 or η_1. From the mathematical equation of elliptical clutter ridge, the major axis equation is determined:

$$m'(s_c', \omega_{gc}') = s_c' - \omega_{gc}' = 0 \qquad \text{(IV.15)}$$

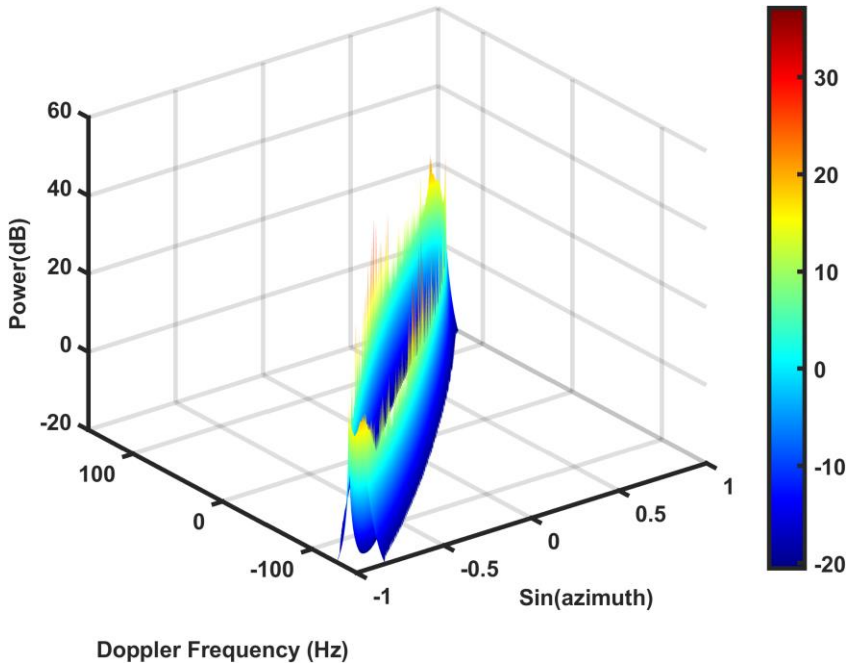

Figure IV. 6 The detected elliptical clutter block in 3D format using the proximity to the major axis of the non-linear clutter

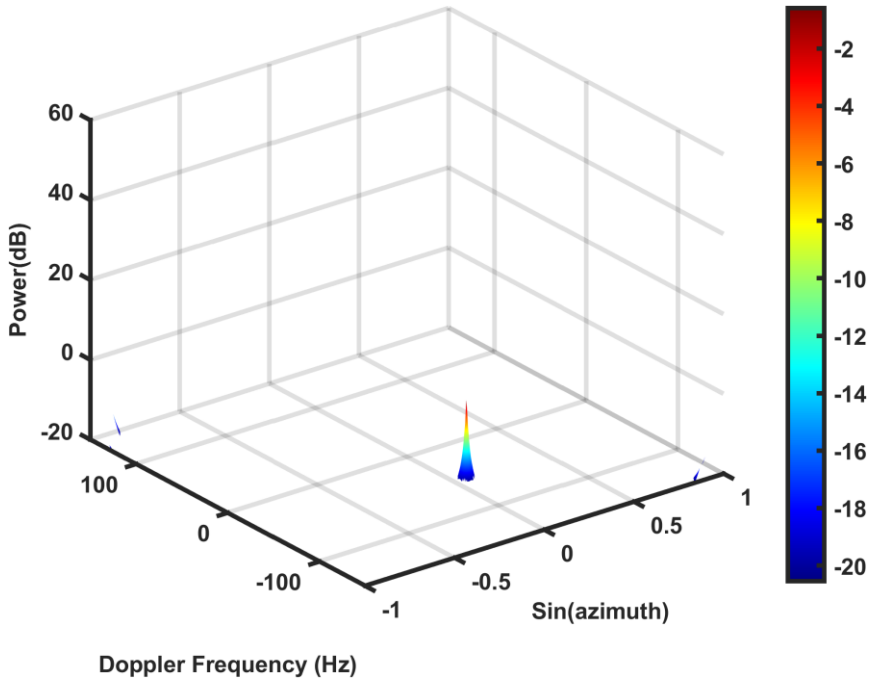

Figure IV. 7 The detected target at −51 Hz of Doppler frequency in 3D format

Where, k_2, k_1 and k_0 are 0.83, -1 and 0 respectively. From the major axis of the clutter

ridge, the maximum distance from any pixel to the elliptical clutter block is 27.21. Likewise, the minimum distance from any pixel of the target block to the major axis is found as 40.26. the detected target and clutter block is shown in Fig. IV.6 and IV.7, respectively. The elliptical clutter block has similar characteristics like a normal ellipse such as:

- The major axis length is 544.67
- The minor axis length 64.12

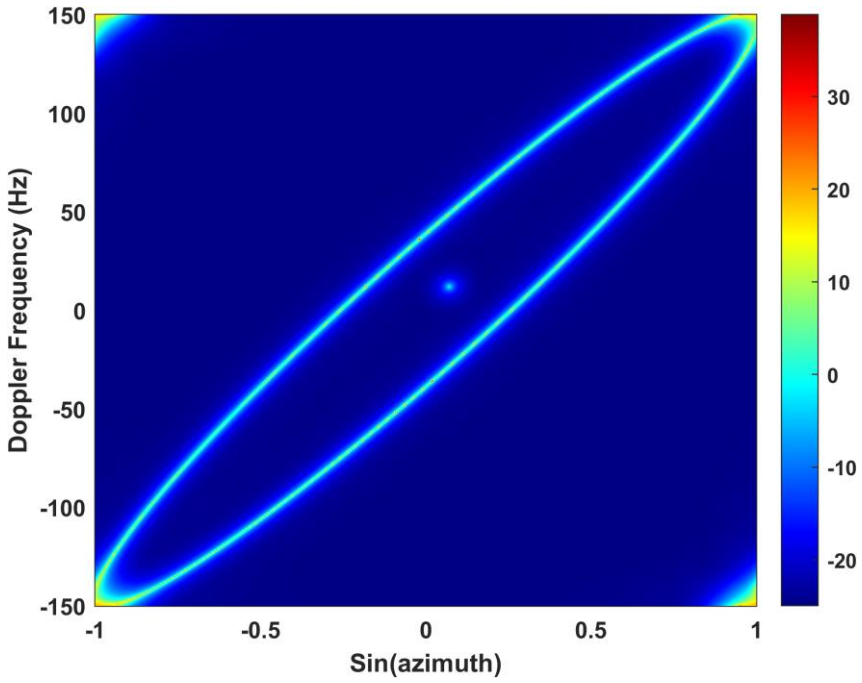

Figure IV. 8 The clutter scenario due to misalignment error angle of 15° with a target set at 12 Hz.

Now if we consider target inside the clutter block (i.e. H1 subspace inside the elliptical clutter), then $g'(s_c', \omega_{gc}') < 0$. Since the target and clutter block do not have overlap with each other, the alignment error angle is fixed at 15°. The target Doppler frequency is set at 12 Hz. Fig. IV.8 and IV.9 show the 2D and 3D formats of transformed radar image for

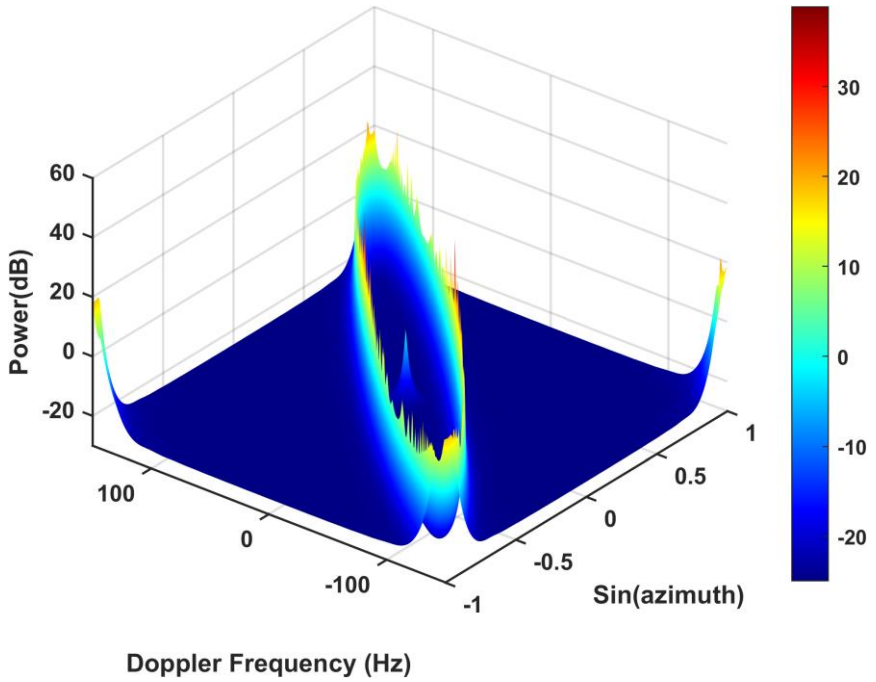

Figure IV. 9 The point target spread at 12 Hz in the middle of the clutter ridge.

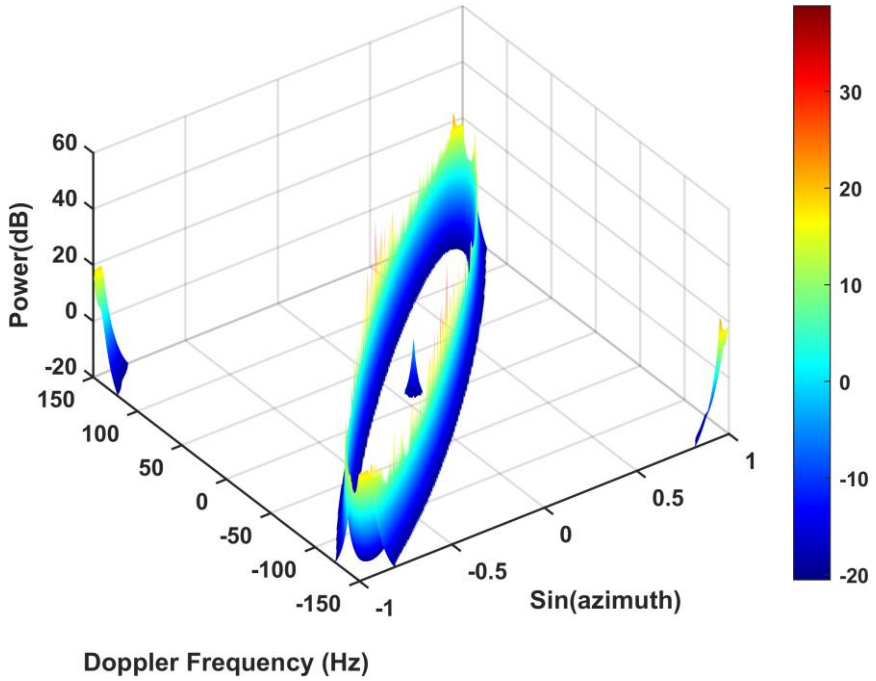

Figure IV. 10 The denoised radar scene with target inside the clutter forming non-linear shape.

this velocity misalignment. After denoising processing, the white noise is greatly reduced

in the radar image as shown in Fig. IV.10. Here some of the distance calculation for this radar scenario:

- the maximum distance from any pixel to the elliptical clutter block is 28.21.
- the minimum distance from any pixel of the target block to the major axis is found as 0. Since the some of the target pixels fall in exactly at major axis, the minimum distance becomes 0. Alternatively, it can be proved with the (IV.12) as some of those target pixels will satisfy the equation.
- The detection proximity thresholds for this case are set as 40 (η_0) and 10 (η_1) ,respectively. It should be noted that, the edge pixels are classified as interference signals inside the clutter ridge regardless of the value of proximity thresholds.

The major and minor axis length are the same as before since the clutter length has not increased rather clutter spread has increased for the alignment error angle. As can be seen

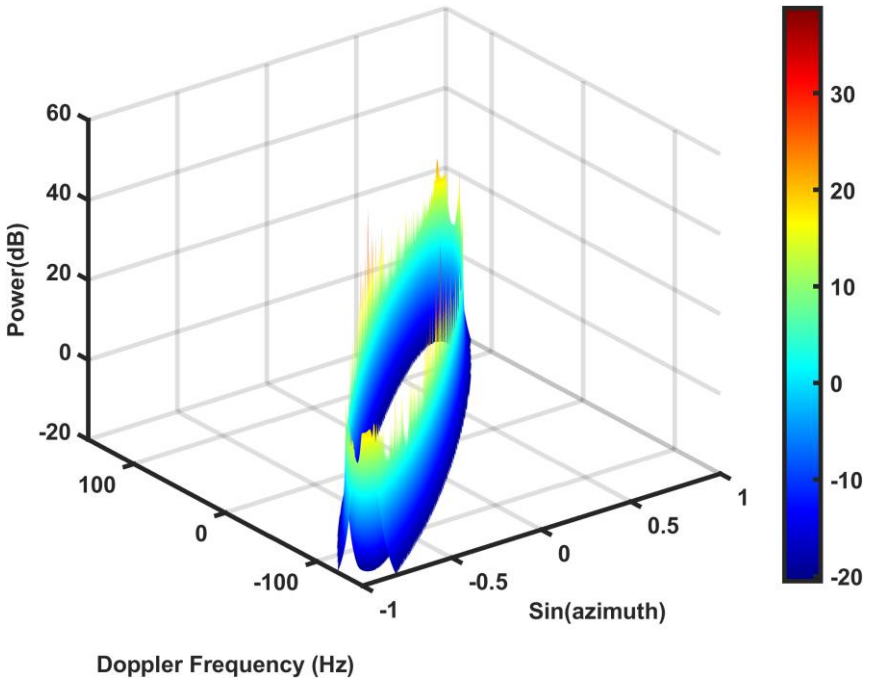

Figure IV. 11 The detected clutter block in the angle-Doppler 3D plane where the clutter is non-linear

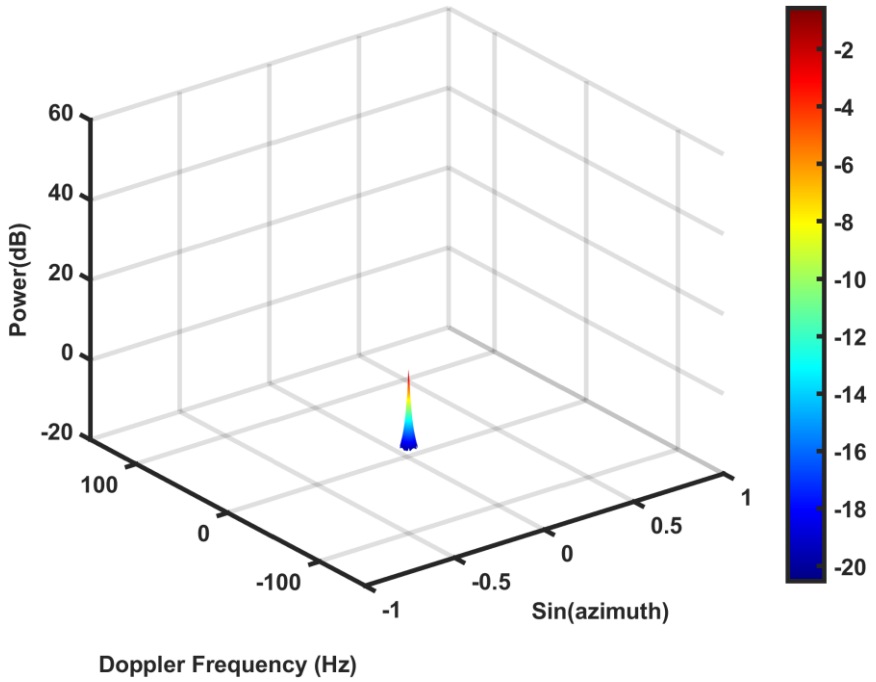

Figure IV. 12 The detected target block in the angle-Doppler 3D plane.

from the Fig. IV.11 and IV.12, the detected clutter block and the target inside it, respectively. It should also be noted that, there are some

The major difference between this case and the previous case is the target location. According to the H_1 hypothesis, target could be located inside or outside the non-linear clutter. The target detection outside the clutter subspace is comparatively easy if the target is not overlapped with the clutter region. However, if it is inside the clutter block's H_1 subspace, then it will be sometimes difficult to detect the target. The difficulty usually occurs when the target is very close to the edge of the elliptic clutter. There is a high probability that the target pixels could blend into the clutter pixels and falsely identify as clutter or interference.

For Doppler ambiguous case, the clutter becomes more complex and the proximity feature alone would not work well since the shape of expected clutter ridge

does not maintain appropriate relation that can be utilized. However, the clutter could still be detectable if several other features including geometric attributes could be employed.

IV.4 Summary of chapter IV

A new technique for target detection is proposed using proximity feature of the non-linear clutter ridge. The method does not need any filtering process to cancel clutter and thus very effective to detect targets with slow speed. Furthermore, most of the detection scenes for H_1 hypothesis under Doppler unambiguous case can be successfully recognized irrespective of alignment error angle. The intrinsic clutter motion is also considered for this simulation result and provides satisfactory result in detecting the clutter spectrum. This method is robust and applicable for Doppler ambiguous scenario of non-linear clutters as well. Existing research on clutter mitigation highly depends on adaptive filtering process [5,11–37]. The proximity of the clutter signal using major axis of elliptical clutter does not require such complicated process. Moreover, the proposed approach is a non-adaptive method that has better performance than the other feature based techniques. Size feature-based technique [91,92] could falsely detect the target when it is close to clutter ridge. However, the proximity feature of the elliptical clutter considers the overlapped target and interference block as target.

V. MULTI-FEATURE BASED MACHINE LEARNING APPROACH FOR GROUND-MOVING RADAR TARGET DETECTION

Low-velocity target detection is often very difficult for an airborne radar due to inhomogeneous ground clutters. In the previous chapters, it is assumed that the slow

moving target and interference do not overlap with each other in the angle-Doppler space. However, when they overlap, feature based approaches such as, proximity to clutter ridge, block size features could not detect the target due to their connected pixels in the radar image scene. To resolve the overlapping problem, two remedies can be adopted:

- Slightly changing the radar parameters such as, PRF. The change of the PRF can eliminate the overlapping problem
- Using multiple features to detect the overlapped target with clutters.

The first solution can normally prevent the target to overlap with clutter. However, the radar needs to either manually or electronically change the PRF. This might make the radar system complex and sometimes ineffective in real-time application.

Focusing on the reduction of the system complexity, this chapter proposes a multi-feature based machine learning approach to increase the robustness of the target detection approach. Several features such as proximity to the clutter ridge, block size, roundness ratio, and bending energy are utilized in order to detect the target in both overlapped and non-overlapped with clutter scenarios. It should be noted that, these features are independent and mutually uncorrelated from each other. The estimation of these features can be approximated by different classifiers such as, Bayes classifier. However, it is quite difficult to derive such an approximation mathematically with simple classification technique since the distribution of the feature is unknown. Moreover, there are several features and obtaining the estimation for them tends to be very cumbersome yet achievable. To avoid such intricacy, the introduced method utilizes a simple deep neural network (DNN). DNNs are very suitable where the feature data distribution is

unknown. This work utilizes deep feed forward neural network (FFNN) to learn the hypothesis of the radar data in angle-Doppler domain. After pre-possessing the feature data, these attributes are fed to a feed forward neural network (FFNN) that consists of four layers. Since there are two classes (target or clutter) considered in this dissertation, FFNN can effectively classifies the target. It also recognizes the overlapped targets and detects them via boundary information using image processing. The work also provides a detailed data generation technique for the synthetic samples of the target-clutter classification.

The opening section of this chapter contains a brief overview of the signal model of the target and interference scene. The second section details the connected signal components and boundary detection. The third section discusses about the purpose of the feature extraction and a brief explanation of two attributes such as the proximity feature and block size for both overlapped and non-overlapped target. This section also provides comprehensive description of different geometric features in the angle-Doppler domain. The fourth section elaborates the FFNN model that has been employed to classify the target and clutter. The next section describes a weighted sampling method and synthetic minority over sampling technique (SMOTE) to generate synthetic target and clutter data for all of the features. Section V.6 and V.7 demonstrate the simulation result based on the multi-feature approach. Section V.8 provides a performance comparison with a previous feature based technique known as BDIFR. Lastly, the summary section puts some ending remarks about this work.

V.1. A brief theory of the multi-feature based airborne signal model

The signal model described in chapter 2 will be applied to this work as well. To facilitate the signal theory for the multi-feature approach, some of the symbols and equations are used in different notations. The radar configuration has been kept as same as before with N element of uniform linear antenna array and M coherent pulses for one CPI. The antenna element spacing is d. The azimuth and elevation angles with respect to the radar antenna are ϕ and θ, respectively. The platform is moving with a velocity v in the x-direction. When the platform starts receiving the echoes, the coherent pulses are then sampled G times to obtain $N \times M \times G$ data. For single range, this is expressed as $NM \times 1$ vector or better known as space time snapshot (χ). It is further assumed that the radar echo data is received in a range unambiguous situation.

Usually, the echo data contains clutter, and thermal noise under null ($\boldsymbol{H_0}$) hypothesis. Whereas alternate ($\boldsymbol{H_1}$) hypothesis includes target as well as interference and noise. The covariance matrix under $\boldsymbol{H_1}$ hypothesis can then be expressed as:

$$\boldsymbol{K} = \boldsymbol{K_c} + \boldsymbol{K_n} + \boldsymbol{K_t} \tag{V.1}$$

Where $\boldsymbol{K_c}$, $\boldsymbol{K_n}$, and $\boldsymbol{K_t}$ are the covariance matrices of clutter, thermal noise and target respectively. $\boldsymbol{K_n}$ is related to white noise with variance σ^2. $\boldsymbol{K_c}$ depends on space time steering vector, and clutter-to-noise ratio (CNR) at each clutter patch.

The steering vector can be further represented as the Kronecker product of clutter normalized spatial and Doppler frequency which are given by:

$$\psi_v = \frac{d \cos\theta_{cl} \sin\phi_v}{\lambda} \tag{V.2}$$

$$\varpi_v = \frac{f_{dv}}{f_r} = \frac{2v}{\lambda}\cos\theta_{cl}\sin\phi_v \tag{V.3}$$

where, λ is the radar operating wavelength, f_{dv} is the Doppler frequency at each clutter patch v, and f_r is the PRF. For N_c independent clutter patches each with random complex amplitude Λ, the clutter space time snapshot can be given by:

$$\boldsymbol{\chi}_c = \sum_{v=1}^{N_c} \Lambda_v \boldsymbol{\rho}_t(\varpi_v) \otimes \boldsymbol{\rho}_s(\psi_v) \tag{V.4}$$

where, ⊗ expresses the Kronecker product,

$\boldsymbol{\rho}_t(\varpi_v) = [1, \exp(j2\pi\varpi_v), \ldots, \exp(j2\pi(M-1)\varpi_v)]^T$ and

$\boldsymbol{\rho}_s(\psi_v) = [1, \exp(j2\pi\psi_v), \ldots, \exp(j2\pi(N-1)\psi_v)]^T$

Hence, the clutter covariance matrix can be represented by,

$$\boldsymbol{K}_c = E\{\boldsymbol{\chi}_c \boldsymbol{\chi}_c^H\} \tag{V.5}$$

Since, $E\left\{\left|\Lambda_v^2\right|\right\} = \sigma^2(CNR)_v$,The matrix can be further represented as:

$$\boldsymbol{K}_c = \sum_{v=1}^{N_c} \sigma^2(CNR)_v [\boldsymbol{\rho}_t(\varpi_v)\boldsymbol{\rho}_t{}^H(\varpi_v)] \otimes [\boldsymbol{\rho}_s(\psi_v)\boldsymbol{\rho}_s{}^H(\psi_v)] \tag{V.6}$$

Since thermal noise is always present in the radar receiver and is uncorrelated both in spatial and temporal domain, this leads to a uniform noise distribution in the angle-Doppler domain. The noise can be given in terms of identity matrix $\boldsymbol{I_M}$ and $\boldsymbol{I_N}$,

$$\boldsymbol{K}_n = E\{\boldsymbol{\chi}_n \boldsymbol{\chi}_n^H\} = \sigma^2 \boldsymbol{I}_M \otimes \boldsymbol{I}_N \tag{V.7}$$

whereas, $\boldsymbol{K_t}$ is based on target space-time steering vector and signal-to-noise ratio (SNR). Target spatial and Doppler frequency have similar expressions as in (V.2) and (V.3). Thus, following the same method, the target covariance matrix can be given by:

$$\begin{aligned} \boldsymbol{K_t} &= E\{\boldsymbol{\chi}_t \boldsymbol{\chi}_t^H\} \\ &= \sigma^2(SNR)[\boldsymbol{\rho}_t(\varpi_{tr}) \otimes \boldsymbol{\rho}_s(\psi_{tr})][\boldsymbol{\rho}_t(\varpi_{tr}) \otimes \boldsymbol{\rho}_s(\psi_{tr})]^H \end{aligned} \tag{V.8}$$

Where, $\boldsymbol{\rho}_t(\varpi_{tr})$ and $\boldsymbol{\rho}_t(\psi_{tr})$ represent target temporal and spatial vector, respectively. Here, the target radial velocity v_{tr} is related to its Doppler frequency (f_t), i.e. $v_{tr} = f_t\lambda/2$.

In this work, the aforementioned received radar data is transformed into angle-Doppler domain via Capon spectral estimator. This transformation scheme has an advantage of better resolution over the 2-D Fourier transform. The method uses narrowband FIR bandpass filters in spatial-temporal domain to minimize the spectral contribution of undesired angle of arrivals except the mainbeam direction. If $\boldsymbol{\rho}(\varpi)$ and $\boldsymbol{\rho}(\psi)$ represent the desired space and time vector then the space-time steering vector can be written as:

$$\boldsymbol{Q} = \boldsymbol{\rho}(\varpi) \otimes \boldsymbol{\rho}(\psi) \tag{V.9}$$

Therefore, the sensor array output power optimized by Capon estimator can be given as [92,93]:

$$P_C = \frac{1}{\boldsymbol{Q}^H \boldsymbol{K}^{-1} \boldsymbol{Q}} \tag{V.10}$$

Actually, the power spectral density in angle-Doppler image presents the scenario of clutter, thermal noise and possibly target. A subsequent denoising process is applied to greatly reduce the thermal noise. The process assigns zero intensity to pixels which are less than certain denoising threshold. The denoising threshold can be represented as,

$$T_d = \tau\sigma_{th} \tag{V.11}$$

where τ is a constant chosen between 2 and 3, and σ_{th} is the standard deviation of the white noise in the transformed domain. After denoising, the remaining non-zero pixels are either for target or clutter signal.

V.2. Connected Component Cluster Partition and Boundary Pixels Identification

After the application of denoising process, there will be target and clutter signal components in the observable angle-Doppler domain. Typically, the signal and interference inherit connected component properties in their pixels. The connected target and interference can then be processed through a connected component extraction algorithm. The algorithm will facilitate all the non-zero pixels to label them to different sets of clusters. After recognizing the clusters, boundary or edge pixels need to be identified for further information of overlapped target.

V.2.1. Connected Component Algorithm

Numerous algorithms can be applied to extract the connected signal blocks. Region growing (RG) algorithm is widely used to segment non-zero pixels in the field of image processing. However, the process of RG algorithm requires to initiate an arbitrary non-zero pixel and thus increases the computational complexity and may not converge to label all the pixels as clustered to a specific group or block. Hence, another algorithm known as Hoshen-Kopelman (HK) algorithm [102,103].

HK algorithm is a popular method for connected component analysis due to its simplicity. It also does not require any seed pixel to begin its procedure. The algorithm considers two passes on the given image. Since, the work deals with a radar image after the transformation, the first pass sets the unlabeled non-zero pixels to temporary labels and keeps equivalence labels in a structure. The final pass substitutes temporary labels by the

smallest labels of its equivalence structure. To illustrate the algorithm, we need to define the following terms.

Definition 1: a non-zero pixel will be defined as a neighbor of another pixel if the Euclidean distance between them is less than 2.

Definition 2: linked_list is a structure containing cells or fields that group the list of connected pixels' labels with a particular label except the background pixel. For instance, if the label of a certain non-zero pixel is 1, the *linked_list*{1} contains a list of the labels of all non-zero neighboring pixels' labels including the label of that particular pixel (1).

Definition 3: label_matrix is a matrix where each connected cluster or group pixels are labeled with a unique positive integer number. Usually, the matrix is the same size of the original image, and all the pixels are assigned as zeros initially.

Definition 4: Signal block is the cluster of non-zero pixel which can be categorized as interference or target block.

Now, the procedure can be described as follows:

Step 1: Define an empty data structure *linked_list* where each cell contains the list of connected pixel labels.

Step 2: Define a *label_matrix* with same size of the radar image (*I*); initialized with zero pixels.

Step 3: Set a counter named next_label initialized with 1.

Step 4 (*First Pass*): Check non-zero pixels from the radar image indices by row and then column i.e. *I(row,column)*

a. Check for the neighboring pixels with 8-connectivity (i.e. distance between two neighboring pixel<2)

b. If no neighbor is found, set the element of *label_matrix* with next_label; Also, update the cell of *linked_list* with that next label and increment the counter.

c. Else find the smallest label from adjacent 8-connected neighbors and assign it to the current element of the *label_matrix*; update the corresponding cell of the *linked_list* with all non-repeating equivalent neighboring pixel labels.

Step 5 (*Second Pass*): Check the non-zero pixels from the radar image again.

a. Check for the values in the *label_matrix* using *linked_list* and replace the temporary labels in the *label_matrix* with minimum value from the elements of that *link_list's* cell.

Step 6: After finishing the second pass, the *label_matrix* yields the expected connected signal blocks. The connected blocks can also be extracted using the indices of non-zero values of *label_matrix*.

The above procedure extracts the connected signal blocks from the transformed radar image. Now, the target and interference blocks should be labeled as a separate

group of clusters if these two types of signal pixels do not overlap. However, if they overlap, target block merges with clutter block and the connected component algorithms such as HK method can not be able to distinguish target and clutter due to the connection between these two signal blocks. Hence, boundary pixels are needed to be identified to know about the location of a target.

V.2.2. Boundary Pixels Identification

Typically, contour points of a region in a 2D image reveal very important information about the discontinuity regarding its surrounding neighboring pixels. It becomes especially significant when the boundary curvature information is needed for a recognition purpose. In the computer vision community, active contour tracing is very important part for image segmentation method. This tracing can be performed either on edge-based or region-based method. Most of the methods of boundary curvature largely depend on convolution of derivative kernels with original image to extract the edge information[104]. However, edge-based method suffers weak edge detection in the presence of noise. In contrast, region-based methods comparatively perform well with the local statistical and curvature knowledge from neighborhood pixels [105]. In this work, we applied Moore-Neighbor tracing algorithm to detect the outward boundary points. The method utilizes backtracking approach to identify and locate the boundary of the region of interest (ROI). However, the algorithm tends to return to its already visited pixel and stops the search for new non-zero neighboring pixel. Hence, Jacob's stopping criteria is utilized to prevent the unexpected termination [106,107]. The algorithm starts with an image that contains a connected regular polygon (i.e. object) G where X is a connected

component. The outcome of this algorithm is a vector or sequence E (e_1, e_2,…,e_k) of contour pixels. For simplicity, the zero pixel will be denoted as background pixel. The steps for Moore-neighborhood are as follows [107]:

- Consider R(x) is the set of pixels defined as Moore neighborhood of pixel x
- x represents the current boundary element or pixel
- u represents the pixel under the process of examination. Hence, c is in R(x)

Step 1: Initialize E as an empty vector list.

Step 2: Examine each pixel of G until a non-zero pixel z of X is discovered

Step 3: Insert the pixel z in the E

Step 4: Change the current boundary pixel from x to z

Step 5: move back to the position where z was encountered (backtracking approach)

Step 6: Set u as the next pixel from R(x) (next pixel should be in clockwise direction)

Step 7: While u is not equal to z

If u is non-zero (=1 for binary image)

- Append u in E
- Set x as u
- Perform backtracking approach (move back to point where u was encountered from the current position of the pixel u)

Else

- Move forward from the current pixel u to the next pixel in R(x)

End While

The algorithm has a disadvantage of convergence problem. In fact, it might not include all the contour point and loops back to its original starting pixel. Hence, a suitable stopping criterion needs to be utilized to improve the boundary detection with Moore-neighborhood tracing.

The solution to the convergence problem is to use a Jacob's stopping criterion. This criteria ensures the algorithm not to disregard the remaining edge pixels without a process.

Jacob's Criterion: It is defined as a criterion by which the algorithm stops traversing the edge pixels if the initial non-zero edge pixel is visited second time in exactly the same way it was visited at the first time.

If Jacob's criterion is met, then it can be said that the algorithm has examined all the edge contour pixels of the polygon or the object in the region of interest.

V.3. Multiple Feature Extraction

When target and clutters do not overlap, a single feature would suffice for the detection method to be successful. However, when target and clutter overlap, a robust combination of multiple-feature is needed for the target detection in inhomogeneous clutter environment. In non-overlapping scenario, target and clutter can be easily detected either by clutter proximity feature or roundness ratio. However, for overlapping state, proximity feature could falsely detect target pixel as clutter one. As for the roundness ratio, the block considered as target (overlapped with clutter) might have a decreased roundness value that is most likely different from the typical non-overlapped target block.

Therefore, multiple features are the prime necessity to detect the target and clutter properly. The features are detailed into several parts that are described below:

V.3.1. Proximity to the Clutter Ridge in the Angle-Doppler Radar Scene

As described in chapter III, the Euclidean distance from expected clutter ridge to the target signal can be considered an important feature in ground moving target detection. A certain proximity distance threshold needs to be introduced to separate the target pixel from the clutter. This threshold parameter can be determined based on the training data obtained from the same radar or from a different radar. It can also be obtained from radar considering different clutter distribution scenario. One of the advantages of this algorithm is that the proximity feature can consider a block as target if it contains both target and clutter signal.

V.3.2. Block Size Feature in the Angle-Doppler domain

Block size feature is another useful attribute in non-adaptive ground moving target detection. It is defined as the maximum Euclidean distance between two pixels inside a block. The distance is calculated after the connected component cluster extraction. Usually, the target block size is smaller than the interference block for non-overlapped scenarios. However, block size gets bigger for the target block when target and interference such as, clutter blends in and merge into a same block. In such case, there is a tendency to falsely detect target as clutter block.

V.3.3. Geometric Features Observed in the Angle-Doppler Space

The geometric features are very well-known attributes for pattern analysis and recognition. Especially, they are widely used in the field of biological cell shape recognition and detection. Generalizing the idea from biological point of view, we utilize the geometric characteristics of target and interference of echo data in the transformed angle-Doppler domain. There are several features which can improve the detection of target and clutters:

V.4.1. Roundness Ratio (RR)

Since, the target or interference block has distinguishing feature of shape and size, roundness ratio could separate the blocks very well. The roundness ratio basically depends on the perimeter and the area of the block. To further describe the property of this feature, we need to define the following terminologies.

Definition 5: Perimeter is defined as the sum of the Euclidean distances of consecutive two samples of boundary points. If $b_s, s = 1, 2, 3 \ldots N$ are the samples of the boundary, then the perimeter (*P*) is given by:

$$P = \sum_{s=1}^{N-1} \left(\left\| b_{s+1} - b_s \right\| \right) + \left\| b_s - b_1 \right\| \tag{V.12}$$

Definition 6: Area is defined as the sum of the number of non-zero pixels inside a block. If *n* is the number of non-zero pixels and p_i is the amplitude of the pixels inside a block. Then the area (*A*) for a block can be represented as:

$$A = \sum_{i=1}^{n} a_i \tag{V.13}$$

where, $a_i = \begin{cases} 1 \; if \;\; p_i \neq 0 \\ 0 \; otherwise \end{cases}$

With the above definitions, the roundness ratio (RR) can be given as following:

$$RR = \frac{4\pi A}{P^2} \tag{V.14}$$

The value of RR ranges from 0 to 1. This feature works well even when the axis of antenna array is misaligned with platform velocity direction.

V.4.2. Bending Energy (BE)

Target and clutters in the angle-Doppler domain can be detected based on the boundary curvature of their arbitrary contour dimension. Since target or clutters in the transformed domain show distinguishing curvature in their boundaries, one can choose several methods in order to demonstrate substantial difference between them. Bending energy (BE) is one of the widely used parameters to evaluate such curvature relating to outward contour shape of an image object [108,109]. This feature can identify subtle difference in the curvature of target and clutter shapes. Most importantly, it can identify the presence of overlapped target with clutter. This energy determines the average curvature strength of a certain block in the angle-Doppler domain. At first, boundary contours are needed to be calculated, which is discussed in section V.2.2. Afterwards, BE is determined based on the change of boundary shape along the curve. From elasticity theory, the bending energy of a curve at a given point, *s* can be written as in integral form [109]:

$$J = \frac{1}{2}\alpha_c I_c \int_0^l C^2(s)ds \tag{V.15}$$

where α_c is Young's modulus, I_c is the moment of inertia and $C(s)$ is curvature at point *s*. Since α_c and I_c are constants, the bending energy can be represented in normalized form:

$$J_{norm} = BE = \int_0^l |C(s)|^2 \, ds \tag{V.16}$$

Now the average bending energy related to perimeter (P) of a simple connected contour (SCC) can be given by:

$$BE = \frac{1}{P} \int_0^P |C(s)|^2 \, ds \tag{V.17}$$

If there are N samples for boundary contour for a signal block, The equation can be further generalized in summation form:

$$BE = \frac{1}{N} \sum_{n=1}^{N} |C(n)|^2 \tag{V.18}$$

To find the curvature C, change from one connected point to the next is needed to be found. The term relating to this change can be expressed as:

$$C(n) = \frac{a(n)}{w(n)}; \; n = 1, 2 \ldots N \tag{V.19}$$

Where $a(n)$ is the change of curvature in angle and $w(n)$ is the path length of the curve segment. Change of curvature for connected components can be found by various methods. Chain coding is widely used to describe such connected boundary points. In this work, we applied Freeman's chain code with 8 directions to encode the line segments

Table V.1 Angles corresponding to numerical values of chain code

No.	Angle (°)
0	0
1	45
2	90
3	135
4	180
5	225
6	270
7	315

between two adjacent boundary points. This encoding scheme finds the gradient of direction and encode each boundary point index into one of the eight numerical codes, shown in Table V.1. Fig. V.1 delineates the direction paths for these numerical values at the boundary. It should be noted that the boundary contour path is following clockwise direction in this work.

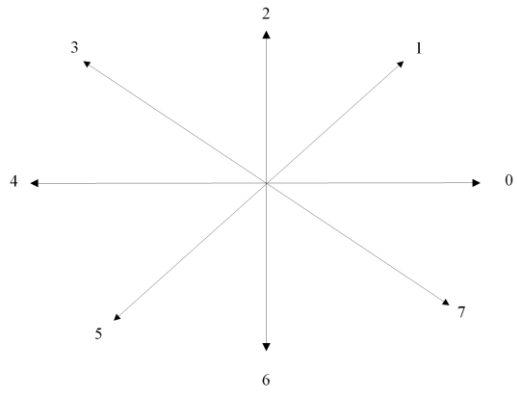

Figure V. 1 Chain Code Direction of Paths

Now, if the two consecutive boundary sample indices are (p_{i-1},q_{j-1}) and (p_i,q_j) and their corresponding difference are *dp* and *dq*, respectively, then the chain-code mapping scheme for n samples can be given by:

$$M_c(n) = 3dq(n) + dp(n) + 4 \qquad \text{(V.20)}$$

Here, it should be noted that, the very first difference is calculated between first and last element of these samples. Moreover, the consecutive two samples are considered as the two end points of a particular curve segment of the boundary.

Using the above concept, steps of chain coding can be described as follows:

Step 1: Find the difference between the indices of each boundary sample to the next one. This will provide sample difference pair *(dp,dq),* for two end points.

Step 2: Calculate the chain code based on the mapping in (V.20) and list the numbers corresponding to every curve segment of the boundary contour.

After obtaining the chain code, one can find the curvature change $\Delta\theta$ by converting the number into an angle using the Table V.1. The curvature change for N points is then expressed as:

$$a(n) = \begin{cases} \Delta\theta(1) - \Delta\theta(N); \ if \ \ n = 1 \\ \Delta\theta(n) - \Delta\theta(n-1); \ if \ \ n = 2,3 \ldots N \end{cases} \tag{V.21}$$

Similarly, the path length can be represented as the half of the curve segment [109]:

$$w(n) = \frac{1}{2}[2 - h(n) - h(n-1)] + \frac{1}{\sqrt{2}}[h(n) + h(n-1)] \tag{V.22}$$

where $h(z) = M_c(z) \mod 2$

Therefore, the average BE in (V.18) can be rewritten as:

$$BE = \frac{1}{N}\sum_{n=1}^{N}\left|\frac{a(n)}{w(n)}\right|^2 \tag{V.23}$$

The steps for finding bending energy are as follows:

Step 1: Find the numerical value for each boundary curvature segment using Freeman's chain code

Step 2: Calculate the curvature angle change and path length for each segment using (V.21) and (V.22), respectively.

Step 3: Find the average of the overall curvature change using (V.23).

The main advantage of this feature is that it can detect the target even if there is an overlapping of target and clutter signal. In fact, the bending energy increases because

of the overlapping between target and clutter sub-space. If this occurs, the usage of chain code identifies the curvature change. Since, the chain code represents the consecutive boundary points' angle direction, the difference from one sample point to another can be simply obtained in order to check the change of the curve. The change can be written as:

$$\Delta M_c(n) = \begin{cases} M_c(n) - M_c(n+1);\ n = 1,2,3,\ldots N-1 \\ M_c(N) - M_c(1);\ n = N \end{cases} \tag{V.24}$$

Most of the times, the maximum change will occur at the points where the target overlaps with the clutter signal. To further describe the phenomenon, we propose the following lemma.

Lemma 1: When clutter and target signal block overlaps with each other, a curvature change will take place at that location, that consequently yields maximum change of curve around the boundary contour of clutter signal block.

The abovementioned lemma is true since the clutter spectrum and target signal have distinguishing shape features. The expected clutter ridges are linearly or elliptically (due to misalignment angle) extended in Doppler-angle plane. In contrast, target signals form a pointed shape with a sufficient number of the transmitted pulse and array elements. This distinctive feature allows them to acquire maximum change at the overlapped region of the curvature all around the clutter signal block. However, the maximum change might not always be valid for the overlapping area in the case of extreme clutter environments such as vegetation and terrains. In such case, a modified PRF (~±15%) could resolve the problem.

To find the largest change over curve, one can use histogram of the boundary pixel angles (or integer number given in Table V.1) to indicate the largest change of curvature. It shows the frequency of values where most of the contour change is located.

Usually, the histogram bin range provides the information corresponding to pixel indices where the maximum curvature change is occurred. Therefore, the boundary of the target can be detected robustly.

Since, the boundary information of target is available from histogram, we can find the non-zero pixels inside the boundary contour using scan-line polygon filling (SLPF) algorithm. SLPF considers scanning the contour from left to right and finds the pixels that lie inside the boundary points. It stores all the edge information in a structured form. Slope of the current edge point index and the previous one is calculated to find the intersections between edge line and current scan line [110]. The method of finding intersection points is known as odd parity test. These points' indices are then sorted in increasing order to provide the pixels inside that boundary contour.

V.4. Deep Learning for Target Detection Using Feed Forward Neural Network (FFNN)

Since there are four features, there are tendencies to use less sophisticated machine learning algorithms such as, logistic regression, support vector machine (SVM). However, these algorithms have major problems dealing with non-linear boundary or unknown feature distribution. Logistic regression assumes linear relationship with the input and output variable of the model and thereby generalize the model without any flexibility. Thus, the model performance will not be satisfactory for the radar data associated with these features. In contrast, SVM has the ability to handle complex boundaries, but it comes at an expense of additional support vectors resulting in more time in training the model.

Considering these drawbacks, FFNN is a better choice for the radar data. A model with several hidden layers is sufficient to provide a satisfactory performance. Furthermore, the FFNN is far less complex than deep CNNs used extensively in the computer vision field. The FFNN also requires much less computational resources than CNN. Therefore, FFNN model is developed for an efficient classification of target and interference in this work.

The data collected from the aforementioned features are fed into simple feed forward neural network (FFNN) with three hidden layers. The samples of the data are normalized before feeding it to the network with a view to avoiding unexpected performance degradation. We build a model using to train, validate and test our proposed method. The details of the model can be further described in the following subsections.

V.4.1. Network Layers

The input layer starts with samples and their corresponding features. After that, there are three intermediate fully connected hidden layers. There is no rigorous set of rules to the number of hidden layers or number of processing elements inside each of the hidden layers. Since the features are not linearly separable, three hidden layers has likelihood of better performance than one or two hidden layers. In addition, more than three hidden layers could also work but the computational load will get higher than the three hidden layers setting. It is always recommended to check for the addition layers' complexity for a network since we need to ensure an efficient model. Likewise, the hidden units do not have specific protocols to follow. Although not unanimously maintained, the number of hidden units should be at least more than the input features

[111,112]. It should also be noted that, a model with fewer hidden units or processing elements (i.e., less than the input features) fail to predict the output labels and thus the probability of detection will decrease momentarily. On the contrary, large amount of processing elements increases the time to train the network. As a result, the model will be more likely prone to the memorization effect. The choice of the hidden units is arbitrary, and considering such circumstances, we experimented with different number of values. With the several trials, we chose 20, 25 and 30 units or processing elements for the first, second and third hidden layers, respectively. These layers use 'relu' activation function to introduce non-linearity in the output of each of them. The fourth or last layer predicts the probability to which the sample belongs to. The softmax activation function is popular in predicting such probabilities. Since, we have two categories (i.e., clutter, and target signal block) in our approach, the last layer has 2 hidden units to classify the expected signal blocks (target or clutter).

V.4.2. Regularization

Regularization is an important step to prevent the model from different performance loss. The procedure is used to regularize or curtail certain network coefficients to avoid memorization. Overfitting or memorization is very common problem in deep neural network (DNN). There is always a tendency from a model to memorize the pattern when it encounters a complex and variable relation between input and output layers. The memorization occurs due to the large values of the coefficients, and they need to be controlled. Thus, additional hyperparameter is introduced to reduce the variance of these coefficients. Furthermore, there are several methods such as ridge

(L2) and lasso (L1) regression to tune or control the hyperparameter that results a flexible model. The hyperparameters for the regularization are tuned empirically from the validation data. Modern DNNs utilized the combination of both regressions to avoid overfitting. The elastic net regularization (ENR) is known as the combination of ridge (L2) and lasso (L1) regression. To prevent overfitting, ENR is utilized in the second and third layer of model.

V.4.3. Optimizer and Loss

The optimizer metric is often very difficult to choose that ensures the success of the network model. The loss function needs to be differentiable to optimize receiver operating characteristics (ROC) metric. However, ROC cannot be optimized for the classification task. Thus, the loss function is used to measure the quantity to minimize the error in the weight vectors of the network. Mean squared error or crossentropy are widely used loss function in such case. However, crossentropy is more suitable with probabilities. It gauges the difference found in the probability distributions of real and predicted data. As for the optimization, there are several optimizers that can be used to adjust the weights of the networks. Mostly use standard or advanced gradient descent algorithm to reach the global minima. In this work, we utilize the RMSprop to calculate the point where the cost/loss function is minimum. This optimizer can automatically control the steps for gradient change towards the minima. Lastly, since our proposed approach deals with binary classification problem that yields probabilities, binary crossentropy is the most suitable loss function to estimate the loss.

V.5. Synthetic Data Generation

The most challenging part of airborne radar target detection is to deal with training data for clutter estimation. The collection of substantial amounts of primary data is very expensive and difficult to achieve. On the contrary, target could be located anywhere in the range of [–PRF/2, +PRF/2] and makes it the majority class. Thus, target data can be generated using a uniform or weighted sampling distribution [113] in that interval. Hence, we propose to generate synthetic data for minority class i.e., clutter subspace using synthetic minority over sampling technique (SMOTE) [114]. The method oversamples the clutter data and increase the data population synthetically without affecting the distribution of the samples. The technique uses k-nearest neighbor algorithm to create synthetic clutter data. The steps are as follows:

1. Select the number of generated sample percentage (G) as a multiple of 100. Divide it by 100 and convert it to the nearest integer i.e.,

$$G = \lfloor G/100 \rceil \tag{V.25}$$

   Here, $\lfloor \bullet \rceil$ denotes the rounding function to obtain the nearest integer.

2. Compute the k-nearest neighbors for the given minority sample matrix $\boldsymbol{M}$ with feature attributes and store the indices of them. (k could be any integer number except 1)
3. Iterate through all the minority sample of $\boldsymbol{M}$ and calculate the difference between each minority sample and randomly selected sample from its k-neighbors. The neighboring sample is chosen randomly such that the index is not equal to the index of current minority sample.

$$diff = M[i] - M[j];\ \begin{matrix} i = 1,2,\ldots S \\ j = 1,2,\ldots S \\ i \neq j \end{matrix} \tag{V.26}$$

4. Multiply the *diff* with another random value *r* (half-open interval [0.0,1.0) range) and then generate new sample by adding it to the previous minority sample.

$$S(h,:) = M(i,:) + r \times diff \tag{V.27}$$

where *h* is the index of the generated synthetic samples.

In this way, one can generate the SMOTE samples for the clutter data synthetically. It should be noted the number of nearest neighbors should be greater than 1 and less than the size of the original clutter samples.

V.6. Simulation Results for Linear Clutter Ridge

In this section, an airborne radar system is considered to simulate a ground moving target scenario in the presence of clutter. The sensor array of the system has 16 isotropic elements with 0.33m spacing between them. The wavelength of the radar is 0.67m. There are 16 pulses in one coherent processing interval (CPI). The pulse repetition frequency (PRF) is set at 300 Hz. The platform height is 9000m. It should be noted that, the simulation considers complex Gaussian distributed clutter with amplitude variation randomly changed with the aid of standard deviation in the primary detection bin. The amplitude distribution is randomly changed from $0.5\partial^2$ to $3\partial^2$ where ∂^2 is the variance of the clutter distribution in the detection bin. The variation is random, and they

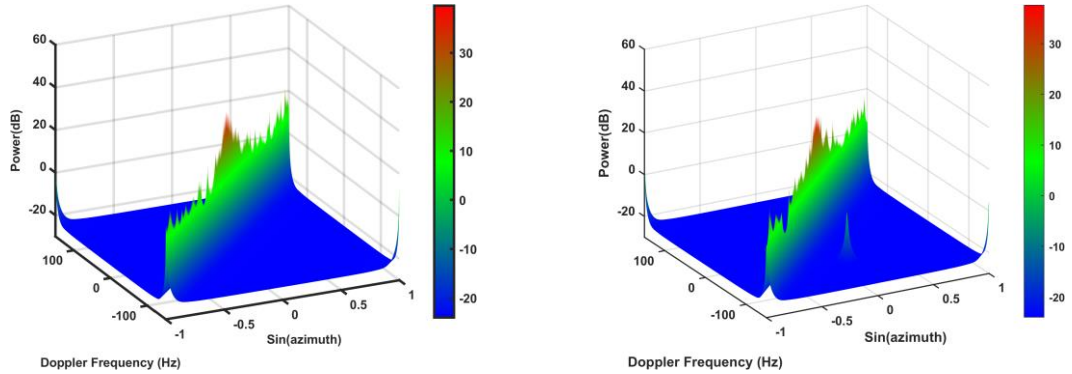

Figure V. 2 Random variation of Gaussian distributed clutter amplitude without Doppler ambiguity under: (a) H_0 hypothesis; (b) H_1 hypothesis

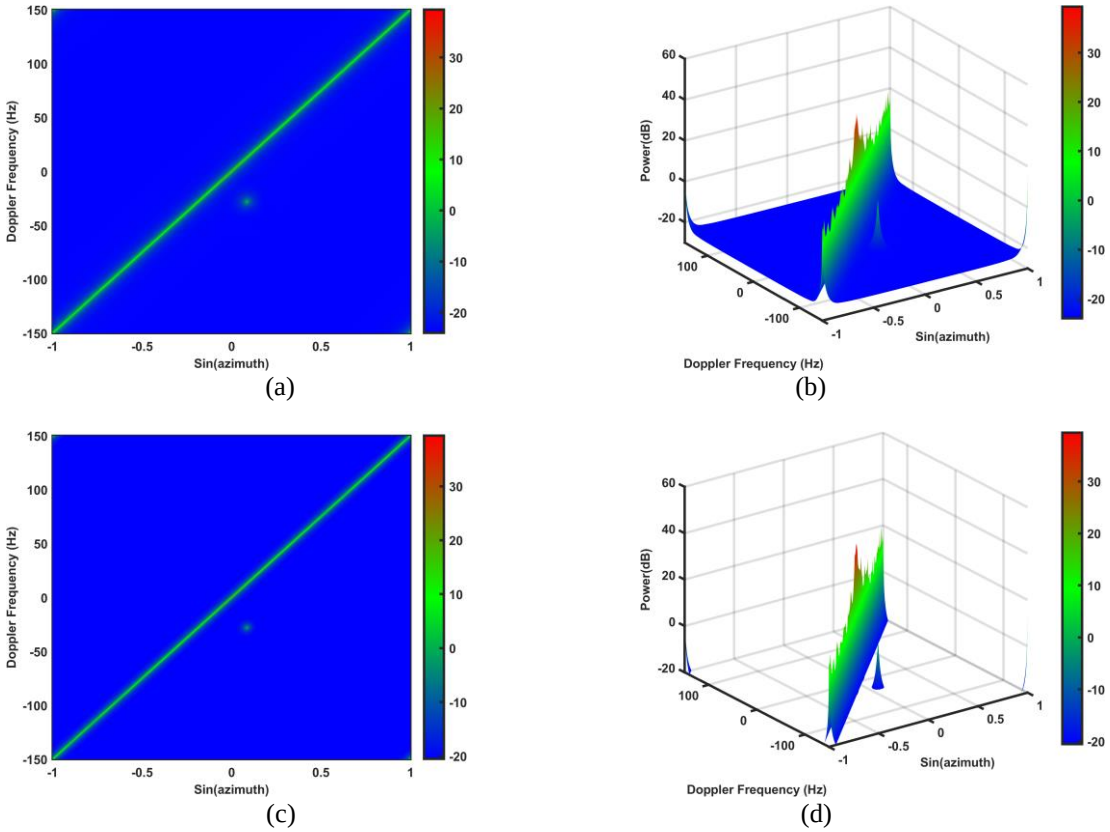

Figure V. 3 Clutter scenario with point target located at −28 Hz in Doppler frequency and angle of arrival at 5° in azimuth: (a) transformed 2D-plot; (b) transformed 3D-plot; (c) denoised radar image in 2D format; (d) denoised image in 3D format.

are evident in the Fig. V.2(a) and (b) under H_0 and H_1 hypothesis, respectively. To build

the FFNN model, we generate a dataset of 6144 samples using over-sampling technique proposed by Chawla *et.al* [114] and weighted sampling method [113] for clutter and target data, respectively. The FFNN model categorizes the samples into two labels such as, target and clutter. Both L1 and L2 hyperparameters for the ENR are fixed at 0.01. The model is then trained with 3456 samples and validated on 1152 samples for 60 epochs.

Table V.2 Different features for target and clutter in doppler unambiguous case

	To the clutter ridge		Block Size	Roundness Ratio	Bending Energy (avg.)	Target Detected?
Maximum distance from any pixel in the clutter block	9.06	Clutter Block	507.70	0.1049	0.0255	No
Minimum distance from any pixel in the Target Block	25.73	Target Block	19.24	0.9613	1.5897	Yes

Training and validation data are shuffled to improve the performance of the model in each epoch. With this radar configuration and platform velocity at 50 m/s, a single target is set at -28 Hz. The azimuth of the target is at 5° with 10km ground range from the

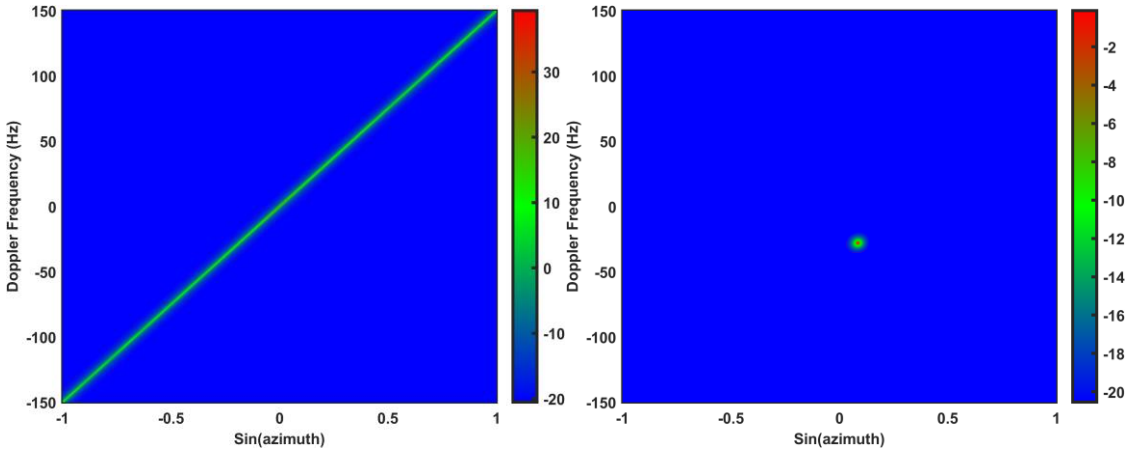

Figure V. 4 Classified clutter and target signal when they are clearly separated: (a) detected clutter block; (b) detected target block

origin. The signal to noise ratio (SNR) and clutter to noise ratio (CNR) are 0dB and 40dB, respectively. Next, the radar echo data collected from primary range bin are transformed into the angle-Doppler domain via Capon estimator (CE). The transformation provides a radar image that contains the clutter, thermal noise and possibly a target. Fig.V.3(a) and (b) shows a typical radar scenario with target Doppler frequency at −28 Hz. The denoised plot of V.2(c) and (d) prove that the noise is significantly reduced. Table V.2 shows different features for target and clutter pixels. The roundness ratio and bending energy clearly distinguishes the target and clutter subspace. These multiple features are fed into the neural network model that predicts whether the detected block is target or clutter. Fig. V.4 shows the detected clutter and target from the prediction of the FFNN. It is also evident that one can detect the target and clutter by using a single feature from the aforementioned features. However, the clutter and target are not always distinctly separated in most of the scenarios. There could be non-ideal

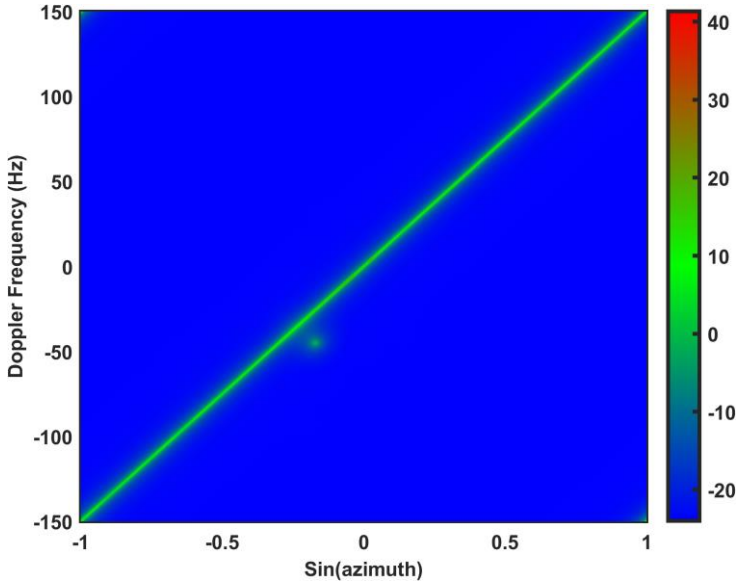

Figure V. 5 Overlapping scenario of the targe-interference classification due to low velocity target at -45 Hz in Doppler frequency with −10° angle of arrival

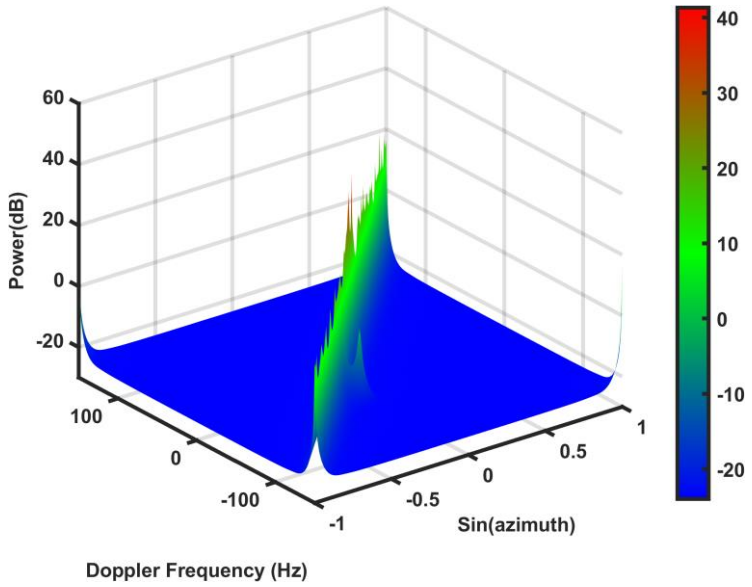

Figure V. 6 The 3D plot of observable low velocity of the overlapping target and single clutter segment under unambiguous Doppler space

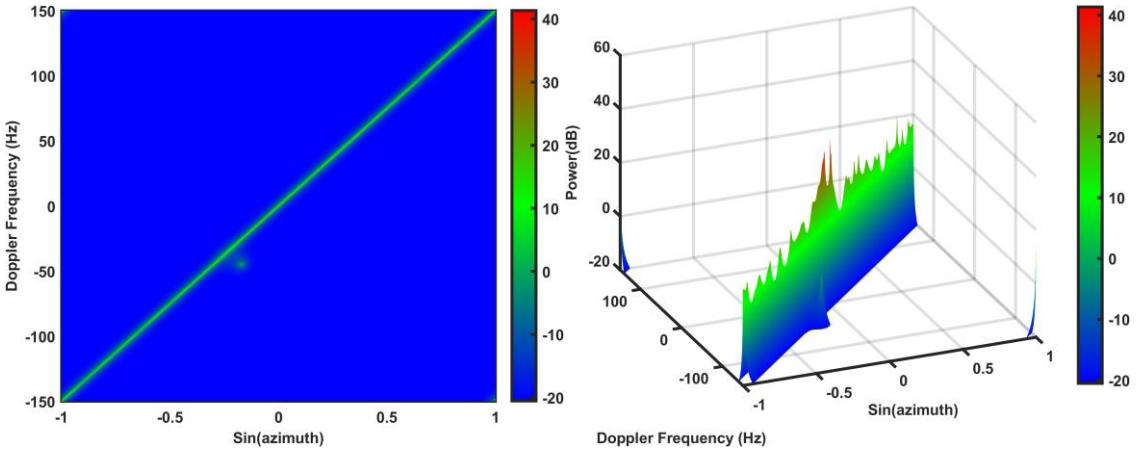

(a) (b)

Figure V. 7 The overlapped scenario of target-interference classification due to low velocity of the target at –45 Hz with azimuth angle of –10° in the angle-Doppler plane (2D plot)

situation due to low velocity of the target or low radar PRF. As a result, target and clutter block could overlap with each other. When target and clutter are merged together, multi-feature based neural network can classify the target and clutter robustly. Consequently, boundary curvature is calculated, and target is detected via maximum change discussed in

Table V.3 Overlapping Target and Clutter Features for Doppler Unambiguous Case

	To the clutter ridge		Block Size	Roundness Ratio	Bending Energy (avg.)	Target Detected?
Maximum distance from any pixel in the clutter block	27.09	Overlapped Target and Clutter Block	507.70	0.1228	0.1505	Yes

section V.3. To evaluate the curvature deviation due to overlap, we set the target at the Doppler frequency of –45 Hz. Fig. V.4 and V.5 shows the overlapping target in 2D and 3D format, respectively. Further denoising process yields the Fig. V.7 where the thermal noise is reduced, and the radar scene contains target and clutter signal only. Also, Table V.3 provides the data for feature attributes. It can be seen from the table that, although the other features are failed to show distinguishing attribute, bending energy indicates an increase in its value. Now, the bending energy of clutter block is 0.1505 which is a significant increase over the previous value of bending energy of the clutter block found in Table V.2. However, the situation is not always the same and the other feature could

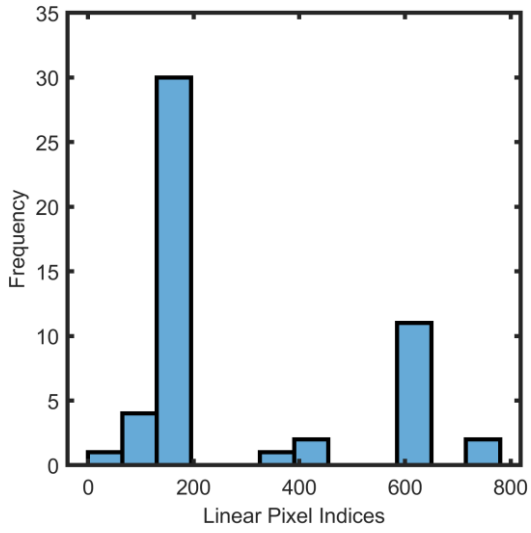

Figure V. 8 Histogram of the curvature change with the maximum change is evident owing to overlapping

show the distinctive characteristics for the classification depending on the constraints in the clutter environment.

Now, if we apply (V.24) to find the difference between the pixel angles, the change in curvature becomes evident. Figure V.8 shows the histogram of the curvature change corresponding to pixel indices. There are 773 boundary pixels detected by Moore-Neighbor

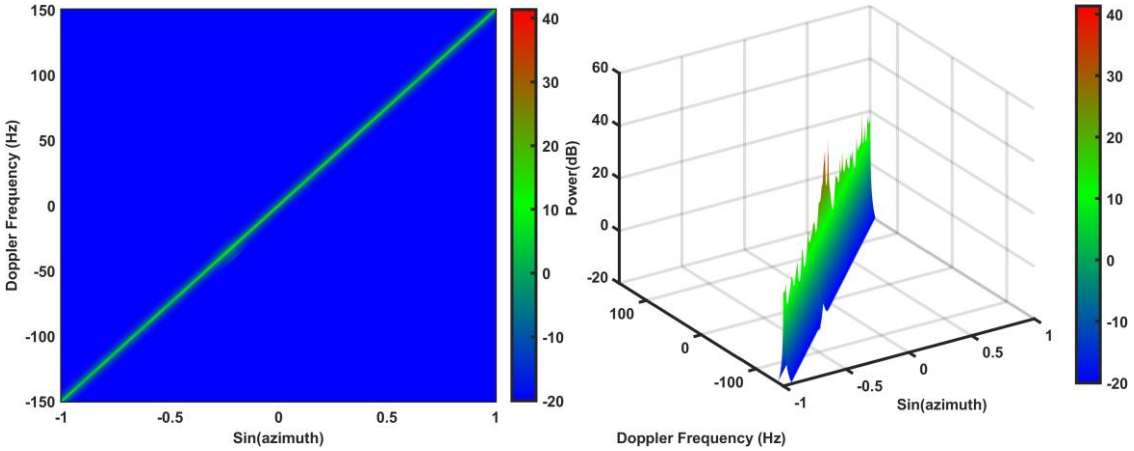

(a) (b)

Figure V. 9 The detected clutter from the overlapping inhomogeneous clutter signal in the angle-Doppler domain; (a) 2D-plot; (b) 3D-plot;

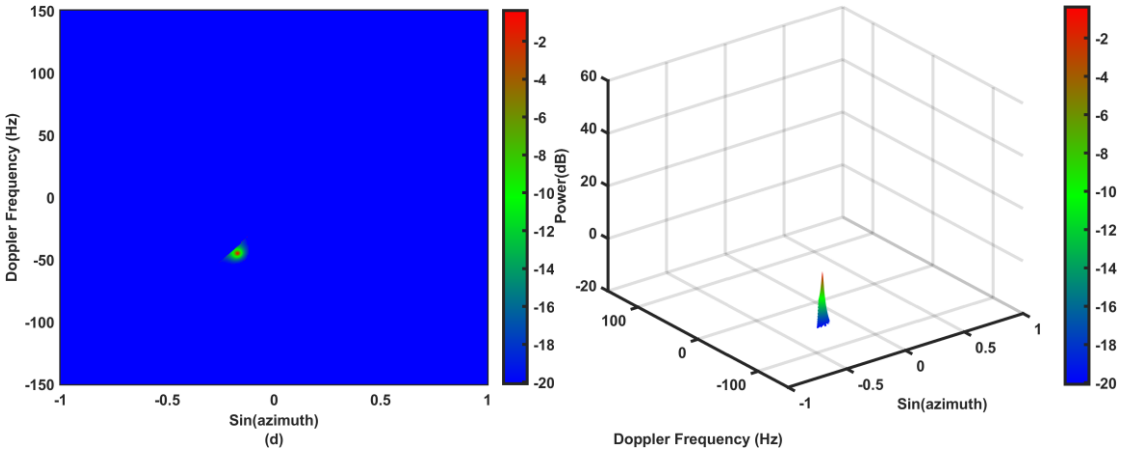

(a) (b)

Figure V. 10 The target block detected from the target-clutter overlapped scenario in the angle-Doppler domain; (a) 2D-plot; (b) 3D-plot;

tracing algorithm. 51 pixels out of them provide information about small to large change in curvature of target block. If we investigate the Fig. V.8, the maximum change of curvature is evident. The corresponding bin edges are considered to search for the indices where the maximum change has occurred.

Afterwards, SLPF algorithm is applied to find the pixels that are inside the boundary contour. Fig. V.9 and 10 show the detected clutter and target, respectively.

Likewise, for the Doppler ambiguous (DA) case, the target signal overlaps with one of the clutter segments. Since, there will be multiple clutter ridges, target subspace becomes narrower than the previous DU case. To simulate the DA case, the platform speed is increased to 100 m/s. The velocity of the platform makes the clutter subspace aliasing int the visible Doppler spectrum. As for the 100 m/s, there will be three multiple clutter segments in the angle-Doppler domain. The shape of the clutters is linearly extended. Other relevant parameters are as same as DU case. In this part of simulation, a single target is set

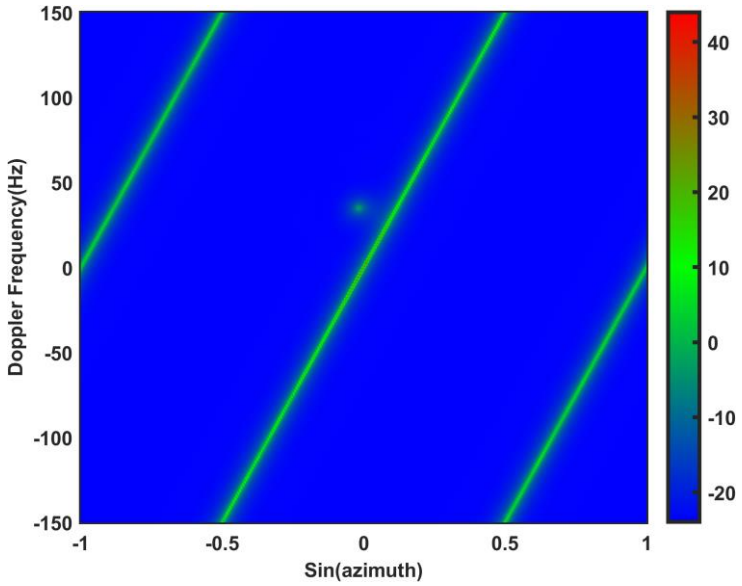

Figure V. 11 Low speed target at the Doppler frequency of 35 Hz overlaps with one of the clutters of the multiple clutter ridge (=3) in a Doppler ambiguous case.

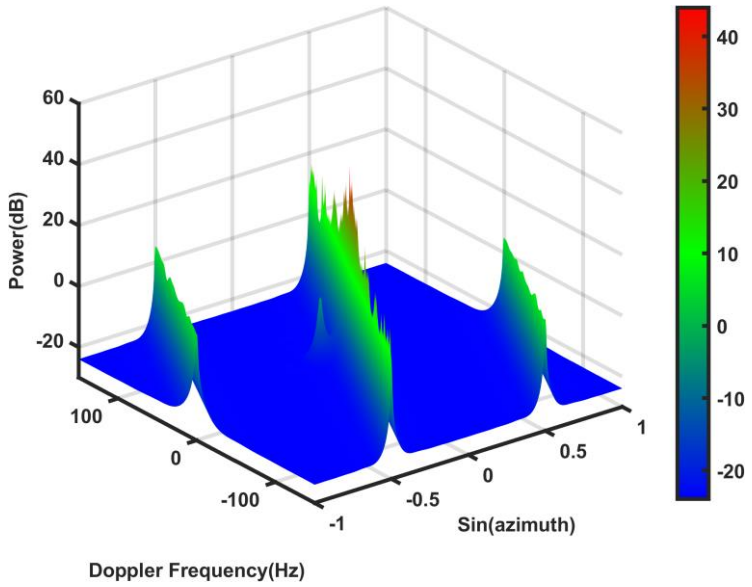

Figure V. 12 3D view of low-speed target that has merged with one of the linearly extended clutters for Doppler ambiguous case.

to be located at 35 Hz. Fig. V.11 shows that a target is closely overlapped with one of the clutter segments in the transformed domain. The scene can be clearly observable from the 3D point of view given in the Fig. V.12. The denoising process is applied to V.11 and thermal noise is mitigated as shown in the 2D and 3D-plot of V.13 and V.14, respectively.

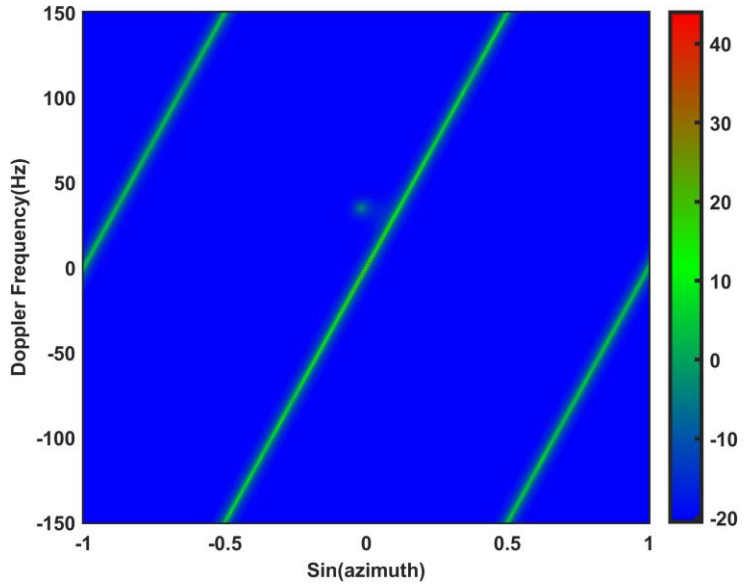

Figure V. 13 Denoising processing significantly reduced the thermal noise in the radar scene with overlapped target and clutter (2D-plot).

The FFNN predicts that the features related to this angle-Doppler image in Fig. V.14, indicates the presence of target which is merged with one of the clutter signal blocks. It implies that, the corresponding block is considered or classified as target block. Table V.4

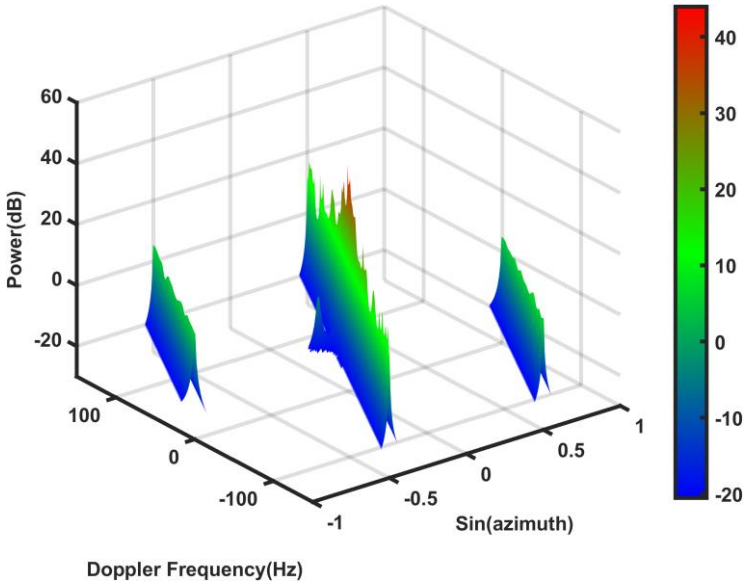

Figure V. 14 Denoised 3D-plot of radar scene with clear evidence of overlapped target and clutter segment.

Table V.4 Overlapping Target and Clutter Features for Doppler Ambiguous Case

	To the nearest clutter ridge		Block Size	Roundness Ratio	Bending Energy (BE)	Target Detected?
Maximum distance from any pixel in the Clutter Block 1	24.71	Overlapped target and Clutter Block 1	267.66	0.1528	0.1115	Yes
Maximum distance from any pixel in the Clutter Block 2	8.50	Clutter Block 2	141.42	0.2872	0.0756	No
Maximum distance from any pixel in the Clutter Block 3	8.66	Clutter Block 3	141.42	0.2872	0.1047	No

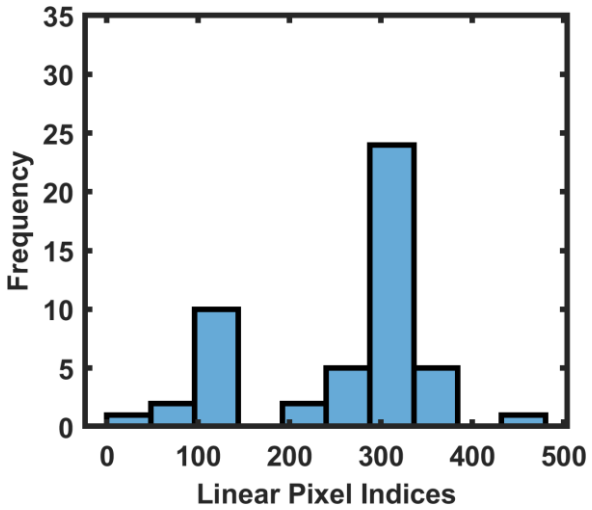

Figure V. 15 The maximum contour change observable in the histogram of the curvature changes for Doppler ambiguous case

shows the values of different feature attributes of the in multiple clutter ridge scenario. Subsequently, boundary information is extracted via chain code and maximum changes among the boundary pixels are identified using histogram like the same procedure applied in the Doppler unambiguous case.

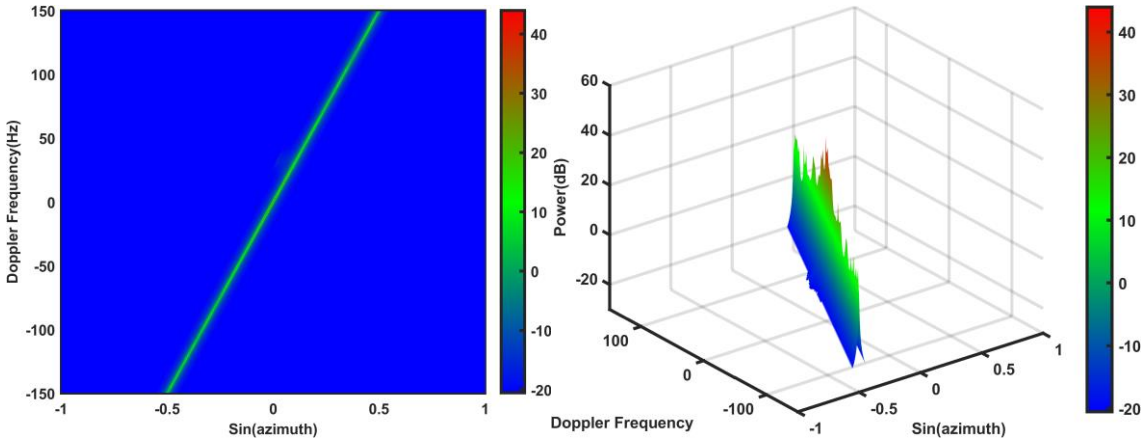

(a) (b)

Figure V. 16 The detected clutter block 1 from the target-clutter overlapped block (i.e. target block) in the angle-Doppler plane; (a) 2D-format; (b) 3D-view of the detected clutter;

Fig. V.15 shows the histogram plot of the corresponding non-zero pixels in the angle-Doppler radar image. There are 435 boundary pixels recognized by Moore-Neighbor

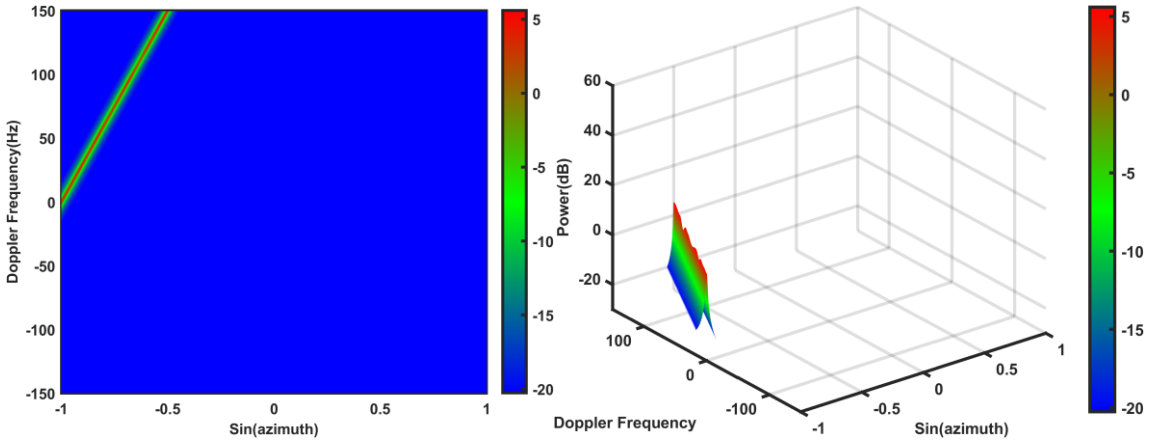

(a) (b)

Figure V. 17 The detected clutter block 2 for multiple clutter scene in the angle-Doppler plane; (a) identified clutter block 1 in 2D-format; (b) 3D-plot of the detected clutter;

tracing algorithm. 50 pixels out of them give information about the small to large change in curvature of target block. The maximum change of curvature is again observed around the contour of the target location. Now, the SLPF algorithm is applied to these boundary

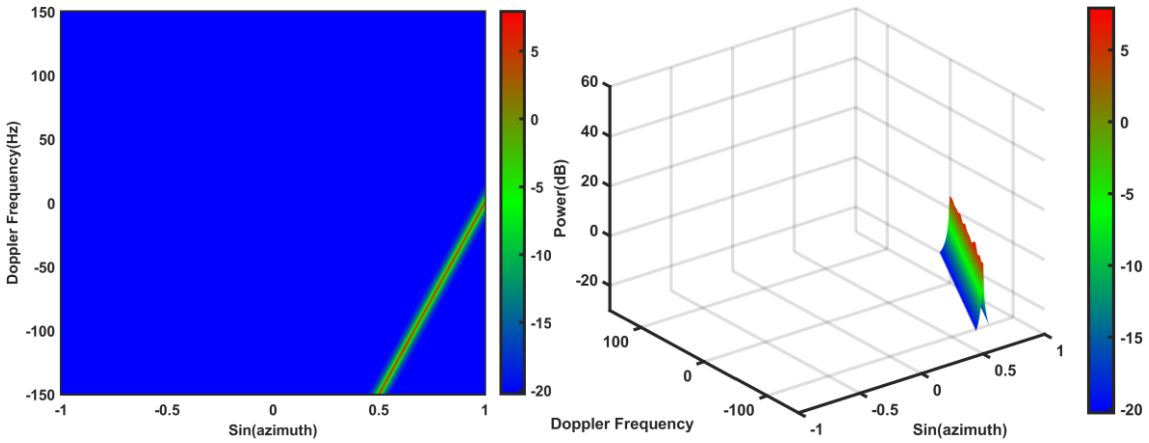

(a) (b)

Figure V. 18 The detected clutter block 3 for multiple clutter scene in the angle-Doppler plane; (a) identified clutter block 1 in 2D-format; (b) 3D-plot of the detected clutter;

points. The algorithm then detects all the non-zero pixels of the target. Fig. V.16 shows the detected clutter signal block that was merged with the target pixels. The clutter signal are segmented based on the SLPF algorithm which is displayed in V.16(a). Whereas the block

shown in Fig. V.16(a) is predicted as a clutter block by the FFNN model. Fig. V.16(b) displays the 3D-plot of the detected clutter block. The remaining block is also identified as a clutter block via the neural network model as shown in Figure V.18. Now, the merged target signal is segmented based on the SLPF algorithm using the boundary curvature information. Fig. V.19 shows the detected target that has merged with the clutter signal. In

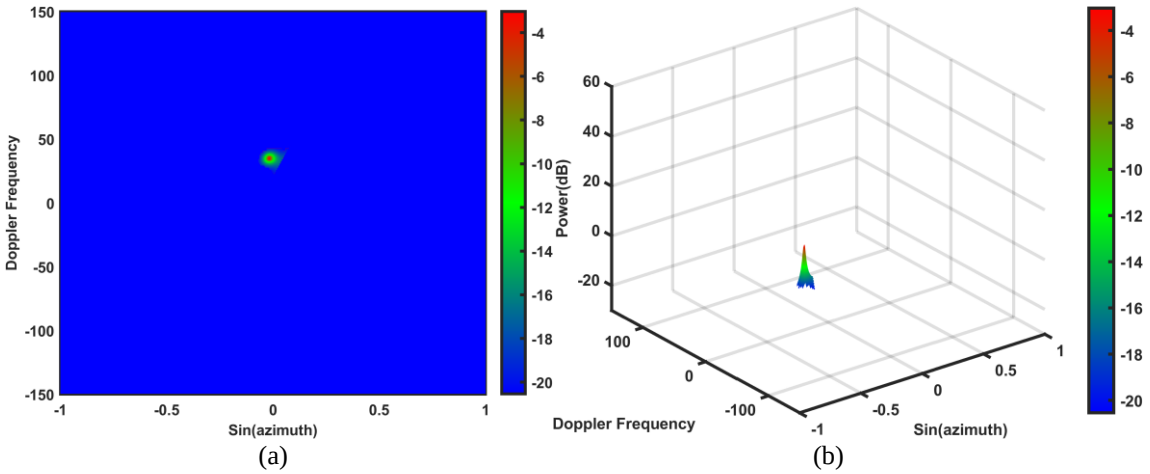

(a) (b)

Figure V. 19 The detected target from the target-clutter overlapped block (i.e. target block) in the angle-Doppler plane; (a) 2D-format; (b) 3D-position of the detected target;

Table V.5 Confusion matrix of multi-feature approach

		Predicted Signal	
		Clutter	Target
Actual Signal	Clutter	100%	0%
	Target	5.1%	94.9%

Fig. V.18(b), it can be seen some of the clutter pixels which are merged with the target are also present in the detection scene.

The deep learning model also has successfully classified target and clutter with few misdetections. The training and validation data helps the model tune to the appropriate values for the hyperparameters to increase the accuracy. 1536 test samples are considered to evaluate the network for the classification. Table V.5 shows the confusion matrix of

classified target and clutter. The misdetections are due to some targets which are totally merged with the clutter without showing much boundary curve variation.

V.7. Simulation Results for Elliptical Clutter Ridge

The proposed method is also applicable to the non-linear clutter ridge. From chapter IV, we know that an alignment error angle will be introduced if the direction of platform velocity is not aligned with antenna array axis. The phenomenon mainly occurs in side-looking antenna or a scanning antenna that rotates continuously. The scanning antenna frequently suffers from this alignment error. The misalignment introduces more occupied clutter subspace in the angle-Doppler space. The proximity feature alone could detect the targets when they are not merged with the non-linear clutter ridge. However, when they overlap, multiple features along with proximity feature are needed to boost up the non-adaptive approach. The multi feature based FFNN method has the capability to detect the target with overlapped clutter even when the clutter ridge is non-linear such as, elliptical clutter.

In this section, simulation results for elliptical shaped clutters are considered. The airborne radar system has the same type of radar parameters. There are 16 isotropic antenna elements and 16 coherent pulses for one CPI. The CNR and SNR are 40 and 0dB, respectively. The alignment error angle is considered to be 12°. The target is set 33 Hz in Doppler frequency. The selected location for the target is overlapping with the non-linear clutter ridge. Now the radar echo data is again transformed into Doppler domain via Capon estimator with fine resolution. Fig. V.20 shows the 2D image scene of merged target and clutter. The overlapped target is more comprehensible in the 3D image in the Fig. V.21.

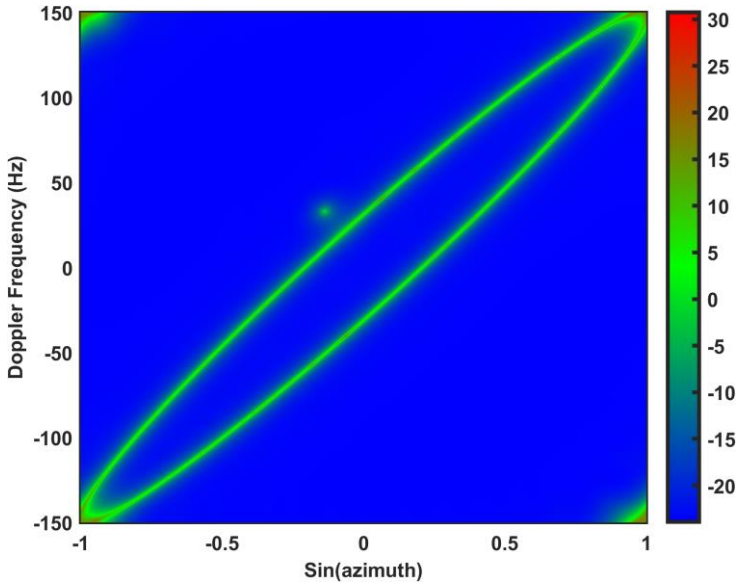

Figure V. 20 Non-linear clutter occupying the observable Doppler spectrum with a point target at 33 Hz and −8° azimuth

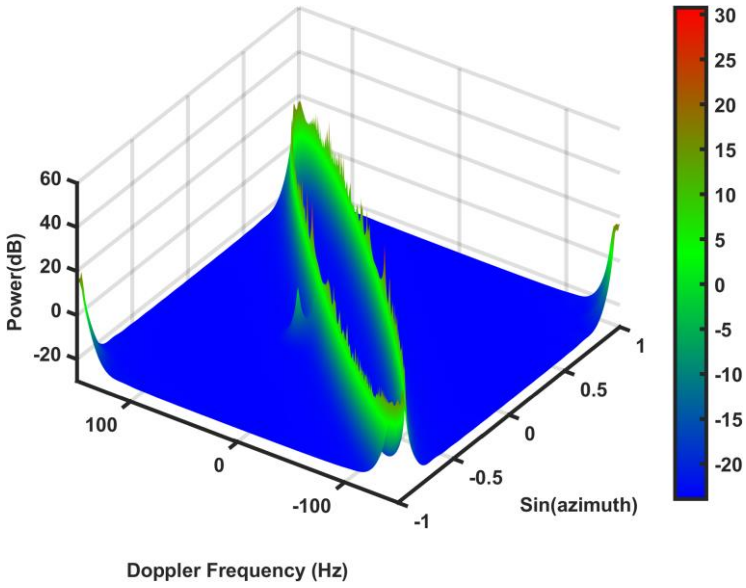

Figure V. 21 3D radar image of the randomly changed Gaussian distributed elliptical clutter ridge and an overlapped target

The next step is to denoise the target and clutter subspace to advance for the classification step. The denoising process removes the thermal noise and there will be

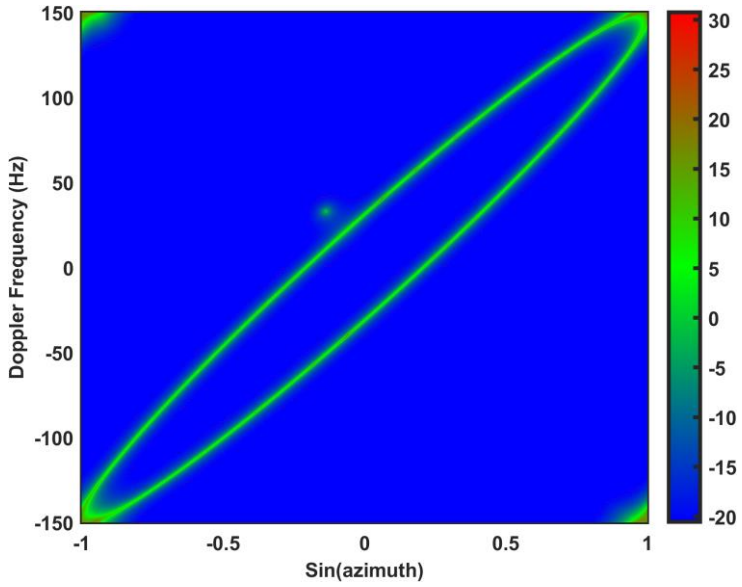

Figure V. 22 Denoised radar image of the elliptical clutter with misalignment error of 12° due to aircraft velocity and antenna array for Doppler unambiguous case

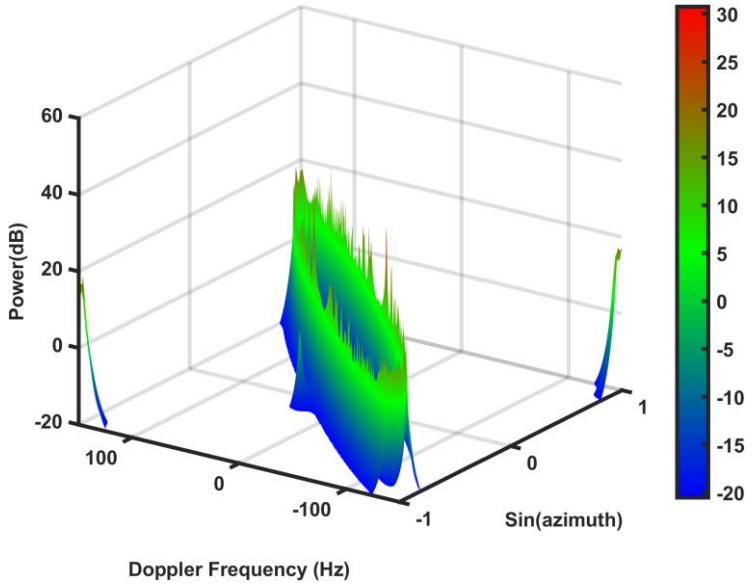

Figure V. 23 Denoised 3D radar image of the elliptical clutter for Doppler unambiguous case where target and clutter are connected and overlapped with each other

only and clutter and target. Fig. V.22 and V.23 show the denoised radar image that clearly indicate the overlapping situation.

After denoising, the target, and clutter are visible in Doppler space. There are also some non-zero edge pixels due to grating lobes. They can be easily removed as those pixels are located at the edges of the angle-Doppler space. Next, the multi feature approach is performed to distinguish the signal blocks. HK algorithm is applied and the there will only one signal block. The feed forward neural network recognizes the block as a target block. The features are calculated and found as:

- The proximity distance is calculated from the major axis of the non-linear clutter ridge.
  - The maximum distance from the non-zero pixel to the major axis is found to be 43.71
  - The minimum distance from the overlapped pixels to the major axis is calculated as 30.70.
  - The maximum distance from the non-linear clutter ridge pixel to the major axis is 25.43
  - The minimum distance from the non-linear clutter ridge pixel to the major axis is 21.46
- The block size for the detected block is measured as 507.70
- The roundness ratio is found to be 0.2154.
- The bending energy is calculated as 0.1141.

Then FFNN model is built based on the features calculated from 1500 radar image scenes. 500 images are used for validation to build the model. The model has same hyperparameters tuned empirically from the training and validation data. The aforementioned test sample has been run through the model and classified as a target

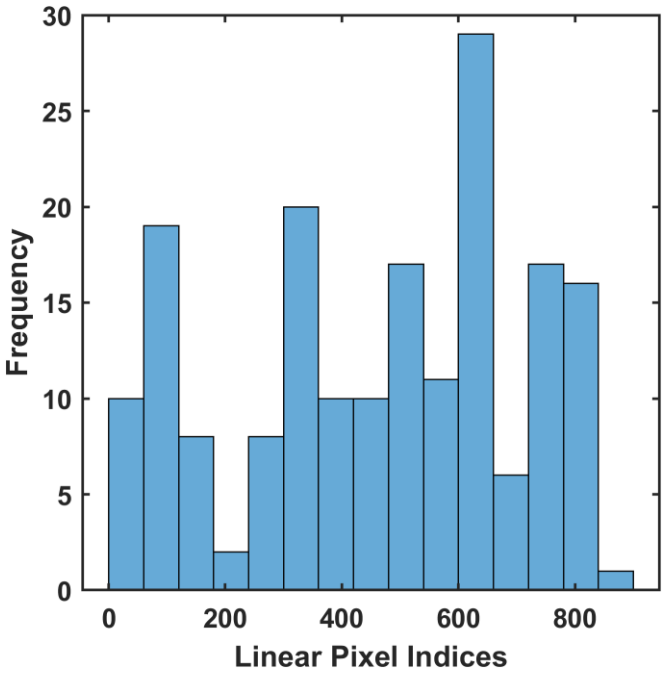

Figure V. 24 Maximum boundary variation observed from the pixel indices 600 to 660 in the histogram plot

block since the target is merged with the clutter signal. Next, the boundary information is processed with the aid of histogram plot. The histogram clearly indicates maximum

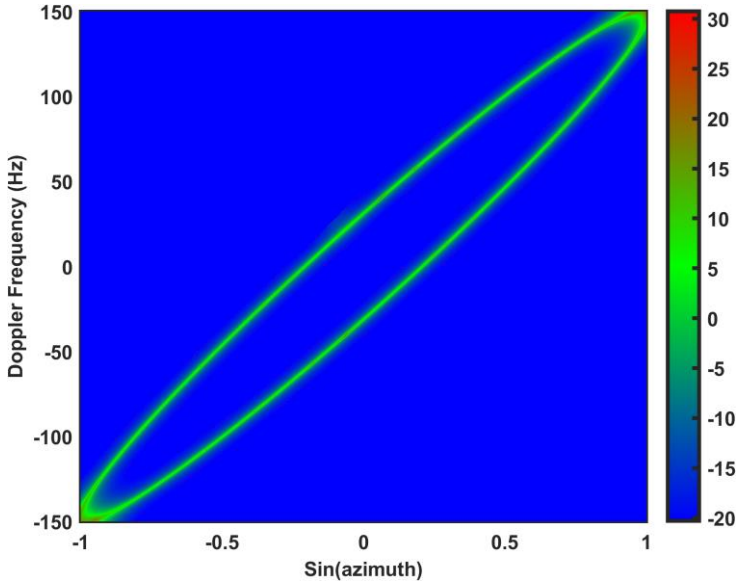

Figure V. 25 Detected non-linear clutter ridge after the segmentation process performe with boundary information from the merged target block predict by FFNN

frequency where target overlaps with clutter. There are 849 boundary pixels found by the tracing algorithm. The chain code maps the pixels coordinate into corresponding angles that ultimately represent the direction change. Fig. V.24 displays the frequency vs. pixel indices for the boundary curve variation using the Moore-neighbor tracing algorithm. 184 pixels out of them show small to large variation of contour curvature.

The pixels are converted to linear indices to obtain the group of pixel which shows maximum frequency or maximum number of change in the boundary. The maximum boundary change is found in the indices of 600 to 660. With the boundary pixels, polygon filling algorithm is applied to find the non-zero pixels inside the boundary. If the pixel inside the boundary is also the member of the radar scene, then it is included in the detected group of target pixels. Some morphological operation is also used to remove some outer pixels from the boundary. These outer pixels could exist due to some criterion error.

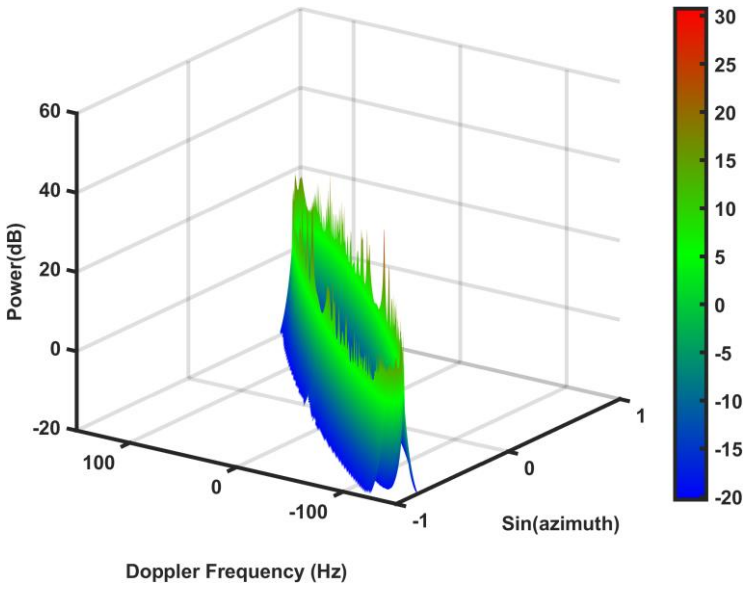

Figure V. 26 Detected non-linear inhomogeneous clutter with 12° alignment error angle (i.e., elliptical shaped clutter) with Gaussian distributed randomly varied amplitude from the merged target block predict by FFNN (3D-plot)

SLPF algorithm is then applied to segment the target pixels from the clutter. Fig. V.25 shows the detected clutter signal that has been separated from the boundary contour information. The 3D plot of figure V.26 displays the detected clutter.

Likewise, the target pixels are also identified the proposed method using the same approach. Since the target overlaps with the clutter, some of the clutter pixel could be

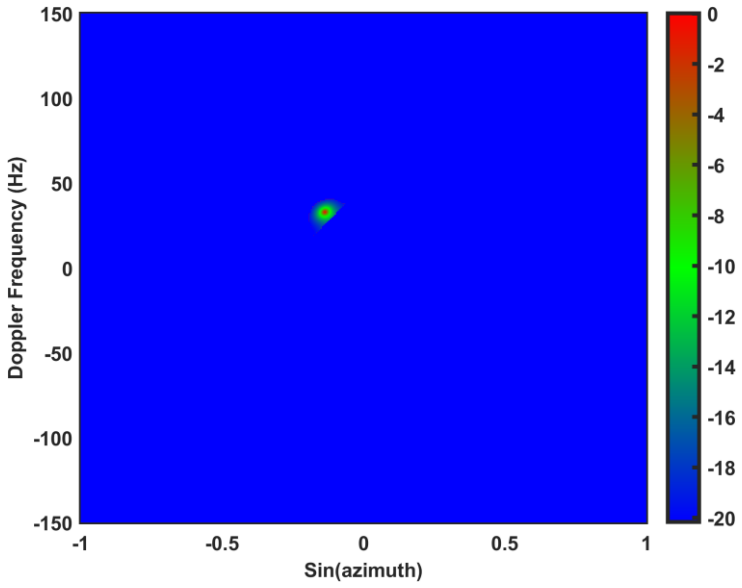

Figure V. 27 Detected target signals at 33 Hz Doppler frequency from the merged target-clutter scenario using boundary curvature information and single line polygon algorithm

included with target signal. As we know, the target forms a pointed shape with effective spread in both angle and Doppler space. The point could include some additional pixels of clutter. However, the target is still be detected from the overlapped scenario of the inhomogeneous clutter. Fig. V.27 shows the 2D image of detected target from the ground clutter environment. The 3D plot of the image also shows the detected target under this Doppler unambiguous scenario.

The simulation result effectively verifies the detectability of target even under the overlapped case of the target. The target could locate inside or outside of the clutter ridge. In such case, the designed algorithm will perform well. That being said, the combination

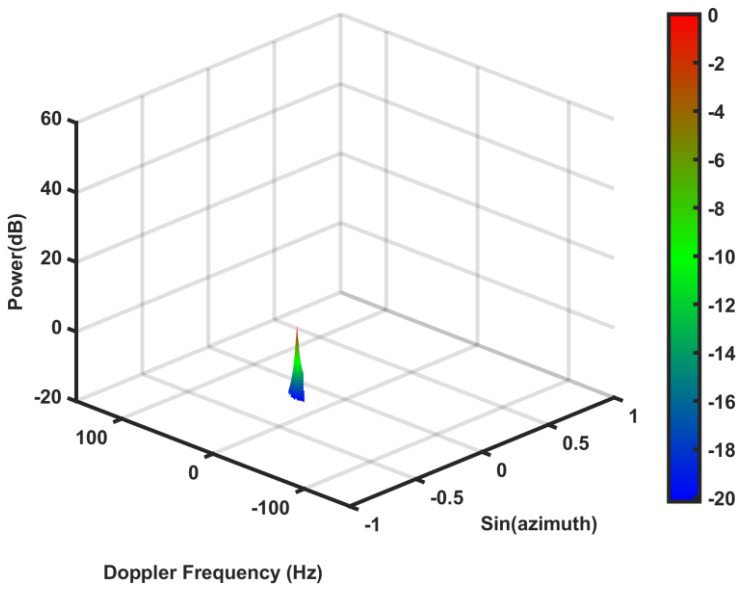

Figure V. 28 The 3D view of detected target pixels (some of the pixels are totally merged with clutter) at 33 Hz of Doppler frequency for non-linear clutter ridge merged with the target

of four features will robustly detect the target and separate it from the clutter if it is merged with the clutter from the inside. The alignment error angle could range from small to large angle. As the error angle increases, it could eventually be a circle. The more the space inside the non-linear clutter, there are more likely to be a chance that target is inside. The small error angle makes the detection more challenging. However, as the angle increases, the chance of the target location inside the clutter will get very high. Thus, the detection probability decreases as the alignment error angle decreases to a small value ($0° < \psi_m < 4°$).

V.8. Performance Comparison

Since the method introduced in this chapter is basically a non-adaptive approach, it is completely unfair to compare with any adaptive approach. Furthermore, the method is feature based technique that does not require any clutter distribution estimation and filtering process. While the adaptive approaches need to estimate the clutter with sufficient clutter samples and then filter out the clutter components. Obviously, conventional adaptive approach fails to recognize and detect inhomogeneous clutter in both cases. In contrast, this feature-based approach will outperform the adaptive method even in the simple circumstances. Therefore, the proposed method is compared with another image feature-based technique known as beam-Doppler image feature recognition (BDIFR) [92]. The comparison is performed with a Doppler ambiguous scenario with same radar parameters. The SNR and CNR are fixed at 0 and 40dB, respectively. The BDIFR method applied RG algorithm to identify the connected region and then detects the target based on the block size feature. The simulation begins with a transformed radar image scene where

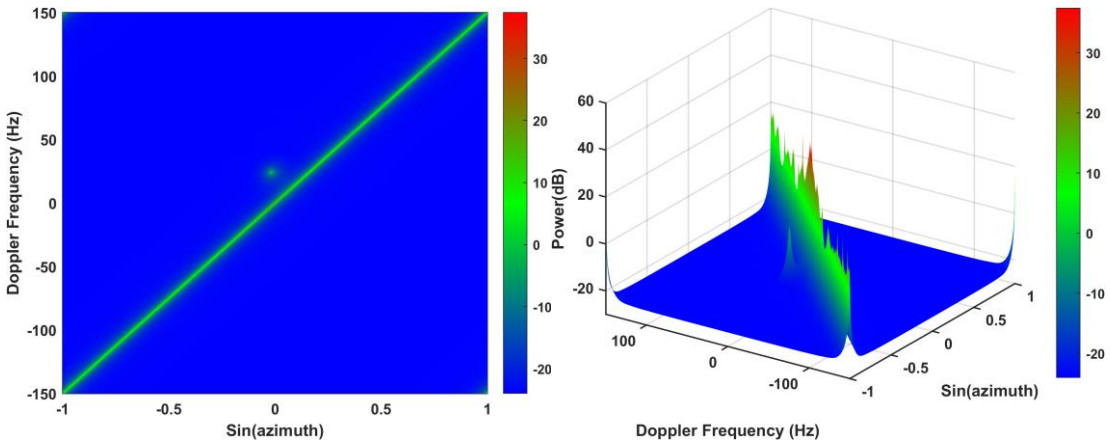

(a) (b)

Figure V. 29 The MV transformed radar image for the performance comparison between the introduced feature-based approach and BDIFR method

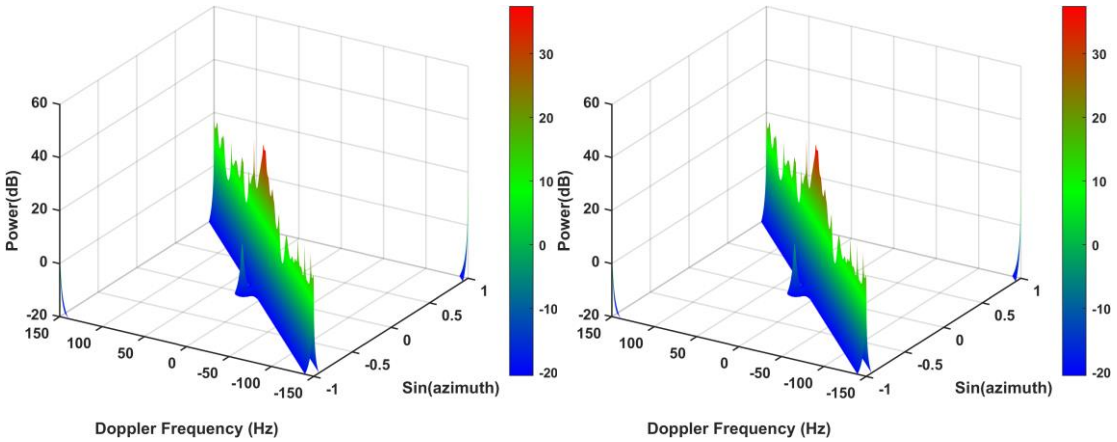

Figure V. 30 Denoised 3D-plots for both of the methods: (a) the proposed approach; (b) the BDIFR method

the target Doppler frequency is set at 24 Hz with −1° in azimuth. Fig. V.29 shows the MV transformed radar data with a single clutter ridge. Both methods remove most of the white noise successfully. Fig. V.30 displays the denoised scenes for both methods. The proposed method then applied HK algorithm to obtain the connected region. On the contrary, the BDIFR method used RG algorithm to get the connected block.

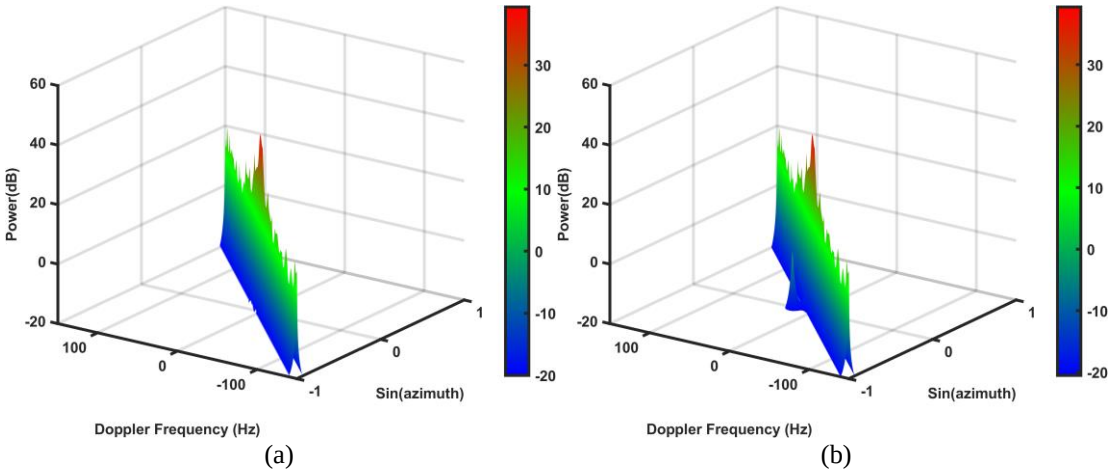

Figure V. 31 Classification of clutter for comparison: (a) Detected clutter block of the proposed method; (b) target signal merged with clutter in BDIFR method

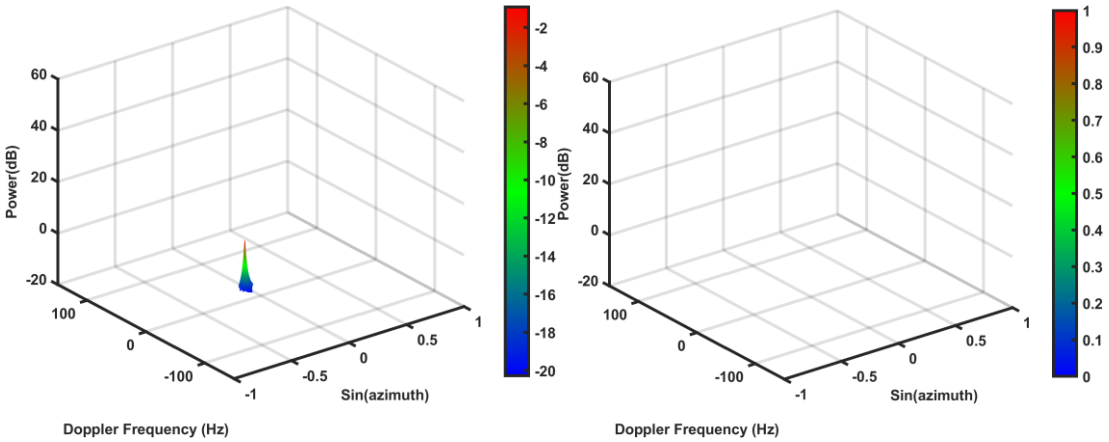

Figure V. 32 Target block detection under H_1 in the angle-Doppler scene : (a) Detected target block of the proposed method; (b) target not detected by BDIFR method

Table V.6 Performance comparison

			Target Detected?
BDIFR	Block Size	507.70	No
Proposed Method	Block Size	507.70	Yes
	Maximum distance to the Clutter Ridge	30.80	
	Roundness Ratio (RR)	0.1028	
	Bending Energy (BE)	0.1009	

Next, the proposed approach extracts the four features such as, proximity to clutter ridge, block size, roundness ratio and bending energy and then test the FFNN model to detect the radar image in V.32(a) as target block. Subsequently, information about boundary contour variation is processed to detect all of the target pixels and detect the target. In contrast, BDIFR approach uses the block size feature to detect the block. The feature falsely classifies the block as clutter instead of target. Fig. V.31 and 32 demonstrate the stark difference between two approaches for target detection. The comparison clearly shows that the proposed method outperforms the BDIFR method in the case of overlapping state. Table V.6 shows the feature comparison between the proposed and BDIFR method. As can be seen from the table, BDIFR method cannot detect the overlapped with the block

size of 507.07. Thus, it falsely recognizes the target as clutter. In contrast, the multi-feature method utilized the geometric feature values of target and interferences along with proximity feature and block size. Hence, the proposed method detects the overlapped target and recognizes it with the target boundary and pixels inside that boundary.

V.9. Summary of Chapter V

An innovative multi-feature based deep learning approach is introduced in this chapter. The method does not depend on the availability of secondary clutter samples. In fact, the data collected from the primary detection bin is sufficient for this approach. Furthermore, the neural network model is appropriate choice for these features since the feature distribution is non-linear and unknown prior to the processing of the algorithm. The method also requires no statistical data about clutter amplitude variance and detects the target both in overlapping and non-overlapping scenarios of clutter spectrum. The detection approach is equally applicable to the non-linear clutter and therefore ensures its viability in real inhomogeneous clutter environment. Jammer is not considered in this machine learning approach. Since the jammer and clutter will show connected property to each other in the radar image, this deep learning feature-based method can also classify the target and interference from such situation. The method also outperforms the previous non-adaptive feature-based methods since it makes decision about target from multiple independent and uncorrelated features. Also, most adaptive [5,11-27] and knowledge-aided approaches [33-49] fail to detect the overlapping target since the filters erroneously remove the target pixels as the clutter echo. In contrast, the multi-feature method detects the overlapping target from the proximity and geometric features. The deep learning model also increases the robustness of the method to recognize the target in the angle-Doppler domain. Furthermore,

traditional methods such as STAP and Reduced dimension techniques suffer performance deterioration for random clutter amplitude and misalignment owing to the velocity direction of the airborne platform and its antenna array. In comparison, this detection method is independent of clutter amplitude and misalignment error and thus detects targets successfully in such inhomogeneous environments.

VI. CONCLUSION AND FUTURE WORK

VI.1. Conclusion

In this dissertation, innovative approaches have been devised to detect the target effectively from the ground clutter environment. Radar interference such as clutter and the receiver noise known as white noise are considered to be the obstacles in this work. The work mainly demonstrates the effectiveness of the proposed detection technique under various real world clutter scenarios such as, Doppler ambiguity, velocity misalignment etc. The mathematical and theoretical aspects of these methods are also shown that proves to be better interference suppression technique over the other conventional and feature based approaches. The target-interference classification techniques proposed in this dissertation are encapsulated as follows:

Chapter III is established on the concept of innovative clutter-proximity feature that describes a machine learning approach to learn about the detection threshold. Once the detection threshold is well approximated, the clutter and target could be classified based on this feature. The radar echo data is transformed via MV method with the few amount of samples from primary detection bin. The denoised image is then processes for proximity

feature. The clutter distribution does not need to be homogeneous for the detection approach. It implies that, the clutter feature will work well in inhomogeneous clutter environment. Moreover, the simulation results validate the effectiveness of the proposed approach. The method also outperforms from typical or conventional adaptive approach.

In chapter IV, a slightly modified proximity feature approach is introduced to suppress the non-linear clutter and thereby detect the target. Since the clutter is non-linear, the major axis parameter is utilized to classify the target and clutter pixel in the angle-Doppler plane. The two proximity detection thresholds are employed to recognize the target. The first threshold works when the target pixels are located outside the clutter and later one works when the target is inside the H_1 subspace of the clutter. The simulation result validates the method with an inhomogeneous DU clutter to detect the target successfully.

In chapter V, an effective multi-feature based deep learning approach is developed to detect the target and suppress the clutter without any adaptive filters. The MV transformed radar data are then utilized and some image as well as geometric features are extracted from the transformed angle-Doppler domain. These feature data are processed with FFNN model that can predict target even when it is low speed. The low-speed targets generally overlap with clutter. The proposed approach can successfully detect the overlapping target and suppress the clutter. The method is not affected by the inhomogeneity of the clutter environment. Since this is a multi-feature approach, it works equally well when the clutter is no longer linearly extended. Furthermore, the proposed method works very well compared to the previous image feature-based techniques.

Nevertheless, there are some pitfalls of these proposed detection techniques that need to be considered. The first problem of these machine learning techniques is the lack of training data. Airborne radar's measured data is very expensive and difficult to achieve. The proposed methods explore the detection performance on simulated data. However, the simulated data does not always consider all plausible scenarios and hence the detection probability deteriorates relating to real world environments. Secondly, some other environments such as, Doppler ambiguous case for velocity misalignment phenomenon, extreme intrinsic clutter motion are not considered in this work. These real world effects could have some adverse effects on the proposed methods.

VI.2. Future Work

Having those constraints in my mind, I would like to extend the research for the multi-feature-based machine learning approach. There are several future approaches that could be employed for better suppression in the real-world clutter environment. They can be explained briefly as follows:

- *Transfer Learning:* Since the real radar data is not readily available, transfer learning with few amounts of training data can be effectively utilized to further improve the performance of the multi-feature based machine learning approach. The transfer of knowledge could be obtained from the same type of radar system or different radar operating in different weather or other turbulence of the environment. The transfer learning will be very effective in the field of ground moving target detection.

- *Adding More Features:* The performance of the multi feature based approach improves greatly due to the different feature attributes. The more feature is utilized, the detection probability of target increases. More image and geometric features such as, number of the corner, Euler characteristic, axial ratio, aspect ratio, image entropy etc. could be utilized along with the aforementioned features to classify target and clutter robustly in real clutter scenario.

REFERENCES

1. G.W. Stimson, Introduction to Airborne Radar, Mendham, NJ, SciTech publishing, inc. , 1998, pp. 25–33.

2. M. I. Skolink, Introduction to Radar Systems, 3rd ed. NY, USA, McGraw-Hill, 2001, pp. 114–117, 139–182.

3. L. N. Ridenour, Radar System Engineering, MIT Radiation Laboratory Series, 1st ed. NY, USA, McGraw-Hill,1947, pp. 116-124.

4. Nanzhi Jiang, Renbiao Wu and Jian Li, Super resolution feature extraction of moving targets, in *IEEE Transactions on Aerospace and Electronic Systems*, vol. 37 no. 3, pp. 781–793, July 2001.

5. J. Ward, Space-time adaptive processing for airborne radar, MIT Lincoln Lab., MA, USA, Dec. 1994, Tech. Rep. 1015.

6. E. C. Barile, R. L. Fante and J. A. Torres, "Some limitations on the effectiveness of airborne adaptive radar," in *IEEE Transactions on Aerospace and Electronic Systems*, vol. 28, no. 4, pp. 1015-1032, Oct. 1992.

7. G. Anderws, Airborne radar motion compensation technique, Evaluation of TACCAR, NRL Report NRL-7407, USA, Apr. 1972.

8. Y. Kwag, M. Choi, C. Jung, J. Bae and I. Jeon, "An Adaptive Compensation of Moving Clutter Doppler Shift for Helicopter MTD Radar," 2006 CIE International Conference on Radar, 2006, pp. 1-4.

9. R. M. Cooper, The impact of TACCAR on STAP algorithm convergence, *IEEE International Radar Conference*, 2005., 2005, pp. 447-452.

10. Zhe Geng, S.M.A. Motahari, Hai Deng, and B. Himed, "Ground moving target detection for airborne radar using clutter doppler compensation and digital beamforming", in *Microwave and Optical Technology Letters*, vol. 60, no. 1, pp. 101-110, 2018.

11. L. Brennan, J. Mallett and I. Reed, Adaptive arrays in airborne MTI radar, in *IEEE Transactions on Antennas and Propagation*, vol. 24, no. 5, pp. 607-615, September 1976.

12. I. S. Reed, J. D. Mallett and L. E. Brennan, Rapid Convergence Rate in Adaptive Arrays, in IEEE Transactions on Aerospace and Electronic Systems, vol. AES-10, no. 6, pp. 853-863, Nov. 1974.

13. R. Nitzberg, An effect of range-heterogeneous clutter on adaptive Doppler filters, in *IEEE Transactions on Aerospace and Electronic Systems*, vol. 26, no. 3, pp. 475-480, May 1990.

14. Y. Wu, T. Wang, J. Wu and J. Duan, Training Sample Selection for Space-Time Adaptive Processing in Heterogeneous Environments, in *IEEE Geoscience and Remote Sensing Letters*, vol. 12, no. 4, pp. 691-695, April 2015.

15. R. Klemm, Introduction to space-time adaptive processing, IEE Colloquium on Space-Time Adaptive Processing (Ref. No. 1998/241), London, UK, 1998, pp. 1/1-111.

16. R. Li, Y. Wang, Z. He, J. Li and G. Sun, "Minimum redundancy space-time adaptive processing utilizing reconstructed covariance matrix," *2017 IEEE Radar Conference (RadarConf)*, 2017, pp. 0722-0726.

17. B. Friedlander, "A subspace method for space time adaptive processing," in *IEEE Transactions on Signal Processing*, vol. 53, no. 1, pp. 74-82, Jan. 2005.

18. W. Zhang, Z. He, J. Li, H. Liu, and Y. Sun, A Method for Finding Best Channels in Beam-Space Post-Doppler Reduced-Dimension Stap, in *IEEE Trans. Aerosp. Electron. Syst.*, vol. 50, no. 1, pp. 254–264, Jan. 2014.

19. R. Klemm, Adaptive airborne MTI: An auxiliary channel approach, IEE Proc. F–Commun. Radar Signal Process. UK, vol. 134, no. 3, pp. 269–276, ,June 1987.

20. R. DiPietro, Extended factored space-time processing for airborne radar systems, in Conference Record of the 26th Asilomar Conference on Signals, Systems & Computers, Pacific Grove, CA, USA, 1992 pp. 425–430.

21. H. Wang and Lujing Cai, On adaptive spatial-temporal processing for airborne surveillance radar systems, in *IEEE Transactions on Aerospace and Electronic Systems*, vol. 30, no. 3, pp. 660-670, July 1994.

22. Y. Guo, G. Liao and W. Feng, Sparse Representation Based Algorithm for Airborne Radar in Beam-Space Post-Doppler Reduced-Dimension Space-Time Adaptive Processing, in IEEE Access, vol. 5, pp. 5896-5903, 2017.

23. Z. Li, Y. Guo, Y. Zhang, H. Zhou and G. Zheng, Sparse Bayesian Learning Based Space-Time Adaptive Processing Against Unknown Mutual Coupling for Airborne Radar Using Middle Subarray, in *IEEE Access*, vol. 7, pp. 6094-6108, 2019.

24. Z. Yang, X. Li, H. Wang and W. Jiang, On Clutter Sparsity Analysis in Space–Time Adaptive Processing Airborne Radar, in IEEE Geoscience and Remote Sensing Letters, vol. 10, no. 5, pp. 1214-1218, Sept. 2013.

25. S. Sen, "Low-Rank Matrix Decomposition and Spatio-Temporal Sparse Recovery for STAP Radar," in IEEE Journal of Selected Topics in Signal Processing, vol. 9, no. 8, pp. 1510–1523, Dec. 2015.

26. S. Han, C. Fan and X. Huang, A Novel STAP Based on Spectrum-Aided Reduced-Dimension Clutter Sparse Recovery, in IEEE Geoscience and Remote Sensing Letters, vol. 14, no. 2, pp. 213-217, Feb. 2017.

27. W. Zhang, Z. He and H. Li, Linear Regression Based Clutter Reconstruction for STAP, in *IEEE Access*, vol. 6, pp. 56862-56869, 2018.

28. A. Haimovich, The eigencanceler: adaptive radar by eigenanalysis methods, in *IEEE Transactions on Aerospace and Electronic Systems*, vol. 32, no. 2, pp. 532-542, April 1996, doi: 10.1109/7.489498.

29. J. S. Goldstein and I. S. Reed, Reduced-rank adaptive filtering, in IEEE Transactions on Signal Processing, vol. 45, no. 2, pp. 492-496, Feb. 1997, doi: 10.1109/78.554317.

30. J. S. Goldstein, I. S. Reed and L. L. Scharf, A multistage representation of the Wiener filter based on orthogonal projections, in *IEEE Transactions on Information Theory*, vol. 44, no. 7, pp. 2943-2959, Nov. 1998, doi: 10.1109/18.737524.

31. D. A. Pados and G. N. Karystinos, "An iterative algorithm for the computation of the MVDR filter," in *IEEE Transactions on Signal Processing*, vol. 49, no. 2, pp. 290-300, Feb. 2001.

32. R. Fa, R. C. de Lamare and L. Wang, Reduced-Rank STAP Schemes for Airborne Radar Based on Switched Joint Interpolation, Decimation and Filtering Algorithm, in *IEEE Transactions on Signal Processing*, vol. 58, no. 8, pp. 4182-4194, Aug. 2010.

33. T. K. Sarkar and N. Sangruji, An adaptive nulling system for a narrow-band signal with a look-direction constraint utilizing the conjugate gradient method, in *IEEE Transactions on Antennas and Propagation*, vol. 37, no. 7, pp. 940-944, July 1989.

34. T. K. Sarkar, S. Park, J. Koh and R. A. Schneible, "A deterministic least square approach to adaptive antennas", Digital Signal Processing Rev. J., vol. 6, pp. 185-194, 1996.

35. T. K. Sarkar et al., "A pragmatic approach to adaptive antennas," in *IEEE Antennas and Propagation Magazine*, vol. 42, no. 2, pp. 39-55, April 2000, doi: 10.1109/74.842124.

36. D. Cristallini and W. Burger, "A Robust Direct Data Domain Approach for STAP," in *IEEE Transactions on Signal Processing*, vol. 60, no. 3, pp. 1283-1294, March 2012, doi: 10.1109/TSP.2011.2176335.

37. Z. Yang, X. Wang, Reduced-rank space-time adaptive processing algorithm based on multistage selections of angle-Doppler filters. *IET Radar Sonar Navig*. vol. 16 no. 2, pp. 327– 345, 2022.

38. G. Sun, Z. He, J. Tong and X. Zhang, Knowledge-Aided Covariance Matrix Estimation via Kronecker Product Expansions for Airborne STAP, in IEEE Geoscience and Remote Sensing Letters, vol. 15, no. 4, pp. 527–531, April 2018.

39. W. L. Melvin and J. R. Guerci, "Knowledge-aided signal processing: a new paradigm for radar and other advanced sensors," in *IEEE Transactions on Aerospace and Electronic Systems*, vol. 42, no. 3, pp. 983-996, July 2006.

40. S. Bidon, O. Besson and J. Tourneret, Knowledge-Aided STAP in Heterogeneous Clutter using a Hierarchical Bayesian Algorithm, in IEEE Transactions on Aerospace and Electronic Systems, vol. 47, no. 3, pp. 1863–1879, July 2011.

41. O. Ledoit and M. Wolf, "A well-conditioned estimator for large-dimensional covariance matrices", J. Multivar. Anal., vol. 88, no. 2, pp. 365-411, 2004.

42. P. Stoica, J. Li, X. Zhu and J. R. Guerci, "On Using a priori Knowledge in Space-Time Adaptive Processing," in *IEEE Transactions on Signal Processing*, vol. 56, no. 6, pp. 2598-2602, June 2008.

43. J. P. Hoffbeck and D. A. Landgrebe, "Covariance matrix estimation and classification with limited training data", IEEE Trans. Pattern Anal. Mach. Intell., vol. 18, no. 7, pp. 763-767, Jul. 1996.

44. P. Wang, Z. Wang, H. Li and B. Himed, "Knowledge-Aided Parametric Adaptive Matched Filter With Automatic Combining for Covariance Estimation," in *IEEE Transactions on Signal Processing*, vol. 62, no. 18, pp. 4713-4722, Sept.15, 2014.

45. M. Riedl and L. C. Potter, Multimodel Shrinkage for Knowledge-Aided Space-Time Adaptive Processing," in *IEEE Transactions on Aerospace and Electronic Systems*, vol. 54, no. 5, pp. 2601-2610, Oct. 2018.

46. F. Jia, G. Sun, Z. He and J. Li, "Grating-Lobe Clutter Suppression in Uniform Subarray for Airborne Radar STAP," in *IEEE Sensors Journal*, vol. 19, no. 16, pp. 6956-6965, 15 Aug.15, 2019, doi: 10.1109/JSEN.2019.2912827.

47. M. Li, G. Sun, J. Tong and Z. He, Training-free moving target detection with uncertain a priori knowledge for airborne radar, *IET Radar, Sonar & Navigation*, vol. 14, no. 3, pp. 372-380, 2020.

48. Y. Wang, W. Xia and Z. He, CFAR Knowledge-Aided Radar Detection With Heterogeneous Samples, in *IEEE Signal Processing Letters*, vol. 24, no. 5, pp. 693-697, May 2017.

49. X. Wang, Z. Yang, J. Huang and R. C. de Lamare, "Robust Two-Stage Reduced-Dimension Sparsity-Aware STAP for Airborne Radar With Coprime Arrays," in *IEEE Transactions on Signal Processing*, vol. 68, pp. 81-96, 2020.

50. D. L. Donoho, "Compressed sensing", *IEEE Trans. Inf. Theory*, vol. 52, no. 4, pp. 1289-1306, 2006.

51. M. Duarte and Y. C. Eldar, "Structured compressed sensing: From theory to applications", *IEEE Trans. Signal Process*, vol. 59, no. 9, pp. 4053-4085, Sep. 2011.

52. E. Cands, J. Romberg and T. Tao, "Stable signal recovery from incomplete and inaccurate measurements", *Comm. Pure Appl. Math*, vol. 59, no. 8, pp. 1207-1223, 2006.

53. M. A. Herman and T. Strohmer, High-resolution radar via compressed sensing, in *IEEE Trans. Signal Process.*, vol. 57, no. 6, pp. 2275-2284, June 2009.

54. B. Demissie, High-resolution range-Doppler imaging by coherent block-sparse estimation, in Proc. Int. Workshop Compress. Sens. Appl. Radar, May 2012.

55. O. Bar-Ilan and Y. C. Eldar, Sub-Nyquist Radar via Doppler Focusing, in *IEEE Transactions on Signal Processing*, vol. 62, no. 7, pp. 1796-1811, April 2014.

56. Q. Feng, J. Huang, S. Liang and L. Kang, "A Pulse Repetition Rate Compressive Sampler for Radar Target Detection," in IEEE Sensors Letters, vol. 4, no. 2, pp. 1-4, Feb. 2020, Art no. 7000604, doi: 10.1109/LSENS.2020.2970722.

57. F. Xi, S. Chen and Z. Liu, Quadrature Compressive Sampling for Radar Signals, in *IEEE Transactions on Signal Processing*, vol. 62, no. 11, pp. 2787-2802, June1, 2014, doi: 10.1109/TSP.2014.2315168.

58. C. Liu, F. Xi, S. Chen, Y. D. Zhang and Z. Liu, Pulse-doppler signal processing with quadrature compressive sampling, in *IEEE Transactions on Aerospace and Electronic Systems*, vol. 51, no. 2, pp. 1217-1230, April 2015.

59. A.H. Oveis, and M.A. Sebt, Compressed sensing-based ground MTI with clutter rejection scheme for synthetic aperture radar. In *IET Signal Process.*, vol 11, no. 2, pp. 155-164, 2017.

60. S. Maria and J. -. Fuchs, "Application of the Global Matched Filter to Stap Data an Efficient Algorithmic Approach," *2006 IEEE International Conference on Acoustics Speech and Signal Processing Proceedings*, 2006, pp. IV-IV.

61. R. Baraniuk and P. Steeghs, "Compressive Radar Imaging," in *2007 IEEE Radar Conference*, 2007, pp. 128-133.

62. W. U. Bajwa, K. Gedalyahu and Y. C. Eldar, Identification of Parametric Underspread Linear Systems and Super-Resolution Radar, in *IEEE Transactions on Signal Processing*, vol. 59, no. 6, pp. 2548-2561, June 2011.

63. J. Zhang, D. Zhu and G. Zhang, "Adaptive Compressed Sensing Radar Oriented Toward Cognitive Detection in Dynamic Sparse Target Scene," in *IEEE Transactions on Signal Processing*, vol. 60, no. 4, pp. 1718-1729, April 2012.

64. S. Haykin, B. W. Currie and S. B. Kesler, "Maximum-entropy spectral analysis of radar clutter," in *Proceedings of the IEEE*, vol. 70, no. 9, pp. 953-962, Sept. 1982, doi: 10.1109/PROC.1982.12426.

65. W. Stehwien and S. Haykin, "A statistical radar clutter classifier," *Proceedings of the IEEE National Radar Conference*, 1989, pp. 164-169.

66. S. Haykin and C. Deng, Classification of radar clutter using neural networks, in *IEEE Transactions on Neural Networks*, vol. 2, no. 6, pp. 589-600, Nov. 1991, doi: 10.1109/72.97936.

67. A. Jakubiak, J. Arabas, K. Grabczak, D. Radomski and J. F. Swiderski, "Radar clutter classification using Kohonen neural network," *Radar 97* (Conf. Publ. No. 449), 1997, pp. 185-188, doi: 10.1049/cp:19971658.

68. X. Li, G. Zhu, H. Cao and S. Wang, A Classifier for Radar Clutter Using Alpha Stable Model, in *2006 CIE International Conference on Radar*, 2006, pp. 1-4, doi: 10.1109/ICR.2006.343454.

69. I. Jouny and C. Wu, Classification of radar clutter using features extracted from the time-frequency domain, in *Proceedings of SPIE*, vol. 3069, pp. 49-56, 1997.

70. I. Bilik, J. Tabrikian and A. Cohen, "GMM-based target classification for ground surveillance Doppler radar," in *IEEE Transactions on Aerospace and Electronic Systems*, vol. 42, no. 1, pp. 267-278, Jan. 2006, doi: 10.1109/TAES.2006.1603422.

71. R. Soleti, L. Cantini, F. Berizzi, A. Capria and D. Calugi, "Neural Network for polarimetric radar target classification", in *2006 14th European Signal Processing Conference*, pp. 1-5, September, 2006.

72. M. A. Darzikolaei, A. Ebrahimzade and E. Gholami, "Classification of radar clutters with Artificial Neural Network," *2015 2nd International Conference on Knowledge-Based Engineering and Innovation (KBEI)*, 2015, pp. 577-581.

73. H. Ghadaki and R. Dizaji, "Target track classification for airport surveillance radar (ASR)," 2006 IEEE Conference on Radar, 2006, pp. 4, doi: 10.1109/RADAR.2006.1631787.

74. D. Callaghan, J. Burger and A. K. Mishra, "A machine learning approach to radar sea clutter suppression," 2017 IEEE Radar Conference (RadarConf), 2017, pp. 1222-1227, doi: 10.1109/RADAR.2017.7944391.

75. P. -L. Shui, X. -Y. Xia and Y. -S. Zhang, "Sea–Land Segmentation in Maritime Surveillance Radars via K-Nearest Neighbor Classifier," in *IEEE Transactions on Aerospace and Electronic Systems*, vol. 56, no. 5, pp. 3854-3867, Oct. 2020, doi: 10.1109/TAES.2020.2981267.

76. A. El Khatib, K. Assaleh and H. Mir, "Learning-based space-time adaptive processing," *2013 1st International Conference on Communications, Signal Processing, and their Applications (ICCSPA)*, 2013, pp. 1-4, doi: 10.1109/ICCSPA.2013.6487279.

77. A. E. Khatib, K. Assaleh and H. Mir, "Space-Time Adaptive Processing Using Pattern Classification," in *IEEE Transactions on Signal Processing*, vol. 63, no. 3, pp. 766-779, Feb.1, 2015, doi: 10.1109/TSP.2014.2385653.

78. L. Wang, J. Tang and Q. Liao, "A Study on Radar Target Detection Based on Deep Neural Networks," in *IEEE Sensors Letters*, vol. 3, no. 3, pp. 1-4, March 2019, Art no. 7000504, doi: 10.1109/LSENS.2019.2896072.

79. E. Mason, B. Yonel and B. Yazici, "Deep learning for radar," *2017 IEEE Radar Conference (RadarConf)*, 2017, pp. 1703-1708, doi: 10.1109/RADAR.2017.7944481.

80. C. Wang, J. Wang and X. Zhang, "Automatic radar waveform recognition based on time-frequency analysis and convolutional neural network", *2017 IEEE International Conference on Acoustics, Speech and Signal Processing (ICASSP)*, 2017, pp. 2437-2441, doi: 10.1109/ICASSP.2017.7952594.

81. D. Zhou, X. Wang, Y. Tian and R. Wang, "A novel radar signal recognition method based on a deep restricted Boltzmann machine", *Engineering Review*, vol. 37, no. 2, pp. 165-171, 2017

82. M. Courbariaux, I. Hubara, D. Soudry, R. El-Yaniv and Y. Bengio, Binarized neural networks: training deep neural networks with weights and activations constrained to + 1 or −1, 2016.

83. Z. Lin, M. Courbariaux, R. Memisevic and Y. Bengio, Neural networks with few multiplications, October 2015.

84. G. J. Mendis, Jin Wei and A. Madanayake, Deep learning cognitive radar for micro UAS detection and classification, *2017 Cognitive Communications for Aerospace Applications Workshop (CCAA)*, 2017, pp. 1-5, doi: 10.1109/CCAAW.2017.8001610.

85. H. Liu, B. Feng, B. Chen and L. Du, "Radar high-resolution range profiles target recognition based on stable dictionary learning", *IET Radar Sonar Navig.*, vol. 10, no. 2, pp. 228-237, 2016

86. Z. Liu, D. K. C. Ho, X. Xu and J. Yang, "Moving Target Indication Using Deep Convolutional Neural Network," in *IEEE Access*, vol. 6, pp. 65651-65660, 2018, doi: 10.1109/ACCESS.2018.2877018.

87. G. W. Titi and D. F. Marshall, "The ARPA/NAVY mountaintop program: Adaptive signal processing for airborne early warning radar", in *Proc. IEEE Int. Conf. Acoust. Speech Signal Process.*, vol. 2, pp. 1165-1168, May 1996.

88. M. Pan, J. Chen, S. Wang and Z. Dong, "A Novel Approach for Marine Small Target Detection Based on Deep Learning," *2019 IEEE 4th International Conference on Signal and Image Processing (ICSIP)*, 2019, pp. 395-399, doi: 10.1109/SIPROCESS.2019.8868862.

89. X. Chen, N. Su, Y. Huang and J. Guan, False-Alarm-Controllable Radar Detection for Marine Target Based on Multi Features Fusion via CNNs, in *IEEE Sensors Journal*, vol. 21, no. 7, pp. 9099-9111, 1 April1, 2021, doi: 10.1109/JSEN.2021.3054744.

90. J. Williams, L. Rosenberg, V. Stamatescu and T. -T. Cao, "Maritime Radar Target Detection Using Convolutional Neural Networks," in *2022 IEEE Radar Conference (RadarConf22)*, 2022, pp. 1-6, doi: 10.1109/RadarConf2248738.2022.9764227.

91. Hai Deng, B. Himed and M. C. Wicks, "Image feature-based space-time processing for ground moving target detection," in *IEEE Signal Processing Letters*, vol. 13, no. 4, pp. 216-219, April 2006, doi: 10.1109/LSP.2005.863676.

92. Z. Geng, H. Deng and B. Himed, Ground Moving Target Detection Using Beam-Doppler Image Feature Recognition, in *IEEE Transactions on Aerospace and Electronic Systems*, vol. 54, no. 5, pp. 2329-2341, Oct. 2018, doi: 10.1109/TAES.2018.2814350.

93. M. H. Hayes, *Statistical Digital Signal Processing and Modeling*. New York, NY, USA: Wiley, 1996. pp. 426–433.

94. J. R. Guerci, *Space-Time Adaptive Processing For Radar*, Norwood, MA, USA: Artech House, 2003. pp. 65–70.

95. K. Duan, H. Chen, W. Xie, and Y. Wang, Deep learning for high-resolution estimation of clutter angle-Doppler spectrum in STAP, in *IET Radar Sonar Navig*., Nov. 2021. doi: 10.1049/rsn2.12176.

96. X. Yang, J. Shi, Y. Zhou, C. Wang, Y. Hu, X. Zhang, and S. Wei, Ground Moving Target Tracking and Refocusing Using Shadow in Video-SAR, in *Remote Sensing*, vol. 12, no. 18, p. 3083, Sep. 2020. doi: 10.3390/rs12183083.

97. J. Zhao, J. Wu, X. Guo, J. Han, K. Yang, and H. Wang, Prediction of radar sea clutter based on LSTM, *J. Ambient Intell. Hum. Comput.*, vol. 4, pp. 1–8, Sep. 2019. doi: 10.1007/s12652-019-01438-4.

98. M. Lim, O. A. Omitaomu and S. J. Bae, A Step-Down Test Procedure for Wavelet Shrinkage Using Bootstrapping, in *IEEE Access*, vol. 8, pp. 174763-174772, 2020, doi: 10.1109/ACCESS.2020.3025103.

99. A. Khosravi, S. Nahavandi, D. Srinivasan and R. Khosravi, Constructing Optimal Prediction Intervals by Using Neural Networks and Bootstrap Method, in *IEEE Transactions on Neural Networks and Learning Systems*, vol. 26, no. 8, pp. 1810-1815, Aug. 2015, doi: 10.1109/TNNLS.2014.2354418.

100. B. Efron and R. J. Tibshirani, *An Introduction to the Bootstrap*. New York, NY, USA: Chapman & Hall, 1993, pp. 45–56, 170–173.

101. S. M. Kay, *Fundamentals of Statistical Signal Processing: Detection Theory*, Upper Saddle River, NJ, USA:Prentice-Hall, 1993, pp. 67–71.

102. J. Hoshen, R. Kopelman, Percolation and cluster distribution. I. Cluster multiple labeling technique and critical concentration algorithm, in *Phys. Rev. B*, vol. 14, no. 8, 1976, pp. 3438–3444. doi: 10.1103/PhysRevB.14.3438.

103. J. Hoshen, The application of the enhanced Hoshen-Kopelman algorithm for processing unbounded images, in *IEEE Trans Image Process.*, vol. 8, no. 3, March 1999, pp. 421–425, doi: 10.1109/83.748896.

104. P. Arbeláez, M. Maire, C. Fowlkes and J. Malik, Contour Detection and Hierarchical Image Segmentation, in *IEEE Transactions on Pattern Analysis and Machine Intelligence*, vol. 33, no. 5, pp. 898-916, May 2011, doi: 10.1109/TPAMI.2010.161.

105. F. Akram, M. A. Garcia, D. Puig, Active contours driven by local and global fitted image models for image segmentation robust to intensity inhomogeneity, in *PLoS ONE*, vol. 12, no. 4: e0174813, 2017. doi: 10.1371/journal.pone.0174813.

106. R. C. Gonzalez, R. E. Woods, S. L. Eddins, *Digital Image Processing Using MATLAB*, Pearson Prentice Hall, 2nd edn., 2004, pp. 598–603.

107. A. G. Ghuneim, 'Contour Tracing'. Available: http://www.imageprocessingplace.com/downloads_V3/root_downloads/tutorials/contour_tracing_Abeer_George_Ghuneim/index.html, accessed 16 April 2022.

108. V. J. L. Vliet and W. P. Verbeek, Curvature and bending energy in digitized 2D and 3D images, *Proc. 8th Scandinavian Conf. Image Analysis*, pp. 1403-1410, 1993.

109. I. T. Young, J. E. Walker, and J. E. Bowie, An analysis technique for biological shape. I, Information and control, 1974, vol. 25, no. 4, pp. 357–370, doi: 10.1016/S0019-9958(74)91038-9

110. B. D. Agkland and N. H. Weste, The edge flag algorithm — A fill method for raster scan displays, in *IEEE Transactions on Computers*, vol. C-30, no. 1, pp. 41–48, Jan. 1981, doi: 10.1109/TC.1981.6312155.

111. M.J.A. Berry and G.S. Linoff, *Data Mining Techniques: For Marketing Sales and Customer Relationship Management*, New York: Wiley, 1997, pp. 323.

112. A. Blum, *Neural Networks in C++: An Object-Oriented Framework for Building Connectionist Systems*, New York, NY, USA:Wiley, 1992, pp. 60.

113. C. K. Wong and M. C. Easton, "An efficient method for weighted sampling without replacement", SIAM J. Comput., vol. 9, no. 1, pp. 111–113, 1980

114. N. V. Chawla, K. W. Bowyer, L. O. Hall, W. P. Kegelmeyer, SMOTE: Synthetic minority over-sampling technique, J. Artif. Intell. Res., vol. 16, Jun. 2002, pp. 321–357. doi: 10.1613/jair.953.

VITA

RAFI AHMED

Born, Dhaka, Bangladesh

2009-2013	B.S., Electronics and Communication Engineering Khulna University of Engineering and Technology (KUET) Khulna, Bangladesh
2018-2021	M.S., Electrical Engineering Florida International University (FIU) Miami, Florida
2018-2019	Graduate Research Assistant Sensor and Systems Research Laboratory Florida International University (FIU) Miami, Florida
2019-2022	Graduate Teaching Assistant Florida International University (FIU) Miami, Florida
2021 -2022	Doctoral Candidate Florida International University (FIU) Miami, Florida

PUBLICATIONS AND PRESENTATIONS

[1] Rafi Ahmed, B.M. Golam Kibria, “Robust ground moving target detection for airborne radar using a novel feature-based machine learning approach”, *Journal of the Franklin Institute*, 2022, ISSN 0016-0032.

[2] R. Ahmed and H. Deng, “Proximity Feature Based Target Detection for Airborne Radar with Misaligned Antenna Array,” *2021 IEEE International Symposium on Antennas and Propagation and USNC-URSI Radio Science Meeting (APS/URSI)*, 2021, pp. 957-958.

[3] R. Ahmed and H. Deng, “Airborne Radar Clutter Suppression in Angle-Doppler Domain Using Clutter-Proximity Feature,” *2021 IEEE International Symposium on Antennas and Propagation and USNC-URSI Radio Science Meeting (APS/URSI)*, 2021, pp. 1117-1118.

[4] Rafi Ahmed, and Hai Deng, "A Multi-Feature Based Machine Learning Approach for Ground-Moving Radar Target Detection," 2022 *IEEE International Symposium on Antennas and Propagation and USNC-URSI Radio Science Meeting (APS/URSI)*, 2022. (accepted)

[5] R. Ahmed “Ground moving radar target detection using a novel feature-based machine learning approach” Presented at the Statistics conference organized by the Division of Statistics, Dept. of Mathematics & Statistics, Florida International University, April 2022.